

Copyright is owned by the Author of the thesis. Permission is given for a copy to be downloaded by an individual for the purpose of research and private study only. The thesis may not be reproduced elsewhere without the permission of the Author.

**Teasing apart the interaction
between HDAC4 and Ankyrin2 in
Drosophila neuronal function**

*A thesis presented in partial fulfilment of the requirements
for the degree of*

Master of Science

in

Biochemistry

School of Fundamental Sciences
Massey University, Manawatu, New Zealand

Sarah Jean Wilson

2021

Abstract

Histone deacetylase 4 (HDAC4) is a class IIa histone deacetylase that has previously been implicated in a range of neurodevelopmental and neurodegenerative diseases which involve deficits in memory and cognition. Overexpression of *HDAC4* in the *Drosophila* brain impairs memory, therefore making *Drosophila* an ideal genetic model system to further investigate the molecular pathways through which HDAC4 acts. A recent genetic screen in *Drosophila* for genes that interact in the same molecular pathway as *HDAC4* identified the cytoskeletal regulator *Ankyrin2* (*Ank2*). The *Ank2* protein plays a pivotal role in maintaining the stability and plasticity of the spectrin-actin cytoskeleton by organising the distribution of ion channels and cell adhesion molecules, which is essential to normal learning and memory formation. Both overexpression of *HDAC4* and knockdown of *Ank2* result in similar deficits in *Drosophila* brain development and long-term memory formation, suggesting that these two proteins may interact together in such processes.

HDAC4 contains an N-terminal ankyrin repeat binding motif and it was hypothesised that HDAC4 interacts physically with the ankyrin repeat region at the N-terminus of *Ank2*, however, no physical interaction was detected via co-immunoprecipitation. Further investigation was then carried out to elucidate the nature of the genetic interaction proposed between *HDAC4* and *Ank2*. In doing so, it was observed that nuclear accumulation of HDAC4 is required for this interaction, however, the presence of the HDAC4 ankyrin repeat binding motif is not required. This is consistent with the finding that HDAC4 does not bind *Ank2* and indicates that the interaction between HDAC4 and *Ank2* is indirect.

It was also identified that *Ank2* and *HDAC4* are both required for *Drosophila* eye development as knockdown of *Ank2* paired with overexpression of *HDAC4* resulted in a severe novel “blueberry” phenotype that has not yet been characterised for these genes. Furthermore, it was observed that *Ank2* was required for normal growth and morphogenesis of dendrites in the visual system, whereby both knockdown of *Ank2* and overexpression of *HDAC4* disrupt dendrite morphogenesis. These data provide further understanding of the roles of HDAC4 and *Ank2* in *Drosophila* neuronal function, and the establishment of the molecular pathway in which *HDAC4* and *Ank2* act will be essential in unravelling additional mechanisms involved in the processes of learning and memory.

Acknowledgements

What an experience 2020 has been. Coronavirus hit, lockdown was imminent and before we knew it, we were ringing in the New Year.

First and foremost, I would like to thank my supervisor Dr. Helen Fitzsimons for this incredible opportunity and endless support. Her enthusiasm, patience and guidance has helped me get through the massive amount of reading, writing, re-writing, and experimentation which I undertook in this project. Again, thank-you.

To my lab mates, come friends, Andy, Hannah, Maddie and Wei, thank-you all for your support and helpful suggestions as well as the welcome conversations about coronavirus and politics, it is suffice to say, I have learnt a lot over the past two years. I would also like to thank the biomedical lab group for the weekly lab meetings, it has been a pleasure to learn what everyone's projects are all about.

A special thank-you to Ana Claasen for all that you do for our lab, from finishing off experiments to making fly food. I would also like to thank you for taking me under your wing and teaching me many of the basic techniques that we use on a daily basis.

To Dr. Matthew Savoian and Raoul Solomon of the Manawatu Microscopy and Imaging Centre (MMIC) thank you both for the patience, guidance and assistance when I was learning to use the Confocal and Scanning Electron Microscopes.

I would also like to thank Ann Truter and Cynthia Cresswell, without whom SFS would struggle to function.

A special thanks to Dr. Silvia Schwartz, whose PhD lead to this Masters project, and without her prior knowledge and preliminary experiments, I would have been seriously out of my depth.

This project was funded by the Royal Society of New Zealand Marsden Fund, and I would again like to thank Dr. Helen Fitzsimons for granting me a scholarship through this fund, in which I am most grateful for.

Lastly, I would like to express my deepest gratitude to my friends and family, without their unconditional love and support I would not have been able to get through these past two years. To my parents, thank you for everything you have done and continue to do for

me, I am eternally grateful. To Glen, my wonderful fiancée, thank you for your continuous support, love and patience, I could not have done this without you.

Coronavirus Statement

As a consequence of the New Zealand nationwide lockdown, Massey University closed down between March 23rd 2020 to May 18th 2020. The ramifications of this closure period were not limited to those two months outside of the laboratory as all experiments involving fly crosses that were set prior to the lockdown had to be abandoned. Following the University re-opening, these crosses required resetting for a second time, which entailed approximately eight weeks of preparation before the progeny required for the experimental assays emerged. This resulted in a loss of approximately four months of time in the lab and as a consequence, several objectives were unable to be completed as planned, which are described below:

Objective 2: Due to time constraints, the western blot performed was only able to be completed once without any semi-quantitative analysis, rather than the minimum three repetitions. This was due to it being one of the last experiments to be started.

Objective 3: Due to time constraints, the western blot was performed in duplicate to allow for a semi-quantitative analysis to be performed, however the results remain inconclusive due to variability. This blot was planned to have been repeated at least one more time.

Objective 5: The experiment on the effect of *HDAC4* overexpression and *Ank2* knockdown on the morphogenesis of dendrites in the visual system was completed, however, it was initially planned that the *DmHDAC4* nuclear-restricted transgene and *DmHDAC4* transgene with a mutated ankyrin repeat binding domain would also be expressed in combination with *Ank2* knockdown in the visual system, to compare these effects to those that were seen in the *Drosophila* eye.

Objective 6: It was initially planned that approximately 20 brains per genotype would be analysed for the phenotypes from either knockdown of *Ank2*, overexpression of *HDAC4*, or both in combination, however, *HDAC4* overexpression alone resulted in a phenotype that was too severe, requiring this experiment to be repeated at a lower temperature (which would result in a lower level of transgene expression). Due to time constraints crosses were unable to be set and raised at a lower temperature, therefore, this experiment remains incomplete.

A further experiment was removed entirely from the project due to lack of time. This experiment was to examine the impact of altering the expression of *Ank2* and *HDAC4*

on the arrangement of the actin cytoskeleton by measuring the ratio of filamentous actin (F-actin) to monomeric globular actin (G-actin).

Table of Contents

Abstract	iii
Acknowledgements	iv
Coronavirus Statement	vi
Table of Contents	viii
List of Figures	xii
List of Tables	xiv
Abbreviations	xv
1 Introduction	1
1.1 Neurodegenerative and neurodevelopmental disorders	2
1.2 Studies of learning and memory	2
1.3 <i>Drosophila</i> as a model system for neuroscientific research	4
1.3.1 The mushroom body	5
1.3.2 The <i>Drosophila</i> compound eye	6
1.3.3 The <i>Drosophila</i> visual system.....	8
1.3.4 Genetic manipulation of <i>Drosophila</i>	9
1.3.4.1 The UAS/GAL4 system.....	10
1.3.4.2 The TARGET system.....	11
1.4 Epigenetic regulators of memory formation	12
1.4.1 Histone deacetylases	13
1.5 HDAC4	15
1.5.1 HDAC4 and neurodevelopmental and neurodegenerative disease.....	17
1.5.2 HDAC4 and memory	18
1.6 Ankyrin proteins	20
1.6.1 Mammalian ANKYRIN-G.....	22
1.6.2 <i>Drosophila</i> Ankyrin2	23
1.7 A relationship between HDAC4 and Ank2	26

2	Materials and Methods.....	29
2.1	<i>Drosophila melanogaster</i> fly strains	30
2.1.1	Fly strain maintenance	30
2.2	Genetic Crosses.....	30
2.3	<i>Drosophila</i> brain isolation	31
2.3.1	Immunohistochemistry on isolated fly brains.....	31
2.4	<i>Drosophila</i> protein extraction.....	33
2.4.1	Fly head isolation	33
2.4.2	Total protein isolation from <i>Drosophila</i> heads.....	33
2.4.3	Cell fractionation from <i>Drosophila</i> heads	34
2.5	Protein quantification.....	34
2.6	SDS-PAGE and Western Blotting.....	35
2.7	Immunoprecipitation / Co-immunoprecipitation	36
2.8	<i>Drosophila</i> eye phenotype analysis.....	37
2.8.1	Light microscopy.....	37
2.8.2	Scanning electron microscopy	38
3	Results.....	39
3.1	Investigating a physical interaction between HDAC4 and <i>Ank2</i>	40
3.1.1	Confirmation of expression of <i>Ank2</i> ₁₉₀₋₉₄₆ -HA via western blot	42
3.1.2	Confirmation of co-expression of <i>Ank2</i> ₁₉₀₋₉₄₆ -HA and DmHDAC4-Myc via immunohistochemistry	44
3.1.3	Immunoprecipitation of <i>Ank2</i> ₁₉₀₋₉₄₆ -HA and DmHDAC4-Myc	47
3.1.4	Positive co-IP control	50
3.1.5	A physical interaction was not detected between <i>Ank2</i> ₁₉₀₋₉₄₆ -HA and DmHDAC4-Myc via co-IP.....	51
3.2	What is the molecular basis of the genetic interaction between <i>HDAC4</i> and <i>Ank2</i> ?	54
3.2.1	Does HDAC4 regulate <i>Ank2</i> expression?.....	54
3.2.2	Does <i>Ank2</i> regulate expression and/or subcellular distribution of HDAC4 protein?.....	56

3.3 Examining the genetic interaction between <i>HDAC4</i> and <i>Ank2</i> in photoreceptors.....	62
3.3.1 A phenotypic eye screen showing the effect of <i>Ank2</i> knockdown in combination with <i>Drosophila HDAC4</i> mutants.....	63
3.3.2 Characterisation of additional eye phenotypes that were observed.....	73
3.4 Investigation of the neurodevelopmental role of <i>HDAC4</i> and <i>Ank2</i> in dendrite morphogenesis	75
3.4.1 Characterisation of the genetic interaction between <i>HDAC4</i> and <i>Ank2</i> in dendrite morphogenesis	79
3.5 Investigation of the neurodevelopmental role of <i>Ank2</i> and <i>HDAC4</i> in axon morphogenesis in the mushroom body.....	83
4 Discussion and Future Directions	87
4.1 There is not a direct physical interaction between HDAC4 and <i>Ank2</i>.....	88
4.2 <i>Ank2</i> may regulate the level of HDAC4 protein	89
4.3 Nuclear HDAC4 interacts genetically with <i>Ank2</i>.....	91
4.3.1 The genetic interaction does not depend on the presence of the ankyrin binding domain on HDAC4.....	92
4.4 What is the nature of the interaction between HDAC4 and <i>Ank2</i>?	94
4.4.1 The role in the mushroom body.....	95
4.4.2 The role in memory formation	97
4.5 What is the molecular basis of the observed rough eye phenotypes?	98
4.5.1 Reduction of eye sizes attributed to apoptosis	98
4.5.2 The “blueberry” phenotype	99
4.6 Wild-type levels of HDAC4 and <i>Ank2</i> are required for normal dendrite morphogenesis in the optic lobes	100
4.7 Conclusion.....	101
5 References	103

6	Appendix	123
	6.1 Fly strains.....	124
	6.2 Ank2₁₉₀₋₉₄₆-HA sequence.....	125
	6.3 HDAC4 variant sequences.....	126
	6.4 <i>Ank2</i> RNAi transcript targets	132

List of Figures

Figure 1.1. Schematic of the synaptic connection between an axon and dendrite	3
Figure 1.2. Schematic depiction of the <i>Drosophila</i> brain	6
Figure 1.3. Rough eye phenotype enhancement screen	8
Figure 1.4. Schematic of the UAS/GAL4 bipartite system in <i>Drosophila</i>	10
Figure 1.5. The TARGET system in <i>Drosophila</i>	11
Figure 1.6. Schematic showing the composition of a nucleosome	12
Figure 1.7. Schematic representations of the domain structures of human HDACs	14
Figure 1.8. Conserved domains of <i>Drosophila</i> and human HDAC4	16
Figure 1.9. Schematic of a canonical long ankyrin isoform	21
Figure 1.10. The conservation of the ankyrin repeat binding domain of HDAC4.	22
Figure 2.1. Schematic of the process involved in immunoprecipitation and co- immunoprecipitation assays	37
Figure 3.1. The HDAC4::YFP construct	40
Figure 3.2. Endogenous expression of HDAC4 and Ankyrin2 in HDAC4::YFP brains	41
Figure 3.3. Example of a genetic crossing scheme	43
Figure 3.4. Characterising expression of Ank2 ₁₉₀₋₉₄₆ -HA	43
Figure 3.5. Crossing scheme to generate a <i>UAS-Ank2₁₉₀₋₉₄₆-HA; UAS-DmHDAC4-Myc</i> homozygous line	45
Figure 3.6. Characterising the expression and co-distribution of Ank2 ₁₉₀₋₉₄₆ -HA and DmHDAC4-Myc	47
Figure 3.7. Immunoprecipitation of Ank2 ₁₉₀₋₉₄₆ -HA and DmHDAC4-Myc	49
Figure 3.8. Positive co-IP control blots	51
Figure 3.9. Ank2 ₁₉₀₋₉₄₆ -HA and DmHDAC4-Myc do not physically interact via co-IP	53
Figure 3.10. The effect of <i>DmHDAC4</i> regulation on Ank2 protein level	56
Figure 3.11. <i>Ank2</i> knockdown alters total HDAC4 protein levels	58
Figure 3.12. Cellular fractionation optimisation	59
Figure 3.13. <i>Ank2</i> knockdown during development does not significantly affect <i>HDAC4</i> expression and subcellular localisation	60
Figure 3.14. <i>Ank2</i> knockdown in the adult brain does not significantly affect <i>HDAC4</i> expression and subcellular localisation	62
Figure 3.15. <i>Ank2</i> RNAi enhancement of the <i>DmHDAC4</i> overexpression-induced rough eye phenotype	67

Figure 3.16. Phenotype scores for the <i>DmHDAC4</i> transgenes and <i>Ank2</i> RNAi	69
Figure 3.17. Reduced eye sizes observed when <i>DmHDAC4</i> transgenes are co-expressed with <i>Ank2</i> RNAi	71
Figure 3.18. Box and whisker plot showing eye area changes observed by co-expression of <i>DmHDAC4</i> transgenes and <i>Ank2</i> RNAi	72
Figure 3.19. “Blueberry” phenotype observed upon <i>Ank2</i> RNAi and <i>DmHDAC4</i> transgene co-expression	74
Figure 3.20. Characteristic normal dendrite growth in the visual system LPTCs.....	77
Figure 3.21. Representative images of the phenotypes observed in the LPTCs	78
Figure 3.22. Tracing plot of a characteristic LPTC dendritic arbour	79
Figure 3.23. The percentage of abnormal phenotypes in LPTCs induced by <i>HDAC4</i> mutants and <i>Ank2</i> RNAi.....	81
Figure 3.24. Alterations in the level of <i>HDAC4</i> and <i>Ank2</i> do not affect the growth and extension of the visual system LPTCs	82
Figure 3.25. Mushroom body phenotypes resulting from <i>Ank2</i> RNAi at 25°C.....	84
Figure 3.26. Mushroom body phenotypes from <i>HDAC4</i> overexpression and <i>Ank2</i> RNAi at 25°C.....	85
Figure 4.1. Model of the proposed genetic interaction between <i>HDAC4</i> , <i>Ank2</i> and unidentified ankyrin repeat-containing protein(s)	94
Figure 4.2. The ternary complex found in <i>Drosophila</i> mushroom body axons	96
Figure 6.1. <i>Ank2</i> gene and transcript targets by the <i>Ank2</i> RNAi construct.....	132

List of Tables

Table 2.1. List of primary antibodies used in immunohistochemistry and western blotting with corresponding dilutions	32
Table 2.2. List of secondary antibodies used in immunohistochemistry and western blotting with corresponding dilutions	33
Table 3.1. Semi-quantitative rough eye phenotype analysis	65
Table 3.2. Rough eye phenotype scores	68
Table 3.3. Proportion of normal vs abnormal phenotypes induced by <i>HDAC4</i> mutants and <i>Ank2</i> RNAi in the visual system LPTCs.....	80
Table 6.1. Genotypes and sources of <i>Drosophila melanogaster</i> strains used in this study	125

Abbreviations

°C	Degrees Celsius
ADHD	Attention Deficit Hyperactivity Disorder
α -syn	Alpha-synuclein
Ank1	Ankyrin1
Ank2	Ankyrin2
Ank2-L	Ankyrin2-Long
Ank2-M	Ankyrin2-Medium
Ank2-S	Ankyrin2-Short
Ank2-XL	Ankyrin2-Extra Long
Ank3	Ankyrin3
ANK-G	Ankyrin-G
ANKRA2	Ankyrin repeat family A protein 2
AL	Antennal Lobe
APP	Amyloid Precursor Protein
A.U	Arbitrary Units
BDSC	Bloomington Drosophila Stock Centre
bp	Base pair
Ca ²⁺	Calcium
CaMK	Calcium/calmodulin-dependent kinase
CF	Cytoplasmic Fraction
CO ₂	Carbon Dioxide
Co-IP	Co-Immunoprecipitation
cs	Canton special
CyO	Curly of Oster balancer chromosome
dH ₂ O	Distilled water
DmHDAC4	<i>Drosophila</i> HDAC4
DNA	Deoxyribonucleic acid
DSHB	Developmental Studies Hybridoma Bank
dsRNA	Double stranded Ribonucleic acid

DTT	Dithiothreitol
EDTA	Ethylenediaminetetraacetic acid
EGFP	Enhanced green fluorescent protein
elav	Embryonic lethal abnormal visual system
ER	Endoplasmic Reticulum
F-actin	Filamentous Actin
FasII	Fasciclin II
g	Gram
G-actin	Globular Actin
GFP	Green fluorescent protein
GMR	Glass multimer reporter
GST	Glutathione S-transferase
H ⁺	Hydrogen
HAT	Histone acetyltransferase
HCl	Hydrochloric acid
HDAC	Histone deacetylase
HDAC4	Histone deacetylase 4
hHDAC4	Human HDAC4
HRP	Horseradish Peroxidase
IHC	Immunohistochemistry
IgG	Immunoglobulin G
IP	Immunoprecipitation
IP-MS	Immunoprecipitation-Mass Spectrometry
K ⁺	Potassium
kb	Kilobase
kDa	Kilodalton
kV	Kilovolts
L	Litre
L1-CaM	L1 cell adhesion molecule
LPTC	Lobula Plate Tangential Cells

M	Molar
MARCM	Mosaic Analysis with a Repressible Cell Marker
MEF2	Myocyte Enhancer Factor 2
mg	Milligram
mL	Millilitre
mM	Millimolar
mRNA	Messenger RNA
MS	Mass Spectrometry
Na ⁺	Sodium
NAD ⁺	Nicotinamide adenine dinucleotide
NES	Nuclear export signal
NF	Nuclear Fraction
NLS	Nuclear Localisation Sequence
nm	Nanometre
n.s	Not Significant
OL	Optic Lobe
padj	P value adjusted for multiple testing
RFXANK	Regulatory factor X associated ankyrin-containing protein
R	Rhabdomic
RNA	Ribonucleic acid
RNAi	RNA interference
RNA-seq	RNA sequencing
RT	Room Temperature
Sb	Stubble
Sco	Scutoid
SDS	Sodium Dodecyl Sulfate
SDS-PAGE	Sodium Dodecyl Sulfate-Polyacrylamide Gel Electrophoresis
SEM	Scanning Electron Microscopy
SEM	Standard Error of the Mean
sev	sevenless

shRNA	Short hairpin RNA
SNP	Single nucleotide polymorphism
TARGET	Temporal and regional gene expression targeting
TM3	3 rd multiply inverted balancer chromosome
ts	Temperature sensitive
Tub	Alpha-tubulin promoter
UAS	Upstream activating sequence
V	Volt
VDRC	Vienna Drosophila Resource Centre
VS	Vertical System
w ⁺	Mini-white gene
W1	Wash 1
W2	Wash 2
WB	Western blotting
YFP	Yellow Fluorescent Protein
Zn ⁺	Zinc
µg	Microgram
µL	Microlitre
µm	Micrometre

1 Introduction

1.1 Neurodegenerative and neurodevelopmental disorders

Precise spatial and temporal regulation of gene expression is necessary for the correct development of the brain, which involves the morphogenesis of billions of neurons and organisation of trillions of synapses into functional neuronal networks. Genetic and epigenetic dysregulation of these processes can lead to a range of neurodevelopmental disorders that result in clinical features including intellectual disability, developmental delay and autism, the underlying causes of which are usually undetermined.

Late-onset neurodegenerative disorders cause gradual degeneration of the nervous system, impaired cognitive function and death of neurons. Such disorders include Alzheimer's disease (Weller & Budson, 2018), Parkinson's disease (Przedborski, 2017) and Huntington's disease (Kumar et al., 2015). Characteristics of these include impaired motor function, loss of cognitive abilities and memory impairments. In recent years, as healthcare continues to improve the aging population continues to rise, resulting in an ever-increasing incidence of dementia. Alzheimer's disease makes up between 60-80% of dementia diagnoses (Neugroschl & Wang, 2011). In New Zealand there was a 29% increase in Alzheimer's prevalence over a five-year timespan between 2011 and 2016 resulting in 62,287 individuals being diagnosed. This number is expected to increase by more than double to 170,212 by the year 2050 (*Dementia economic impact report 2016*, 2017). Worldwide there are 50 million individuals living with dementia, with a new case being identified every three seconds, this number is expected to triple by 2050 to a massive 152 million people suffering from dementia (Patterson, 2018). As there are currently no effective treatments for dementia, a better understanding of the molecular processes that are required for normal cognitive function and how these processes are disrupted in neurodegenerative disease is imperative.

1.2 Studies of learning and memory

Neurons transmit and receive signals to and from other neurons via synapses, the junctions through which electrochemical signals are transferred (Sudhof & Malenka, 2008). Neurons are comprised of dendrites that receive signals from neighbouring neurons (Sidiropoulou et al., 2006), the axon initial segment; which initiates an action potential (Foust et al., 2010), the axon; which transmits the action potential signal over a

long distance, and the axon terminal where this signal is transmitted through the synapse (Sudhof & Malenka, 2008). Neurotransmitters are small molecules released into the synapse following firing of an action potential. This action potential travels down the axon to the axon terminal which depolarizes the membrane, triggering opening of the voltage-gated calcium channels allowing for an influx of calcium to enter the presynaptic axon terminal resulting in the release of a neurotransmitter (Reece et al., 2014; van der Kloot & Kita, 1974). These neurotransmitters are released into the synaptic cleft and bind to receptors on the post-synaptic dendrite which triggers an action potential in the following neuron (Figure 1.1). Neurotransmitters can also bind to voltage-gated sodium channels which then open and allow positive charge to flood the negative resting cell (Cantrell et al., 1999). This influx of positive charge depolarizes the cell and activates the firing of an action potential (van der Kloot & Kita, 1974). This action potential is initiated at the axon initial segment and is propagated down the axon by the myelin sheaths and nodes of Ranvier to the axon terminal (Arancibia-Carcamo & Attwell, 2014; Foust et al., 2010; Nickel & Gu, 2018).

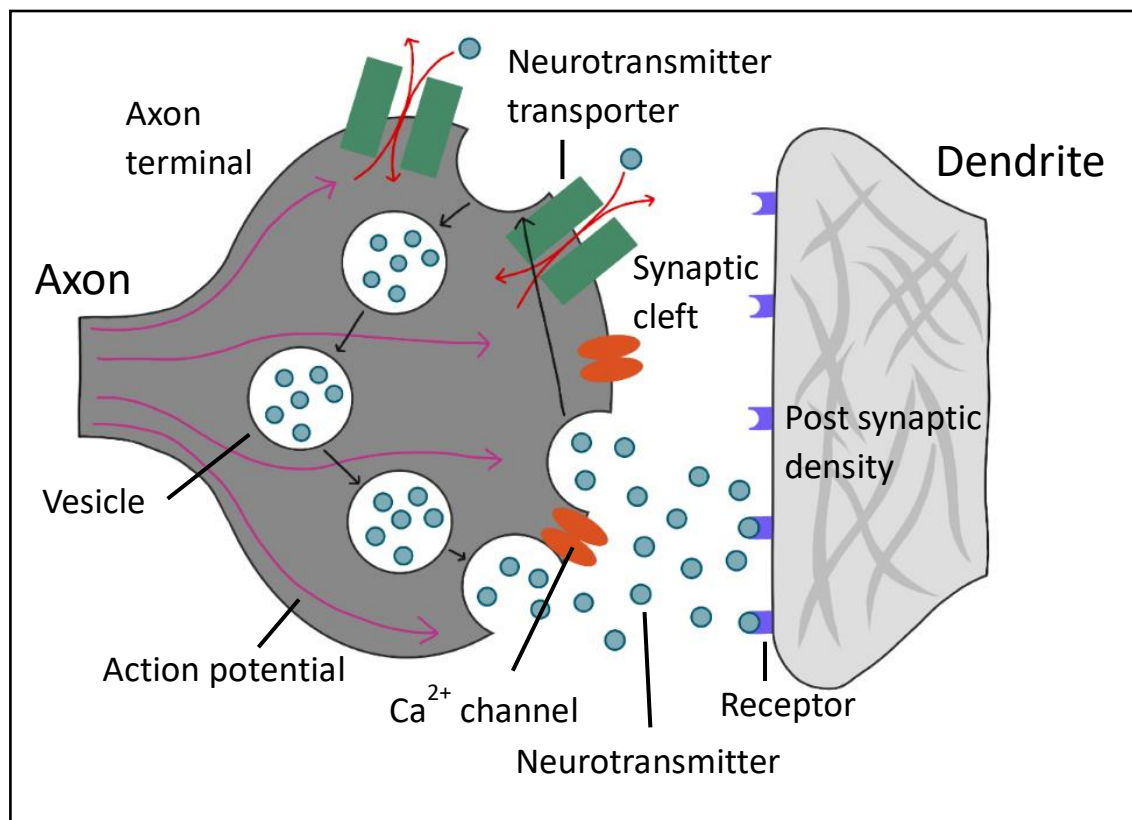


Figure 1.1. Schematic of the synaptic connection between an axon and dendrite. In the axonal presynaptic terminal, neurotransmitters are gathered into synaptic vesicles where they are released into the synaptic cleft following depolarization of the membrane by the firing of an action potential. This causes the voltage-gated Ca²⁺ channels to open allowing an influx of calcium to enter the presynaptic terminal. Neurotransmitters then bind to receptors on the postsynaptic

dendrite or are recaptured by the presynaptic terminal and repackaged into new synaptic vesicles. Abbreviations: Ca^{2+} = Calcium. *Original artwork created with reference to Thomas Spletstoeser (www.scistyle.com) and Sudhof and Malenka (2008).*

Learning is the biological process of acquiring information and knowledge from the surrounding environment, and memory is the retention and storage of information that can be recalled (Bailey & Kandel, 1993).

Two independent types of memory are formed which utilise different systems. Short-term memory is formed via covalent modifications of pre-existing proteins which facilitate transient alterations in the synapse including increased neurotransmitter release and increased clustering of ion channels. This type of memory results in a transient increase in synaptic strength, i.e. an increase in the size of the post-synaptic response following activation and lasts between a few minutes to an hour. Long-term memory is retained for a longer period of time and requires synthesis of new proteins to form new synaptic connections, whereas short-term memory is protein synthesis independent (Alberini, 2011; Guan et al., 2002; Kandel et al., 2014; Kennedy, 2013).

The formation of long-term memory requires expression of genes that encode proteins involved in rearrangement of the actin cytoskeleton to enable the growth of synapses as well as other plasticity-related genes (Lamprecht & LeDoux, 2004). There are approximately 100,000 synapses per neuron, albeit only a small subset of these undergo synaptic plasticity when a memory is formed (Halassa et al., 2007). Further research is therefore required to understand how gene expression is regulated during memory formation and how signals are sent to and from specific synapses for appropriate synaptic growth.

1.3 *Drosophila* as a model system for neuroscientific research

The use of the small model organism *Drosophila melanogaster* is ideal for molecular dissection of memory processes due to the abundance of tools that have been developed for genetic manipulation in order to alter the expression of a specific gene (Brand & Perrimon, 1993; Dukas, 2008; McGuire et al., 2004) to activate or suppress specific neuronal pathways to determine the effect on learning and memory (Margulies et al., 2005). In addition, 75% of genes that have been implicated in human genetic disorders

are conserved in *Drosophila* (Lloyd & Taylor, 2010; Pandey & Nichols, 2011; Reiter et al., 2001).

Behavioural assays have also been developed to evaluate learning and memory in a quantitative manner, for example, the courtship suppression assay. This assay utilises the associative learning of a male fly following rejection from a non-receptive female fly. Following the learned rejection, the male fly is then placed with a new non-receptive female where his courting abilities are monitored. If the memory of the male is intact, he remembers the rejection he was shown during training and will display reduced courtship behaviour towards the unresponsive mated female (Ejima & Griffith, 2011).

The *Drosophila* brain is comprised of approximately 100,000 neurons (Chiang et al., 2011; Huang et al., 2018), and a region of the brain that is of particular focus in memory research is the mushroom body. This region has gained attention as McBride et al. (1999) previously demonstrated that a structurally intact mushroom body is essential for normal memory formation, whereby both chemical ablation and mutations causing defects in the mushroom body structure resulted in impairments in short and long-term memory formation.

1.3.1 The mushroom body

The *Drosophila* mushroom body is a bilateral structure which was compared to the cerebral cortex in vertebrates when it was initially identified by Félix Dujardin in 1850. The mushroom body receives input from olfactory projection neurons which sense odorants. The axons of these olfactory projection neurons synapse with the dendrites of Kenyon cells, which are the intrinsic neurons of the mushroom body (Turner et al., 2008). There are approximately 2,500 Kenyon cells which cluster their cell bodies at the posterior dorsal region of the brain and extend their dendrites anteriorly into the calyx. The Kenyon cell axons are then bundled to form the ventrally projecting peduncle which then bifurcates into vertical and medial lobes (Technau & Heisenberg, 1982) (Figure 1.2).

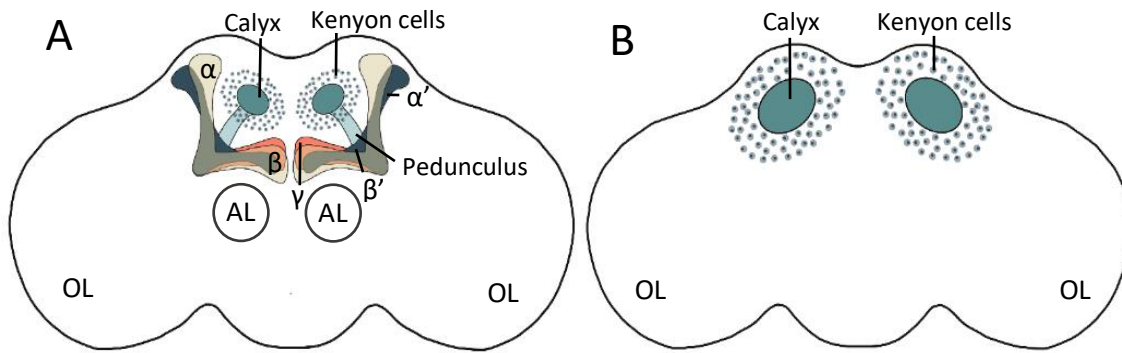


Figure 1.2. Schematic depiction of the *Drosophila* brain. (A) Anterior depiction of the *Drosophila* brain showing the Kenyon cell bodies extending their axons through the ventrally projecting pedunculus where these axons then bifurcate to form the distinct α/α' vertical lobes and β/β' and γ medial lobes. (B) Posterior depiction of the *Drosophila* brain showing the organisation of the Kenyon cell bodies which extend their dendrites anteriorly into the calyx. Abbreviations: AL = antennal lobe, OL = optic lobe. *Original artwork created with reference to Lee et al. (1999), Schwartz (2016), and Technau and Heisenberg (1982).*

There are three Kenyon cell subtypes which differentiate sequentially throughout larval and pupae development. The first population of Kenyon cells to be born are the γ neurons, which form between the initial larval and the mid-third instar larval stages, where axons are bundled to form the medial γ lobes. The α'/β' neurons are then formed between the mid-third instar larval stage and pupal formation before lastly the α/β neurons are formed following pupation. The α/α' axons bundle together to form vertical lobe structures, while the β/β' axons bundle to form additional medial lobes (Lee et al., 1999). These axonal bundles create the L-shape characteristic of the *Drosophila* mushroom body.

The Kenyon cells are also innervated by extrinsic modulatory neurons, which includes several types of dopaminergic neurons, the activity of which is critical for normal memory formation (Ito et al., 1998; Kim et al., 2007).

1.3.2 The *Drosophila* compound eye

The *Drosophila* compound eye is also a valuable model system for neuroscientific research where neurodevelopmental and neurodegenerative abnormalities can be easily visualised as perturbations in ommatidial patterning and these phenotypes can be semi-quantitatively assessed. Furthermore, photoreceptors are specialised neurons, and the molecular pathways that occur within photoreceptors are likely to be conserved in other

neuronal populations. The compound eye is comprised of between 700 and 800 neatly aligned hexagonal ommatidia with evenly dispersed mechanosensory bristles. Each wild-type ommatidium is composed of eight rhabdomeric (R) photoreceptor cells (R1-8), two primary, six secondary and three tertiary pigmentation cells as well as four cone cells that secrete lens matter. Differentiation in the ommatidial cells occurs in the posterior of the eye imaginal discs (Freeman, 1997). The morphogenetic furrow sweeps anteriorly across the imaginal discs leaving a wake of differentiated ommatidial cells (Ready et al., 1976). The eight photoreceptor cells differentiate in a specific order, R8 is first to differentiate posterior to the furrow before R2 and R5, followed by R3 and R4, then R1 and R6, and lastly R7. (Freeman, 1996; Tomlinson & Ready, 1987). Next to form are the cone cells and pigmentation cells which are configured during the second mitotic wave a few rows posterior to the morphogenetic furrow (Ready et al., 1976). The development and differentiation of the R7 photoreceptor is the most well-characterised due to analysis of the *sevenless* (*sev*) gene. A fly with a background devoid of *sev* resulted in progeny lacking the formation of the R7 photoreceptor while the rest of the eye developed normally (Campos-Ortega et al., 1979; Harris et al., 1976). *Sev* was shown to drive R7 differentiation, however *sev* was not sufficient for R7 formation, nor is it involved in determining the identity of the cell (Freeman, 1997).

A single ommatidium shares three interommatidial mechanosensory bristles with its neighbouring ommatidia (Kumar, 2012). The organisation of the ommatidia and bristles is invariant amongst wildtype flies and disruption, or disorganisation of these features is easily observable as a “rough eye” phenotype, which can be semi-quantitatively scored through analysis of light micrographs or scanning electron micrographs.

Analysis of the rough eye phenotype is a common method used to determine whether two genes interact genetically (Figure 1.3). A genetic interaction occurs when two or more genes act in the same molecular pathway. It is suggested that if the resulting phenotype from the combination of two genetic mutations is more severe than the additive effect of each mutation individually, synergy is occurring (Perez-Perez et al., 2009). A genetic interaction suggests a functional relationship between the two genes; however, it does not provide evidence as to whether the protein products interact physically. If a genetic interaction is identified between two genes, then further analysis, such as investigation of their expression patterns, subcellular distribution or binding partners can be carried out in order to further understand how these genes act together in a particular cellular process.

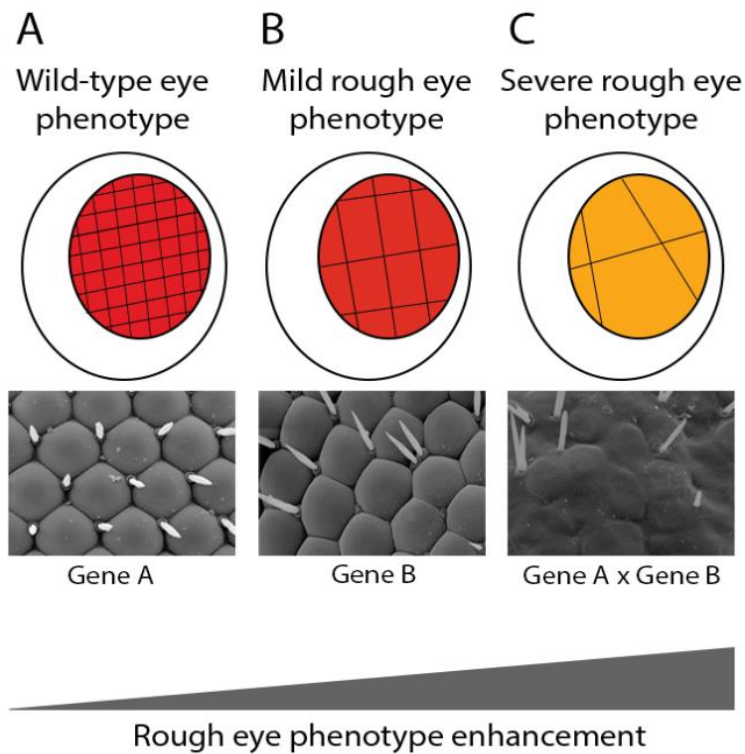


Figure 1.3. Rough eye phenotype enhancement screen. This is a genetic eye screen that is performed on the *Drosophila* compound eye to identify a genetic interaction. (A) No change in phenotype was observed when the expression level of gene A is altered in the eye (eg, by overexpression, RNAi knockdown or mutation). (B) A mild rough eye phenotype is observed when expression of gene B is altered, resulting in mild ommatidia disorganisation. (C) Alteration in expression of genes A and B result in a severe rough eye phenotype where fusion and severe disorganisation is observed. The resulting phenotype is more severe than the additive effect of each phenotype associated with gene A and gene B individually, therefore, this is indicative of a synergistic interaction, meaning that these genes are involved in the same genetic pathway. *Figure from Schwartz (2016), reproduced with permission.*

1.3.3 The *Drosophila* visual system

As rearrangement and growth of the actin cytoskeleton at dendritic spines is required for both neuronal morphogenesis and memory formation (Borczyk et al., 2019), it would be ideal to assess the impact of alterations in expression of candidate memory genes on dendritic growth. The morphology of dendrites differs greatly among neuronal subtypes, dependent on location and function. Dendritic arbours can range from singular thin fibres to large intricate complexes of dendritic spine-like protrusions (Cline, 2001; Libersat & Duch, 2004).

The Kenyon cells of the mushroom body are an ideal model system when looking at abnormalities of the brain as the mushroom body is a prominent structure and defects in

development of the mushroom body lobes (bundled axons) are relatively simple to visualise and score. Kenyon cells also contain dendritic arbours; however, these are small and appear to be more variable (Zhu et al., 2003), making them difficult to study.

In contrast to the Kenyon cells, the visual system contains giant dendritic arbours that develop in a stereotypical fashion and have been well-characterised. Flying insects rely heavily on vision and these visual inputs are largely carried out by giant neurons in the lobula plate of the lobula complex (Dvorak et al., 1975). The lobula plate of a common housefly contains two systems of giant neurons, namely the horizontal and vertical systems. The horizontal system is comprised of three giant neurons, whereas the vertical system contains nine which span their dendritic arbours across the dorsal-ventral axis of the lobula plate (Scott et al., 2002). In the *Drosophila* optic lobe there is a group of six visual interneurons called lobula plate tangential cells (LPTCs) which are structurally similar to the vertical system neurons seen in the housefly. These LPTCs contain spine-like protrusions that are enriched in actin. This enrichment drives dynamic processes making the spines a site of synaptic contact. (Leiss et al., 2009). The development of these spines can be easily assessed via confocal microscopy, where alterations in branching patterns, number of branches, and spine density can be quantitatively measured (Freymuth & Fitzsimons, 2017). Further morphological analyses have been undertaken to fully characterise the dendritic tracing of each of the six LPTCs using mosaic analysis with a repressible cell marker (MARCM) single cell labelling techniques to allow for independent identification of each neuron (Scott et al., 2002).

1.3.4 Genetic manipulation of *Drosophila*

A favourable feature of *Drosophila* as a model system is its amenability to be genetically manipulated, which allows for analysis of gene function as well as neuronal circuitry. The generation of transgenic flies is a simple and routine procedure and flies can be engineered to express any transgene in almost any tissue. The development of the UAS/GAL4 system for tissue specific regulation of gene expression significantly enhanced the utility of gene manipulation in *Drosophila* tissues by way of its “mix ‘n’ match” system in which any promoter can be paired with any transgene for tissue-specific expression (Brand & Perrimon, 1993).

1.3.4.1 The UAS/GAL4 system

The UAS/GAL4 system is a bipartite system that takes advantage of the yeast transcriptional transactivator GAL4, which binds an upstream activating sequence (UAS). Transgenic flies are generated which carry a construct with the GAL4 gene fused downstream of a tissue-specific enhancer, termed a GAL4 driver. These flies are then crossed with a second line carrying the UAS fused with a downstream target transgene of interest. In the F1 progeny of this cross, GAL4 is expressed and binds to regulatory sites on the UAS to induce expression of the downstream transgene in a specific tissue (Brand & Perrimon, 1993; Fischer et al., 1988) (Figure 1.4). Thousands of GAL4 driver lines that express GAL4 in specific tissues and cell-types are available for purchase from stock centres, thus a transgene can be expressed in a tissue or cell-specific manner simply by crossing a UAS-transgene line to the appropriate GAL4 driver (Jenett et al., 2012). UAS lines have also been developed for expression of many *Drosophila* genes, as well as libraries carrying UAS elements fused to inverted repeats or short hairpin RNA (shRNAs) that target specific *Drosophila* genes for RNA interference (RNAi) mediated knockdown (Dietzl et al., 2007).

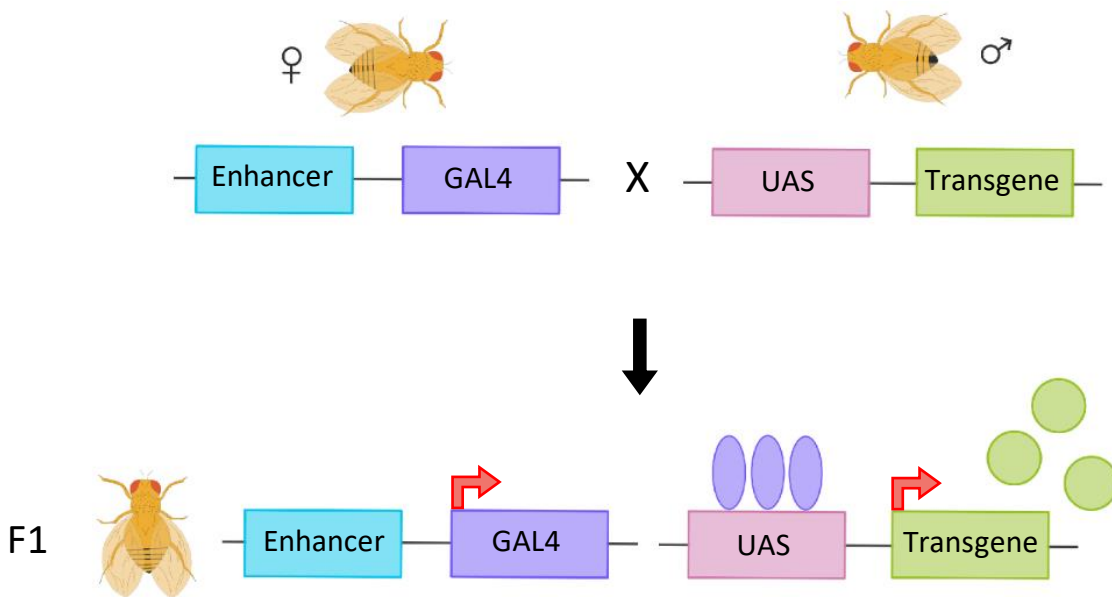


Figure 1.4. Schematic of the UAS/GAL4 bipartite system in *Drosophila*. This system allows for tissue-specific expression of a transgene of interest. Virgin female flies carrying a tissue specific enhancer fused upstream of the transcriptional transactivator GAL4 are crossed to male flies carrying an UAS fused to a transgene of interest. In the F1 progeny, GAL4 binds to regulatory sites on the UAS-inducing tissue-specific expression of the downstream transgene. *Original artwork created with reference to Brand and Perrimon (1993).*

1.3.4.2 The TARGET system

The utility of the UAS/GAL4 system can be further increased through a modified version referred to as the Temporal And Regional Gene Expression Targeting (TARGET) system. This system utilises the GAL80 protein which binds to GAL4 to inactivate it, thus repressing transcription. The TARGET system allows for spatiotemporal gene expression regulation by using a temperature sensitive mutant of GAL80, referred to as GAL80ts which inhibits GAL4 activated transcription at 18°C. When the temperature is raised to 30°C, GAL80ts is inactivated through a conformational change, allowing initiation of GAL4-dependent transcription (McGuire et al., 2004; Suster et al., 2004) (Figure 1.5). The temporal regulation of gene expression is particularly important in the study of memory as many genes involved in molecular pathways of memory are also required for normal brain development, thus, the ability to induce overexpression or knockdown of a gene in the adult brain will avoid any potential confounding developmental effects.

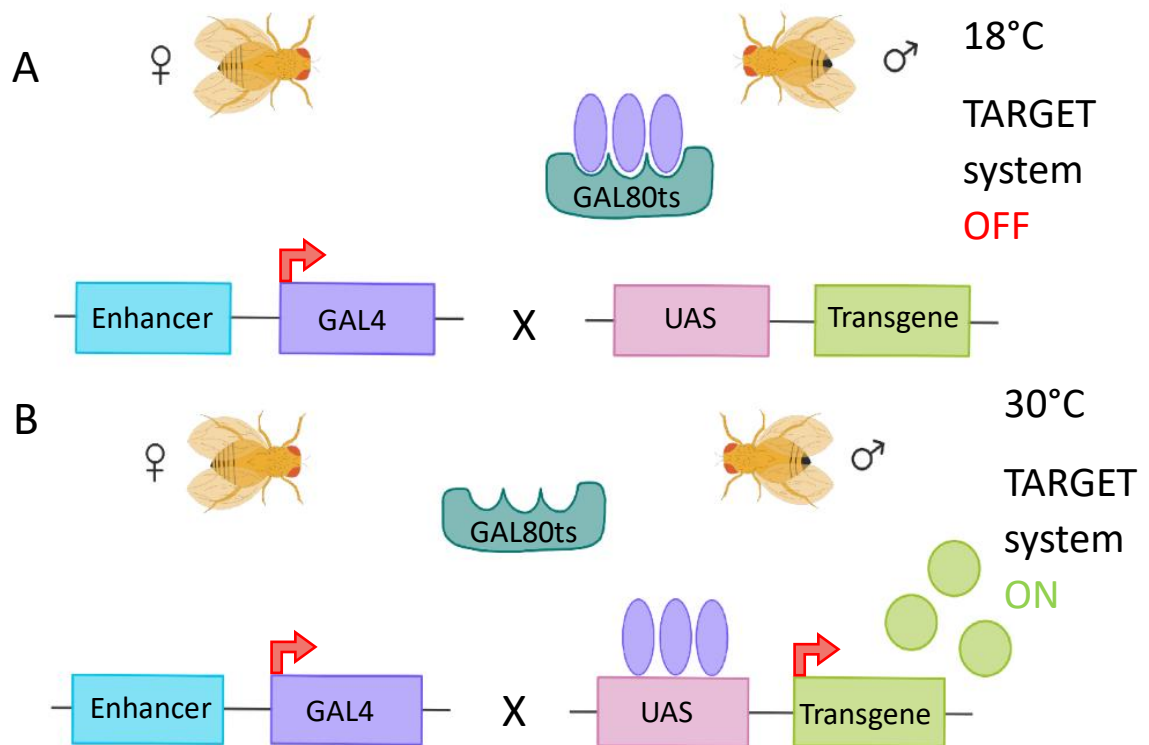


Figure 1.5. The TARGET system in *Drosophila*. (A) At 18°C GAL80ts is active and binds to GAL4 preventing GAL4 from binding to regulatory sites on the UAS and initiating transgene expression. (B) Once the temperature is raised to 30°C, GAL80ts is no longer able to bind GAL4 due to a conformational change, thus GAL4 is now free to bind to regulatory sites on the UAS and initiate downstream transgene expression. *Original artwork created with reference to McGuire et al. (2004).*

1.4 Epigenetic regulators of memory formation

The formation of memories is reliant on precise spatial and temporal regulation of expression of genes required for synaptic plasticity and memory. In the last decade there has been an increased focus on epigenetics and the role that it plays in the regulation of gene expression. Epigenetic regulation refers to the alteration of gene expression without changing the DNA sequence. Instead, epigenetic regulators modify chromatin by the addition of epigenetic marks which results in increased or decreased expression of a specific gene (Jaenisch & Bird, 2003).

Chromatin is a complex of DNA and protein found in the nucleus of eukaryotic cells and is highly structured allowing for compact organisation of DNA inside the nucleus as well as regulation of transcription. Chromatin is comprised of double stranded DNA wrapped 1.67 times around a histone octamer containing two of each of the four core histone proteins (histones H2A, H2B, H3, and H4), creating a nucleosome. Nucleosomes are connected by a short piece of linker DNA creating the characteristic “beads on a string” conformation (Heslop-Harrison & Schwarzacher, 2013; Rattner & Hamkalo, 1978; Verreault, 2000) (Figure 1.6).

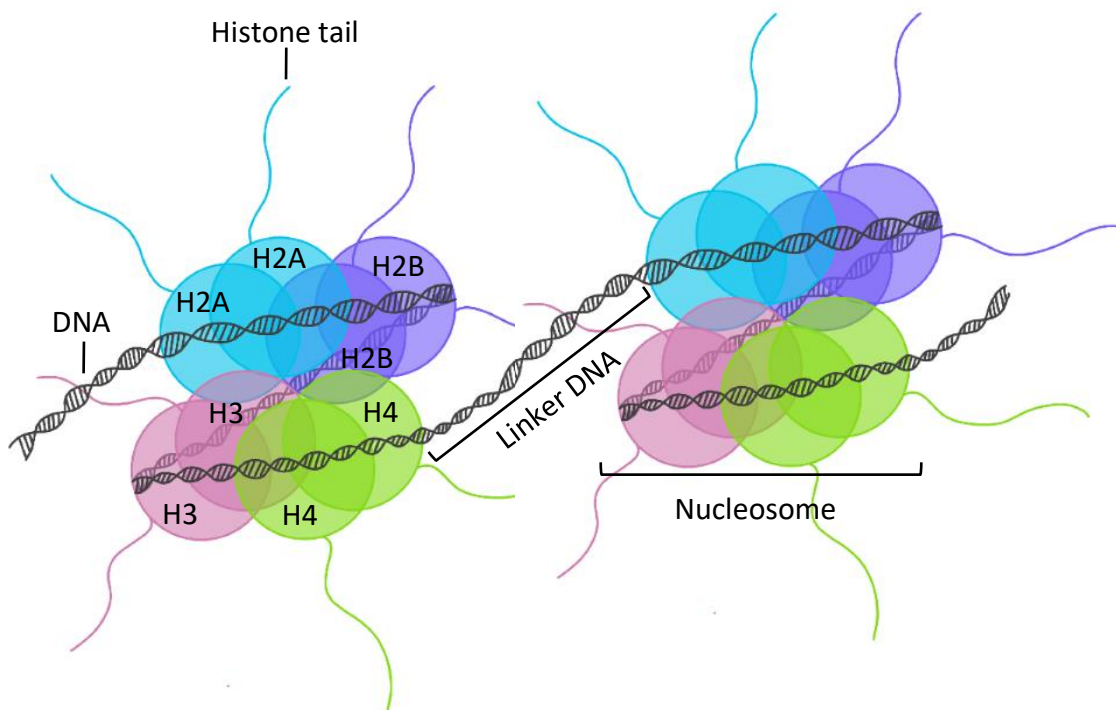


Figure 1.6. Schematic showing the composition of a nucleosome. A single nucleosome consists of eight core histones (H2A, H2B, H3, and H4). Each octamer is then wrapped 1.67 times with double stranded DNA consisting of 146 base pairs (bp) (Richmond & Davey, 2003). A length of linker DNA joins two nucleosomes together to form the classic “beads on a string” (Rattner &

Hamkalo, 1978) chromatin structure. *Original artwork created with reference to Starkman et al. (2012).*

Opposing post-translational modifications to the nucleosome such as acetylation/deacetylation (Sterner & Berger, 2000), methylation/demethylation (Zhang & Reinberg, 2001), and phosphorylation/dephosphorylation (Nowak & Corces, 2004) on core histone tails determine how tightly packed the nucleosomes are by changing the conformation of the histone tails leading to differences in nucleosome packing which in turn establishes the accessibility of the DNA to RNA polymerase and other transcription factors. Histone acetyl transferases (HATs) acetylate N-terminal lysine residues to neutralise their positive charge leading to a weaker interaction between the histone tail and the DNA, resulting in a relaxed chromatin conformation. Histone deacetylases (HDACs) remove these active chromatin marks, thereby condensing chromatin to a point at which transcription factors can no longer access the DNA, therefore, repressing transcription (Cho et al., 2005; Foglietti et al., 2006). Opposing activities of HATs and HDACs modify histone tails of core histones to epigenetically regulate gene expression.

1.4.1 Histone deacetylases

HDACs are a family of enzymes that are best known for their role in transcriptional repression via histone deacetylation. There is however, increasing focus on their roles in both deacetylation of non-histone targets as well as the roles of some HDAC family members that are independent of histone deacetylation (Gaughan et al., 2002; Glozak et al., 2005; Schwartz et al., 2016).

In vertebrates there are eleven HDACs that are separated into four different classes based on their homology to yeast HDACs. Class I is comprised of HDAC1, 2, 3, and 8 which have high deacetylase activity and are primarily localised in the nucleus (Grozingler et al., 1999; Grozingler & Schreiber, 2002; Hildmann et al., 2006; Kao et al., 1999; Somoza et al., 2004). The class II HDACs lack deacetylase activity and are separated into Class IIa and IIb, Class IIa consists of HDAC4, 5, 7, and 9 and Class IIb consists of HDAC6 and 10. Class IIb are primarily localised to the cytoplasm, whereas Class IIa HDACs shuttle between the nucleus and cytoplasm (Bertos et al., 2001; Chawla et al., 2003; Fischle et al., 2001; Grozingler et al., 1999; Grozingler & Schreiber, 2002; Hildmann et al., 2006;

Kao et al., 1999; Schlumm et al., 2013). Class IV contains only HDAC11, which localises to both the cytoplasm and nucleus and is the least well-characterised of all the HDACs. Class I, II and IV HDACs share similarities with yeast HDACs in that they are all zinc (Zn^+) dependent and NAD^+ independent. Lastly, Class III HDACs are Sirtuins which are NAD^+ dependent and Zn^+ independent. Sirtuins 1-7 exhibit their deacetylase activity on a wide range of proteins and are not limited to histone deacetylation (Grozinger & Schreiber, 2002) (Figure 1.7).












Class	Human	Protein structure	Length (aa)	Primary Localisation
I	HDAC1		482	Nucleus
	HDAC2		488	Nucleus
	HDAC3		428	Cytoplasm/ Nucleus
	HDAC8		377	Nucleus
IIa	HDAC4		1084	Cytoplasm/ Nucleus
	HDAC5		1122	Cytoplasm/ Nucleus
	HDAC7		912	Cytoplasm/ Nucleus
	HDAC9		1011	Cytoplasm/ Nucleus
IIb	HDAC6		1215	Cytoplasm
	HDAC10		669	Cytoplasm
IV	HDAC11		347	Nucleus

Figure 1.7. Schematic representations of the domain structures of human HDACs. The catalytic domain is represented in black; serine sites for phosphorylation are highlighted in yellow; the MEF2 binding domain is detailed in green; the zinc finger domain on HDAC6 is shown in blue and the leucine rich region of HDAC10 is shown in purple. Sirtuins 1-7 are not illustrated in this figure. Abbreviations: aa = amino acids. *Original figure created with reference to Morris and Monteggia (2013).*

There are five highly conserved HDACs in *Drosophila*: Rpd3 (Fitzsimons & Scott, 2011; Gregoret et al., 2004; Rundlett et al., 1996) and HDAC3 (Zhu et al., 2008) are homologous to Class I mammalian HDACs. HDAC4 is the sole Class IIa HDAC, HDAC6 is homologous to the human Class IIb HDACs, and HDAC11 is homologous to the Class IV human HDAC11 (Cho et al., 2005; Foglietti et al., 2006).

1.5 HDAC4

HDAC4 contains a number of important regulatory domains that are highly conserved across vertebrates and invertebrates. These include a Myocyte Enhancer Factor-2 (MEF2) binding domain, a nuclear localisation sequence (NLS) and a conserved ankyrin repeat binding domain, all located at the N-terminus (Miska et al., 1999; Wang et al., 2005; Wang & Yang, 2001; Zhao et al., 2005). HDAC4 also contains a nuclear export sequence (NES) and a deacetylase domain at the C-terminus (Wang et al., 1999; Wang & Yang, 2001).

Regulation of the subcellular distribution of HDAC4 occurs via nucleocytoplasmic shuttling in response to synaptic activation. HDAC4 nuclear import requires binding of the transcription factor MEF2 to HDAC4, however, upon binding, the transcriptional activity of MEF2 in the nucleus is inhibited (Chawla et al., 2003; Wang & Yang, 2001). The HDAC4/MEF2 repressive complex is relieved by a calcium/calmodulin dependent kinase (CaMK) that phosphorylates three conserved serine residues on HDAC4 (S246, S467 and S632 of human HDAC4). This phosphorylation creates docking sites on HDAC4 for protein chaperone 14-3-3 to bind to dissociate HDAC4 from MEF2. During this detachment, the nuclear export sequence (NES) located at the C-terminus of HDAC4 is unmasked, resulting in HDAC4 being sequestered into the cytoplasm (Bertos et al., 2001; Chawla et al., 2003; Grozinger & Schreiber, 2000; McKinsey et al., 2006; Z. Wang et al., 2014).

Drosophila HDAC4 shares 57% amino acid identity and 84% sequence similarity with human HDAC4 (Fitzsimons et al., 2013) (Figure 1.8). A key point of difference between human and *Drosophila* HDAC4 is that human HDAC4 has a tyrosine to histidine mutation that renders it catalytically inactive. In contrast, *Drosophila* HDAC4 does not contain this mutation, therefore, retaining its catalytic activity (Lahm et al., 2007;

Mielcarek et al., 2013; Sando et al., 2012). Human HDAC4 can however recruit the deacetylase activity of Class I HDACs to indirectly repress transcription and also repress transcription in a deacetylase-independent manner by binding to and inhibiting the activity of transcription factors such as MEF2 as mentioned above (Lu et al., 2000; Miska et al., 1999; Wang et al., 1999).

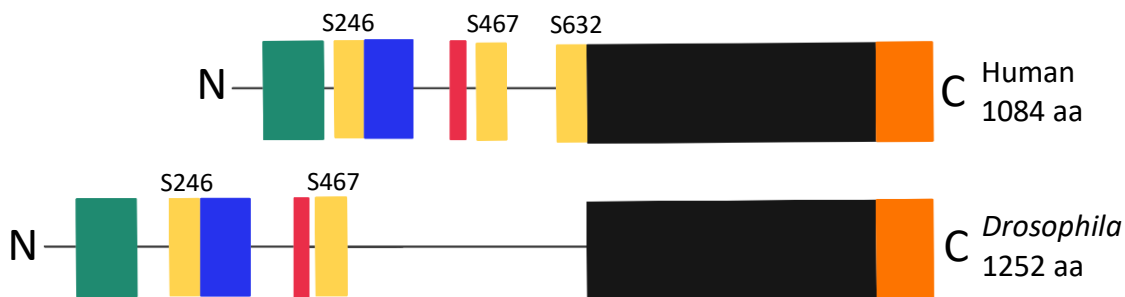


Figure 1.8. Conserved domains of *Drosophila* and human HDAC4. A single isoform of each HDAC4 protein, (Human HDAC4 GenBank accession NP_006028 and *Drosophila* HDAC4, isoform D, GenBank accession NP_572868). The MEF2 binding domain is highlighted in green; 14-3-3 binding sites are detailed in yellow; the nuclear localisation sequence is highlighted in blue, the ankyrin repeat binding domain is shown in red; the deacetylase domain is seen in black and the nuclear export sequence is highlighted in orange. Abbreviations: aa = amino acids. *Original artwork created with reference to Fitzsimons et al. (2013).*

There is a wide distribution of HDAC4 in the vertebrate nervous system and it has been seen that the rodent brain is enriched in HDAC4 mRNA (Grozinger et al., 1999; Wang et al., 1999). Within the mouse brain HDAC4 is predominantly localised to the cytoplasm, which includes the axons and dendrites in most brain regions, however, this varies with respect to nuclear localisation. For example, immunostaining for HDAC4 in the hippocampus revealed that HDAC4 was present in the majority of neuronal nuclei as well as in the cytoplasm. However, in specific cell populations like the dentate granule cells, HDAC4 was absent from nuclei. HDAC4 has also been observed at synapses, but because it dynamically shuttles between the nucleus and cytoplasm in a calcium dependent manner, the level of HDAC4 at specific synapses may also be dynamic leading to inconsistent visualisation (Darcy et al., 2010).

Drosophila HDAC4 is expressed throughout the brain including the mushroom body, where it localises to the axons that bundle to form the mushroom body lobes as well as the calyx in which the Kenyon cell dendrites project into (Technau & Heisenberg, 1982). Similarly to the pattern observed in the mouse brain, nuclear localisation of HDAC4

occurred in only a subset of Kenyon cells containing nuclear puncta (Fitzsimons et al., 2013), indicating that regulation of the subcellular distribution of HDAC4 differs among populations of neurons.

1.5.1 HDAC4 and neurodevelopmental and neurodegenerative disease

Over recent years data from numerous studies have implicated the dysregulation of HDAC4 expression and/or subcellular distribution in several neurodevelopmental and neurodegenerative disorders. A deletion of the human chromosomal region 2q37, in which *HDAC4* resides, results in 2q37 deletion syndrome (previously referred to as Brachydactyly mental retardation syndrome), with clinical features including developmental delay, behavioural issues, autism spectrum disorder and a phenotypically severe facial dysmorphism (Morris et al., 2012; Williams et al., 2010). Haploinsufficiency of *HDAC4* is thought to be the underlying genetic cause (Villavicencio-Lorini et al., 2013; Williams et al., 2010).

Dysregulation of nucleocytoplasmic shuttling resulting in increased nuclear accumulation of HDAC4 has also been associated with Alzheimer's disease (Wu et al., 2016), Parkinson's disease (Wu et al., 2017) and ataxia telangiectasia (Li et al., 2012). Alzheimer's disease is a progressive neurodegenerative disease that is the most common form of dementia (Neugroschl & Wang, 2011). It is associated with the presence of β -amyloid oligomers, plaques and neurofibrillary tangles in the cerebral cortex, resulting in synaptic loss and neuronal death (Alonso et al., 1996; Shen et al., 2016). An analysis of the brains of mice expressing amyloid precursor protein (APP), the proteolysis of which produces β -amyloid, and post-mortem brains from individuals with Alzheimer's disease revealed that the level of accumulation of HDAC4 in the nucleus directly correlated with the severity and onset of the disease in both cases (Herrup et al., 2013; Shen et al., 2016).

Alpha-synuclein (α -syn) deposits in neurons have been associated with Lewy body disease which is a family of disorders that include Parkinson's disease. α -syn is seen to play a central role in Parkinson's disease as point mutations of the *α -syn* gene have been associated with familial Parkinson's (Polymeropoulos et al., 1997). Model systems including transgenic mice and *Drosophila* have been utilised to model these mutations which have resulted in phenotypes which share similarities with features associated with Parkinson's disease (Masliah et al., 2005). In a mouse model of Parkinson's disease,

overexpression of the A53T mutant of α -syn followed by treatment with the neurotoxin 1-methyl-4-phenylpyridinium (MPP⁺) resulted in nuclear accumulation of HDAC4 in dopaminergic neurons (Wu et al., 2017).

Furthermore, HDAC4 has been associated with ataxia telangiectasia which is a neurodegenerative disease caused by a mutation of the *Atm* gene. In a mouse *Atm*^{-/-} model, neurodegeneration was associated with nuclear accumulation of HDAC4, which was due to hypophosphorylation. In contrast, expression of cytoplasmic HDAC4 improved the *Atm*^{-/-} phenotype suggesting a neuroprotective role of cytoplasmic HDAC4 (Li et al., 2012).

These disorders are all associated with impairments in cognitive function, and as HDAC4 is also required for synaptic plasticity and memory formation in animal models (Fitzsimons et al., 2013; Kim et al., 2012; Sando et al., 2012) this suggests that dysregulation of HDAC4 could be involved in the cognitive deficits associated with these disorders.

1.5.2 HDAC4 and memory

Kim et al. (2012) generated mice with a brain-specific conditional knockout of *HDAC4* (thereby avoiding skeletal deformities that had been observed in *HDAC4* null mice) and observed that these mice displayed impaired spatial memory (Kim et al., 2012). Similarly, in *Drosophila*, RNAi knockdown of *HDAC4* in the mushroom body prevented long-term memory formation but not short-term memory or learning, which are protein synthesis independent (Fitzsimons et al., 2013). Together these studies demonstrate that HDAC4 is essential for long-term memory formation. However, it has also been observed that increased levels of HDAC4 also impairs memory formation (Fitzsimons et al., 2013). Notably, the expression of a nuclear-restricted HDAC4 mutant in the mouse brain prevented spatial memory formation. This mutant was lacking the entire C-terminal domain of HDAC4, which includes the deacetylase domain, indicating that this effect is independent of deacetylation (Sando et al., 2012). In *Drosophila*, overexpression of *HDAC4* in the mushroom body impairs long-term memory formation, however, short-term memory was unaffected. Similarly to the observations in mice, an *HDAC4* mutant carrying an amino acid substitution in the active site rendering the deacetylase domain

catalytically inactive, also impaired long-term memory acquisition (Fitzsimons et al., 2013).

HDAC4 mutants with altered subcellular distribution were then generated to further investigate whether the impairments in long-term memory were due to the nuclear or cytoplasmic pools of HDAC4. Expression of a nuclear-restricted mutant (*3SA*) in the adult brain via the TARGET system significantly reduced the formation of long-term memory compared to wild-type, whereas expression of a cytoplasmically-restricted mutant (*LI75A*) had no effect (Main, 2019). The effect of nuclear-restricted HDAC4 on development of the mushroom body was also investigated where this nuclear accumulation induced a range of mushroom body defects including impaired axon elongation and termination. In comparison, expression of *LI75A* resulted in few mushroom body defects, with the majority of brains appearing wild-type (Main, 2019). In eye development, expression of *3SA* resulted in a severe rough eye phenotype with a significant loss of pigmentation, whereas *LI75A* resulted in a wild-type array of ommatidia and normal pigmentation (Main, 2019). Taken together, the data from these studies indicate that memory and neurodevelopmental impairments in *Drosophila* are attributed to a nuclear accumulation of HDAC4.

To investigate transcriptional changes associated with the *Drosophila HDAC4* overexpression-induced impairments, RNA sequencing (RNA-seq) was performed on the heads of brains in which *HDAC4* was overexpressed. Global gene expression changes were not observed as a total of only 26 genes were differentially expressed (Schwartz et al., 2016). Similarly, when *hHDAC4 3SA* was overexpressed in the *Drosophila* brain, a mere 28 genes were differentially regulated (Main, 2019). Together, these data suggest that HDAC4 has minimal effect on transcription and is likely to also act through non-transcriptional mechanisms.

A subsequent investigation into genes which genetically interact with *HDAC4* was then carried out by Schwartz et al. (2016) to identify genes in the same molecular pathway as *HDAC4* via a rough eye phenotype enhancer screen (Section 1.3.2). Overexpression of *HDAC4* in photoreceptors produced a mild rough eye phenotype, thus regulators of *HDAC4* can be identified as genes that enhance or suppress the rough eye phenotype when their expression is altered in the presence of *HDAC4* overexpression. One hundred and twenty-five RNAi lines were screened to find target genes that had minimal

phenotypes when individually knocked down, but when combined with *HDAC4* overexpression resulted in an enhanced rough eye phenotype, indicative of a genetic interaction. From this screen, the cytoskeletal regulator Ankyrin2 was identified and selected for further investigation into the nature of its interaction with *HDAC4* and whether this interaction is important in neuronal development and/or memory formation (Schwartz, 2016).

1.6 Ankyrin proteins

Ankyrins are adapter proteins that aid in the binding of integral transmembrane proteins to the underlying spectrin-actin cytoskeleton (Cunha & Mohler, 2009). Since they were first documented in erythrocytes, three vertebrate ankyrin genes have been identified. *ANKYRIN1* is localised to neurons and a range of tissues including brain, heart and skeletal muscle (Birkenmeier et al., 1993; Gallagher et al., 1997; Lambert et al., 1990). *ANKYRIN2* is also expressed in a variety of tissues including brain, heart, kidney, lung and skeletal muscle (Cunha & Mohler, 2009). *ANKYRIN3* is expressed in heart, kidney, lung and skeletal muscle tissues as well as unmyelinated neurons in the brain where it is an essential component in the assembly of the axon initial segment (Cunha & Mohler, 2009; Devarajan et al., 1996; Kordeli et al., 1995; Thevananther et al., 1998).

The structure of a canonical ankyrin is highly conserved among species. An N-terminal membrane binding domain contains 24 ANK-repeats, where each unit contains a 33 amino acid motif, comprised of two alpha helices connected via a loop region (Mosavi et al., 2002). This ANK-repeat region is then followed by a spectrin binding domain with an inserted ZU5 domain aiding in spectrin based protein interactions, a death domain, and a C-terminal variable regulatory region (C. Wang et al., 2014) (Figure 1.9).

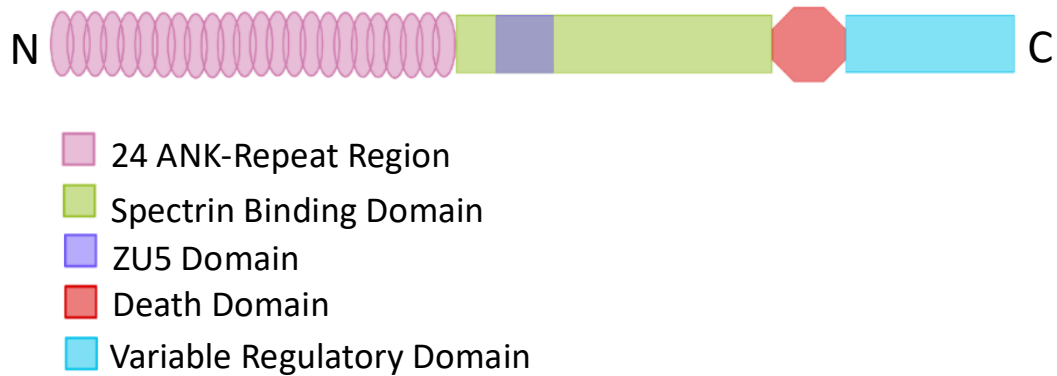


Figure 1.9. Schematic of a canonical long ankyrin isoform. Ankyrins contain an N-terminal membrane binding domain comprised of 24 ANK-repeat units. This is followed by a spectrin binding domain with a ZU5 domain inserted to aid in spectrin binding, followed by a death domain and a C-terminal variable regulatory domain. *Original artwork created with reference to Schwartz (2016).*

Ankyrins play a pivotal role in providing the cell with synaptic and structural stability by regulating the distribution and organisation of integral transmembrane proteins at the spectrin-actin cytoskeleton. Such proteins include cell adhesion molecules; L1-CaMs, neurofascin and neuroglian, clathrin and tubulin, and anion exchangers and ion channels; Na⁺/K⁺ ATPase and H⁺/K⁺ ATPase (Mohler et al., 2002).

When a dendrite receives synaptic input from neighbouring cells, this signal is then propagated to the cell body of the neuron, where an action potential is initiated at the axon initial segment. This signal is then propagated down the axon to the axon terminal. In the majority of vertebrate neurons, the axon initial segment is located at the proximal axons where the polarity of neurons is sustained by ankyrins. At the axon initial segment, ankyrins act as scaffolding proteins in order to maintain a separation between the somatodendritic region (where the cell body and dendrites reside) and the axonal compartment (consisting of the axon and axon initial segment) (Garrido et al., 2003; Pan et al., 2006; Zhou et al., 1998).

In both vertebrates and invertebrates, HDAC4 contains an ankyrin repeat binding domain which mediates protein-protein interactions (McKinsey et al., 2006; Wang et al., 2005). Within the HDAC4 ankyrin repeat binding domain region there is a highly conserved leucine and proline rich region known as the PxLPxI/L motif that is found in a diverse number of binding proteins, including but not limited to HDAC4 and HDAC5 (Xu et al., 2012). The mammalian ankyrin repeat-containing proteins, Ankyrin repeat family A

protein 2 (ANKRA2) and Regulatory factor X associated ankyrin-containing protein (RFXANK) bind to HDAC4 via this highly conserved PxLPxI/L motif (Figure 1.10). The ankyrin repeat region of both proteins share 62% sequence identity and crystal structures have demonstrated that the middle three ankyrin repeats of ANKRA2 bind to specific residues within the PxLPxI/L motif on HDAC4 in a sequence specific lock and key manner. RFXANK however, binds with a much lower affinity. A modification in the PxLPxI/L motif where a serine within the sequence was phosphorylated, resulted in a reduction in the binding affinity of ANKRA2 with HDAC4, consequently this also produced a new docking site for 14-3-3 proteins, sequestering HDAC4 into the cytoplasm (Xu et al., 2012).

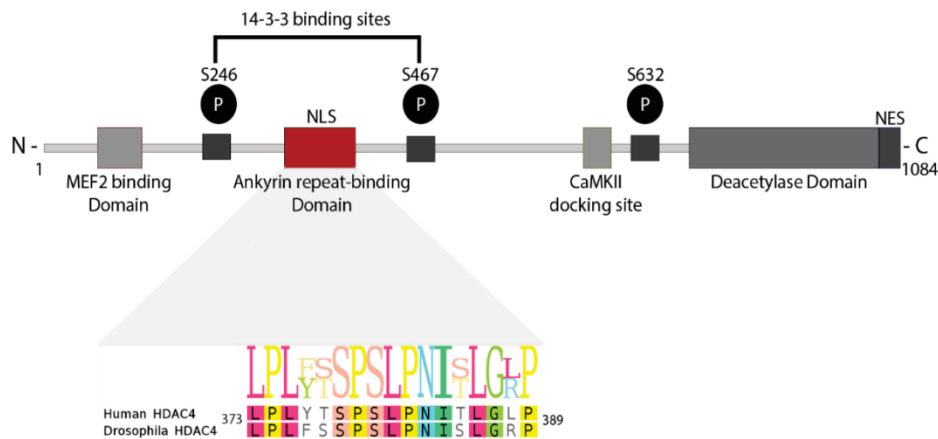


Figure 1.10. The conservation of the ankyrin repeat binding domain of HDAC4. Human and *Drosophila* HDAC4 contain a highly conserved ankyrin repeat binding domain with a 76.5% identity. Figure from Schwartz (2016), reproduced with permission.

1.6.1 Mammalian ANKYRIN-G

Human *ANKYRIN3* (*ANK3*) is expressed throughout the nervous system and encodes the protein ANKYRIN-G (ANK-G) which is a necessary component in the assembly of the axon initial segment, the region that splits the somatodendritic compartment from the axonal compartment in the neuron (Garrido et al., 2003; Pan et al., 2006; Zhou et al., 1998). The long isoforms of ANK-G have been characterised to aid in stabilising the axon initial segment scaffold which spans from the plasma membrane to microtubules (Leterrier et al., 2017). ANK-G recruits and anchors ion channels, which are important in maintaining cell polarity and L1-cell adhesion molecules (L1-CaMs) to the axon initial segment (Huang & Rasband, 2018). This accumulation of membrane bound proteins creates a diffusion barrier separating the somatodendritic compartment from the axonal

compartment, therefore when ANK-G is lost, this recruitment and stabilisation is also lost (Zhou et al., 1998), making ANK-G the master regulator of the axon initial segment.

Recently it has been observed that *ANK3* is implicated in intellectual disability, where a homozygous truncating frameshift mutation affecting only the long isoform of *ANK3* was identified as the first case of a familial mutation of *ANK3*. Along with intellectual disability, this mutation was also associated with epilepsy, hyperactivity, and behavioural issues (Iqbal et al., 2013). *ANK3* has also been implicated in bipolar disorder (Tesli et al., 2011), autism spectrum disorder (Bi et al., 2012), attention deficit hyperactivity disorder (ADHD) (Iqbal et al., 2013) and *ANK3* SNPs have been associated with schizophrenia (Athanasu et al., 2010; Yuan et al., 2012) as well as late onset Alzheimer's disease (Morgan et al., 2008).

The closest homologues to ANK-G in *Drosophila* are Ankyrin1 (Ank1) and Ankyrin2 (Ank2) (Iqbal et al., 2013). The role of Ank1 in *Drosophila* courtship memory was recently investigated and it was found that reducing the amount of Ank1 had no impact on the formation of long-term courtship memory (Schwartz, 2016). Human ANK-G and *Drosophila* Ank2 share 57% amino acid similarity across the entire protein and 71.2% identity over the ankyrin repeat region (Schwartz, 2016).

1.6.2 *Drosophila* Ankyrin2

Ank2 is encoded by the *Dank2* gene from which a large number of *Ank2* splice isoforms are transcribed. The protein products of these isoforms vary in subcellular distribution and functionality. Ank2-S denotes the short isoforms of Ank2 which localise to the cell soma, Ank2-M denotes the medium sized isoform of Ank2 which localises to axons, Ank2-L denotes the long isoform of Ank2 which also localises to axons, and Ank2-XL denotes the extra-long isoform of Ank2 which localises to neuronal cell bodies (Appendix 6.4). The long and extra-long isoforms of Ank2 are required for synaptic plasticity and maintenance whereas the short isoforms are not (Koch et al., 2008). All Ank2 isoforms contain the highly conserved N-terminal ankyrin repeat domain which has recently been demonstrated to control the presynaptic localisation of Ank2. This localisation is important as Ank2 is an essential regulator of synaptic stability in *Drosophila* where it functions by organising the subcellular distribution of transmembrane binding proteins (Weber et al., 2019).

In *Drosophila* the distribution and localisation of Ank2 has been established from embryogenesis through to adulthood. In the embryonic nervous system, the expression of all isoforms of Ank2 are generally restricted to the embryonic peripheral neurons and central neurons. Within the central and peripheral embryonic nervous system, the long isoform of Ank2 is localised specifically to the nerve tracts which are found in the axonal extensions, whereas the short isoforms of Ank2 are localised to the cell bodies (Hortsch et al., 2002). In the adult fly, Ank2 is primarily expressed in the brain, where it localises specifically to the axonal tracts and bundled axons which form the mushroom body lobes, as well as the optic and antennal lobes (Schwartz, 2016).

To date, research in *Drosophila* has focused on the role that Ank2 plays in the larval neuromuscular junction (Koch et al., 2008). The neuromuscular junction is the synapse between a neuron and muscle cell, important for transmitting signals to the muscle cell (Cohen et al., 2007). Mutation of Ank2-L results in disassembly and retraction of the neuromuscular junction due to a lack of protein recruitment, stability and synaptic plasticity, resulting in morphological defects which disrupt neuron excitability (Pielage et al., 2008). A total loss of Ank2 results in synaptic bouton withdrawal and dissolution of the synaptic microtubule cytoskeleton resulting in failure of microtubule binding to associated proteins, and extension to synaptic boutons (Koch et al., 2008). A deletion of part of the ankyrin repeat domain (repeats 7-24) resulted in defects in Ank2-L localisation at the neuromuscular junction where Ank2-L was no longer present in the presynaptic terminal (Weber et al., 2019).

Additional studies have also investigated an interaction between Ank2 and the *Drosophila* L1-CaM homologue Neuroglian and another cytoskeletal regulator Moesin in the mushroom body of axons, specifically in the axon initial segment (Siegenthaler et al., 2015).

In *Drosophila* there is an axon initial segment-like domain which resides in the γ -lobe of the mushroom body (Trunova et al., 2011). As described in section 1.6.1 a loss of ANK-G in the mammalian system leads to issues at the axon initial segment. If there is conservation between mammalian ANK-G and *Drosophila* Ank2 it is proposed that a loss of Ank2 at the axon initial segment-like domain would cause dysregulation and a lack of protein recruitment. This could lead to issues involving cell polarity which could have a destructive effect on action potential firing and axonal protein transport. In larval brains,

a direct *in vivo* interaction between Ank2 and Neuroglian has been established via co-immunoprecipitation (Enneking et al., 2013) as well as a yeast-two-hybrid *in vitro* investigation (Bouley et al., 2000). However, in embryos it was seen that Neuroglian was transported and localised to axons in which Ank2 was lacking, suggesting that in *Drosophila* although there is a direct interaction between the two proteins, Ank2 does not recruit Neuroglian during embryogenesis (Hortsch et al., 2002). It has also been characterised that although Neuroglian is an important binding partner for Ank2 stability and maintenance, it is seen that the localisation of Ank2 is not dependent on Neuroglian (Bouley et al., 2000).

Similarly, *Drosophila* synaptic localisation also relies on the complex formation between Ankyrins and L1-CaMs, as this complex lays down a foundation for the assembly of other binding partners and voltage-gated channels. It has been observed that a deletion of ANK-repeats 13-18 resulted in a large reduction of Ank2 localisation in axons and at the synapse (Weber et al., 2019). The ankyrin repeat domain does not only regulate the targeting and localisation of the ankyrin itself, but also has a role in mediating the localisation of other isoforms of Ank2. It was seen that mutations resulting in a deficiency of the ankyrin repeat domain on Ank2-L resulted in a lack of Ank2-XL targeting at the presynaptic terminal, and vice versa. Therefore, there is a co-dependent relationship between the ankyrin repeat domain of one Ank2 isoform and the localisation of a second Ank2 isoform (Stephan et al., 2015).

Following identification of a genetic interaction between *HDAC4* and *Ank2*, Schwartz et al. (2016) investigated the requirement for Ank2 in development of the mushroom body and in long-term memory formation. RNAi knockdown of *Ank2* in the developing mushroom body resulted in similar defects to those observed for *HDAC4* overexpression including defects in axon elongation and termination as well as guidance deficits. *Ank2* is also specifically required for normal long-term memory formation, as its knockdown in the adult brain resulted in impairments to long-term memory with no effect on short-term memory in the courtship suppression model of memory (Schwartz, 2016). The specific role of Ank2 in long-term memory formation is not yet known.

1.7 A relationship between HDAC4 and Ank2

As described in section 1.5.2, in an attempt to identify the pathway through which HDAC4 regulates memory formation, *Ank2* was identified as a gene which interacted genetically with *HDAC4*. This gene was then selected for further study due to its expression in the mushroom body as well as the presence of an ankyrin repeat binding domain on HDAC4. If these two proteins interact physically, it could then be hypothesised that HDAC4 could influence memory formation by somehow modulating Ank2 activity at the spectrin-actin cytoskeleton. This interaction was further supported through evidence that overexpression of *HDAC4* and knockdown of *Ank2* both result in similar phenotypes including impaired long-term memory formation and developmental deficits in axon elongation and termination in the mushroom body (Fitzsimons et al., 2013; Main, 2019; Schwartz, 2016).

Given that HDAC4 contains an ankyrin repeat binding domain, it is hypothesised that HDAC4 and Ank2 interact physically to regulate the formation of long-term memory and neuronal development, however it has not yet been investigated whether HDAC4 binds physically to Ank2.

The aim of this study is to further investigate the nature of the proposed interaction between HDAC4 and Ank2 and its importance in normal neuronal development in the brain. This will involve firstly investigating whether HDAC4 and Ank2 interact physically via co-immunoprecipitation. Other potential indirect interactions will also be investigated, including whether Ank2 regulates the subcellular distribution of HDAC4. The rationale for this approach is that increased nuclear HDAC4 results in deficits in memory and neuronal development, thus if Ank2 were to bind HDAC4 and tether it outside of the nucleus, a reduction of Ank2 could result in increased nuclear HDAC4 and thus a more severe phenotype. The nature of the genetic interaction in the *Drosophila* eye will also be investigated to determine whether it is through nuclear localisation of HDAC4 and if the interaction is dependent on the presence of the ankyrin repeat binding domain of HDAC4. Finally, it will be investigated whether the genetic interaction between *HDAC4* and *Ank2* is also necessary for normal dendrite and axon morphogenesis in the brain. The specific objectives are as follows:

1. To determine whether there is a physical interaction between HDAC4 and Ankyrin2 in the *Drosophila* brain.
2. To examine whether HDAC4 regulates the expression of *Ank2*.
3. To determine whether *Ank2* regulates the expression and/or subcellular distribution of HDAC4.
4. To investigate the nature of the genetic interaction between *HDAC4* and *Ank2* in the *Drosophila* compound eye.
5. To establish whether a genetic interaction between *HDAC4* and *Ank2* is required for dendrite morphogenesis in the *Drosophila* visual system.
6. To establish whether a genetic interaction between *HDAC4* and *Ank2* is required for axon morphogenesis in the mushroom body.

2 Materials and Methods

2.1 *Drosophila melanogaster* fly strains

The *Drosophila* fly strains that were used in this study are listed in Appendix 6.1. For consistency and clarity, throughout the following sections, all fly strains will be referred to by the shorthand name only, as opposed to their full genotype.

Drosophila gene and protein nomenclature in this thesis is consistent with the established protocols approved by FlyBase and are outlined in (<https://wiki.flybase.org/wiki/FlyBase:Nomenclature>). These protocols detail that if a gene name begins with an uppercase letter, the gene is named after the mutant phenotype that is dominant to the normal wild-type. If a gene name begins with a lowercase letter, the gene is named after the mutant phenotype which is recessive to the normal wild-type. Genes which are named after the product of a protein contain an uppercase first letter and mammalian gene symbols are written in italics, whereas protein symbols are not written in italics.

2.1.1 Fly strain maintenance

Flies used for experimental purposes were raised on a 12-hour light/dark cycle on standard fly media at 25°C, exceptions are otherwise indicated in specific sections.

Standard fly media was produced by combining 10 g agar, 40 g yeast, and 110 g polenta with 1 L of dH₂O which was then brought to the boil before simmering for 2 minutes with constant stirring. This mixture was then taken off the heat and 130 g white sugar was added along with 3.3 g of Moldex (methyl 4-hydroxybenzoate) dissolved in 37 mL 96% ethanol and 20 mL molasses, which was then mixed thoroughly. Approximately 8 mL of this mixture was then poured into 30 mL vials (LabServ) or 40 mL was poured into 100 mL bottles when larger quantities of progeny were required. Once the food was set it was sprinkled with yeast and plugged with either a foam plug (vials) or a sponge plug (bottles).

2.2 Genetic Crosses

To collect virgin female flies for genetic crosses, adult flies were removed from the stock vials/bottles in the morning. Female flies do not mate within eight hours following

eclosion, therefore virgin females can be collected before eight hours have elapsed. Five virgin females and five males were mated together in a 30 mL vial with 8 mL of standard fly media or 15 virgin females and 15 males were mated together in a 100 mL bottle with 40 mL standard fly media. After five to seven days, adult flies were removed, with progeny expected to eclose after ten days at 25°C.

2.3 *Drosophila* brain isolation

Flies were anaesthetised with CO₂ before being placed in a petri dish on ice. Using a pair of sharpened Dumont #5 forceps under a stereomicroscope, each fly was submerged in ice cold PBST (1x PBS and 0.5% Triton X-100), the head capsule was removed to expose the brain, and then fatty tissue and air sacs surrounding the brain were removed. The brains were transferred to a 1.75 mL microcentrifuge tube containing fresh PBST on ice using a glass Pasteur pipette before being fixed in PFAT/DMSO (4% paraformaldehyde in 1x PBS, 0.1% Triton X-100 and 5% DMSO) for 20 minutes. Following this, brains were either washed twice with 100% methanol for 5 minutes each before being stored long term at -20°C in 100% methanol or processed immediately for immunohistochemistry (Section 2.3.1).

2.3.1 Immunohistochemistry on isolated fly brains

Brains stored at -20°C were rehydrated in 50% methanol/PBST for 5 minutes, then washed 4 x 5 minutes in 1x PBST. Brains were then incubated in immunobuffer (5% normal goat serum in 1x PBST) at room temperature (RT) for three hours. Following this, brains were incubated in primary antibody (Table 2.1) diluted in immunobuffer overnight at RT. Brains were then washed with 1x PBST for 2 quick washes then 3 x 5 minute washes before being incubated overnight at 4°C with appropriate fluorescent secondary antibodies (Table 2.2) diluted in immunobuffer.

Following secondary antibody incubation, brains were then again washed with 1x PBST for 2 quick washes then 3 x 5 minute washes. Brains were then mounted onto a microscope slide in 50 µL of antifade (1 mL 10x PBS, 9 mL glycerol and 0.2 mg/mL n-propyl gallate), a coverslip was then added and sealed with nail polish.

Brains were imaged with the Leica SP5 DM6000B confocal microscope (Manawatu Microscopy and Imaging Centre). Z-stacks were collected with an optical section size of 1 μm for mushroom body images and 0.5 μm for LPTC images in the optic lobe. These images were then analysed using ImageJ where maximum projections of each Z-stack produced singular static images for analysis.

Name	Target	Class	Host	Source	Dilution
Ab290	GFP	Polyclonal	Rabbit	Abcam	IHC - 1:20,000 WB - 1:4,000
Nc82	Bruchpilot	Monoclonal	Mouse	DSHB	IHC – 1:100
aa 1655-1912 of SP2523 (<i>Ankyrin2</i>)	Ankyrin2-L	Polyclonal	Rabbit	Dr Aberle. Heinrich Heine University, Düsseldorf	IHC – 1:1,000
Anti-HA High Affinity (3F10)	HA-tag	Monoclonal	Rat	Sigma Aldrich	IHC – 1:500 WB – 1:1,000
Ab9106	Myc-tag	Polyclonal	Rabbit	Abcam	IHC – 1:200 WB – 1:500
12G10 α Tubulin	Tubulin	Monoclonal	Mouse	DSHB	WB – 1:500
1D4 anti-Fasciclin II	Fasciclin (FasII)	Monoclonal	Mouse	DSHB	IHC – 1:20

Table 2.1. List of primary antibodies used in immunohistochemistry and western blotting with corresponding dilutions. Abbreviations: IHC = Immunohistochemistry, WB = Western Blotting, DSHB = Developmental Studies Hybridoma Bank.

Name	Target Species	Origin Species	Source	Dilution
Alexa Anti-Rat 647	Rat	Goat	Sigma Aldrich	IHC – 1:500
Alexa Anti-Mouse 555	Mouse	Goat	Sigma Aldrich	IHC – 1:500
Alexa Anti-Rabbit 488	Rabbit	Goat	Sigma Aldrich	IHC – 1:500
Rat HRP	Rat	Goat	Abcam	WB – 1:10,000
Mouse HRP	Mouse	Goat	Sigma Aldrich	WB – 1:20,000
Rabbit HRP	Rabbit	Goat	Sigma Aldrich	WB – 1:40,000
Veriblot for IP Detection Reagent	Rabbit Total IgG	-	Abcam	WB – 1:4000

Table 2.2. List of secondary antibodies used in immunohistochemistry and western blotting with corresponding dilutions. Abbreviations: IHC = Immunohistochemistry, WB = Western Blotting.

2.4 *Drosophila* protein extraction

2.4.1 Fly head isolation

Adult flies were anaesthetised in FlyNap (Carolina) before a scalpel was used to separate the fly heads from their bodies. The heads were then placed into a 1.75 mL microcentrifuge tube on ice. Heads were then stored at -80°C until total protein was ready to be isolated.

2.4.2 Total protein isolation from *Drosophila* heads

Total protein isolation from *Drosophila* heads was performed by adding 50 µL RIPA buffer (150 mM NaCl, 0.1% Triton X, 0.5% Sodium deoxycholate, 0.1% SDS, 50 mM Tris, pH 8.0, and cOmplete EDTA-free protease inhibitor (Roche)) to approximately 50 fly heads in a 1.75 mL microcentrifuge tube. Using a motorised mortar and pestle, the

tissue was homogenised by pulsing 3 x 10 seconds before centrifuging at 13,000 x g for 2 minutes at 4°C to pellet cellular debris, the supernatant was then transferred to a new chilled 1.75 mL microcentrifuge tube. Whole cell lysates were then quantified immediately using the BCA Protein Kit (Section 2.5) or stored at -80°C.

2.4.3 Cell fractionation from *Drosophila* heads

Cell fractionation was performed on 50 fly heads per sample using the NE-PER Nuclear and Cytoplasmic Extraction Kit (ThermoFisher Scientific) according to the protocol outlined in Maitra et al. (2019). *Drosophila* heads were briefly homogenised in 100 µL Cytoplasmic Extraction Reagent I with 1x protease inhibitors (cOmplete EDTA-free protease inhibitor (Roche)). The lysate was then incubated on ice for 10 minutes before the addition of 5.5 µL of Cytoplasmic Extraction Reagent II followed by centrifugation at 10,000 x g for 5 minutes at 4°C. The resulting supernatant (cytoplasmic fraction) was dispensed into a new chilled 1.75 mL microcentrifuge tube and kept on ice until quantified (Section 2.5) or stored at -80°C. The remaining pellet was then resuspended with 50 µL Cytoplasmic Extraction Reagent I with 1x protease inhibitors. The suspension was then incubated on ice for 10 minutes before 2.75 µL of the Cytoplasmic Extraction Reagent II was added and centrifuged at 10,000 x g for 5 minutes at 4°C. The resulting supernatant (Wash I) was collected into a new chilled 1.75 mL microcentrifuge tube and kept on ice until quantified (Section 2.5) or stored at -80°C. The above wash step was repeated a second time to yield Wash II. The pellet was then resuspended in 50 µL Nuclear Extraction Reagent with 1x protease inhibitors and incubated on ice for 40 minutes before being centrifuged at 10,000 x g for 10 minutes at 4°C. The resulting supernatant (nuclear fraction) was collected into a new chilled 1.75 mL microcentrifuge tube and retained on ice for a short period of time or stored at -80°C (Maitra et al., 2019).

2.5 Protein quantification

The Pierce BCA Protein Assay Kit (ThermoFisher) was used to quantify protein concentrations alongside a set of standards to produce a standard curve according to the manufacturer's instructions. Each standard was measured in duplicate and each sample in triplicate. Absorbances were read using the BioTek PowerWave XS plate reader and

analysed in Excel to determine the protein concentration (mg/mL) from the standard curve.

2.6 SDS-PAGE and Western Blotting

Following lysate preparation and protein quantification, lysates were subject to sodium dodecyl sulfate – polyacrylamide gel electrophoresis (SDS-PAGE) to separate proteins in a sample based on size. For this 30 µg of lysate diluted in RIPA buffer was added to 5x Laemmli buffer (2% SDS, 5% 2-mercaptoethanol, 10% glycerol, 0.01% bromophenol blue, 60 mM Tris HCl, pH 6.8) to a final concentration of 1x. In order to reduce and denature the proteins, samples were then boiled at 95°C for five minutes. Samples were then loaded into a pre-cast polyacrylamide gel (Mini Protean TGX 4%-20%, Bio-Rad) which was then submerged in 1x Running buffer (25 mM Tris, 190 mM glycine, 0.1% SDS) prior to electrophoresis. The gel was then electrophoresed at 200 V for approximately 35 minutes, or until the dye front had reached the bottom of the gel.

The proteins in the gel were then transferred to a nitrocellulose membrane (Amersham Protran premium 0.45 µm nitrocellulose, GE Healthcare LifeScience) by placing the gel with the membrane directly on top of it between two pre-soaked pieces of blotting paper and two pre-soaked sponge pads before tightly closing the sandwich in a plastic cassette. The cassette was then submerged in 1x Transfer buffer (25 mM Tris, 190 mM glycine, 0.1% SDS, 20% methanol) at 4°C. Proteins were transferred to the membrane at 100 V for 60 minutes. The membrane was then stained with Ponceau-S (0.1% Ponceau, 5% acetic acid) for five minutes to confirm the presence of protein before being rinsed with dH₂O until the membrane was clear of Ponceau stain.

The membrane was then incubated with gentle agitation in 5% blocking buffer (5% (w/v) skim milk powder in 1x TBST (20 mM Tris, 150 mM NaCl, 0.1% Tween-20)) at RT for 60 minutes to prevent non-specific antibody binding. The membrane was then washed for 3 x 5 minute washes in 1x TBST before being incubated overnight at 4°C with primary antibody (Table 2.1) specific for the protein of interest diluted in 1% blocking buffer (1% skim milk (w/v) in 1x TBST). The following day, the membrane was washed with 1x TBST for 6 x 5 minute washes before being incubated at RT for 60 minutes with the secondary antibody (Table 2.2) diluted in 1% blocking buffer. The membrane was then

washed for 3 x 5 minute washes in 1x TBST before the secondary antibody was detected using Amersham ECL Prime Western blotting detection reagent (GE Healthcare) and the Azure Biosystems c600 imaging system.

2.7 Immunoprecipitation / Co-immunoprecipitation

The Pierce Classic IP Kit (ThermoFisher Scientific) was used according to the manufacturer's instructions. Total protein was isolated (Section 2.4) and quantified (Section 2.5). Between 500-1000 μ g lysate was combined with 1 μ L of appropriate primary antibody (Table 2.1) to create an antibody/protein complex.

Protein A/G agarose beads were then incorporated to bind to the antibody/protein complex to pull-down the proteins of interest. These proteins were then eluted in 2x Non-reducing lane marker sample buffer (2x Non-reducing lane marker, 20 mM DTT) before being boiled at 100°C for 5 minutes to reduce and denature proteins. The samples were then centrifuged at 1,000 \times g at 4°C for 60 seconds to collect the eluate (Figure 2.1).

Samples were then separated by SDS-PAGE and transferred to a nitrocellulose membrane for detection (Section 2.6) with a specific primary antibody (Table 2.1) and conjugate secondary antibody (Table 2.2).

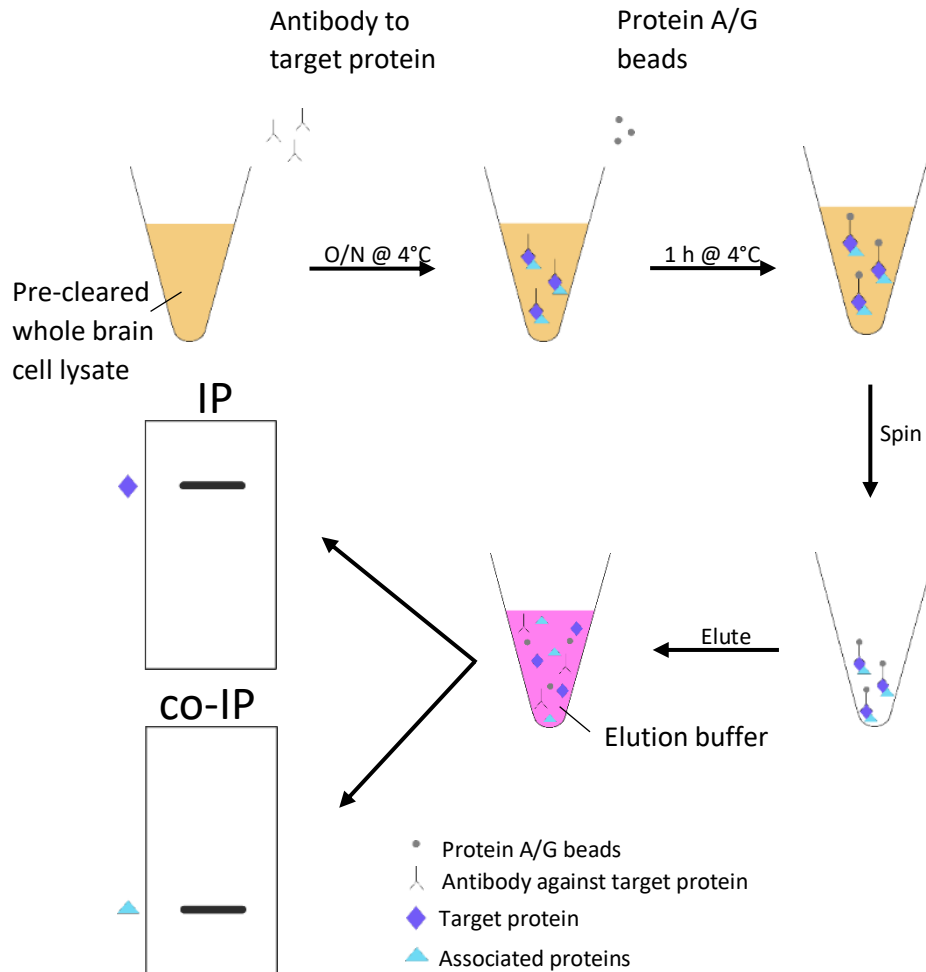


Figure 2.1. Schematic of the process involved in immunoprecipitation and co-immunoprecipitation assays. Primary antibody specific to the target protein is combined with pre-cleared whole cell head lysate and incubated O/N at 4°C. Protein A/G beads were then added, binding specifically to the antibody bound to the target protein of interest and all associated proteins. The lysate was then centrifuged before the elution buffer was added. The Protein A/G beads, antibody, target protein and associated proteins were then dissociated. The eluate was then separated by SDS-PAGE and western blotted. In an IP assay, the target protein was detected using the same antibody used in the pulldown assay. For a co-IP assay, the associated protein can be detected using an antibody specific for the associated protein. Abbreviations: O/N = overnight, IP = immunoprecipitation, co-IP = co-immunoprecipitation.

2.8 *Drosophila* eye phenotype analysis

2.8.1 Light microscopy

Flies were frozen at -20°C overnight, before being thawed and analysed under the stereomicroscope (Olympus SzX12, DP controller imaging software, zoom 108, exposure time: 1/20 seconds). Eye phenotypes were analysed based on pigmentation differences, ommatidia organisation and physical eye size and shape.

2.8.2 Scanning electron microscopy

F1 progeny from the same vials as those that were imaged by light microscopy were placed into a new vial containing a small disc of paper towel soaked in water to allow the flies to remove food residue from their eyes one day prior to scanning electron microscopy (SEM) preparation. Flies were then anaesthetised with FlyNap (Carolina) before being transferred to a vial of primary modified Karnovsky's fixative (3% glutaraldehyde, 2% formaldehyde in 0.1 M phosphate buffer, pH 7.2) and Triton X-100 and vacuum infiltrated until entirely wet. Flies were then transferred into fresh fixative and incubated at RT for eight hours. Three washes, each lasting 10 minutes in phosphate buffer (0.1 M, pH 7.2) were performed before being dehydrated in a series of graded ethanol steps (25%, 50%, 75%, 95%, 100%) each lasting 10 minutes before finally being incubated for 1 hour in 100% ethanol. Following this incubation, samples were then critical point dried using liquid CO₂ and 100% ethanol (Polaron E3000 series II critical point drying apparatus). Following fixation, the abovementioned sample processing was conducted by Mr Raoul Solomon at the Manawatu Microscopy and Imaging Centre (MMIC), School of Fundamental Sciences, Palmerston North.

The samples were then mounted onto aluminium stubs before being sputter coated in gold (Baltex SCD 050 sputter coater), these stubs holding the samples were then imaged using the FEI Quanta 200 Environmental Scanning Electron Microscope at an accelerating voltage of 20 kV. Eye phenotypes were analysed based on bristle formation, ommatidia disorganisation and fusion in accordance with Table 3.1.

3 Results

3.1 Investigating a physical interaction between HDAC4 and Ank2

In an attempt to identify the molecular pathway through which HDAC4 acts in neurons, Schwartz et al. (2016) carried out a genetic enhancer screen in the *Drosophila* eye and identified *Ank2* as a gene that genetically interacts with *HDAC4* during eye development. A subsequent investigation found that knockdown of *Ank2* in the mushroom body also impairs long-term memory formation (Schwartz, 2016) similarly to that seen in *HDAC4* overexpression (Fitzsimons et al., 2013), suggesting that the mechanism through which HDAC4 modulates long-term memory may involve an interaction with Ank2.

The N-terminal region of HDAC4 contains an ankyrin repeat binding domain consisting of a PxLPxI/L motif which in mammalian cells has been characterised to bind to the ankyrin repeat region of proteins such as ANKRA2 and RFXANK (Xu et al., 2012). It can therefore be speculated that *Drosophila* Ank2 may physically interact with *Drosophila* HDAC4 through binding to the conserved PxLPxI/L motif in the ankyrin repeat binding domain.

Prior to investigating a physical interaction, the expression patterns of endogenous Ank2 and HDAC4 were examined, with the rationale that for a physical interaction to occur in the mushroom body *in vivo*, Ank2 and HDAC4 must be endogenously expressed in the same neuronal subtypes in the mushroom body.

There is currently no antibody available that is specific to *Drosophila* HDAC4, therefore a line carrying *HDAC4::YFP* was used to characterise the endogenous expression pattern of HDAC4 in the brain. *HDAC4::YFP* contains an insertion of YFP into the second intron of the endogenous *HDAC4* gene. The *YFP* gene is flanked with splice acceptor and donor sites, resulting in an internal fusion of YFP into the HDAC4 protein (Figure 3.1).



Figure 3.1. The HDAC4::YFP construct. The 22.6 kb HDAC4 locus is shown. The exons are shown as open boxes and the black boxes are representative of the translated regions. The YFP open reading frame is inserted into the HDAC4 gene downstream of the second exon at 1310 bp (Fitzsimons et al., 2013). The YFP is flanked by splice sites resulting in an in frame insertion into the HDAC4 protein. *Figure from Fitzsimons et al. (2013), modified and used under the Creative Commons Attribution 4.0 International licence (doi: [10.1371/journal.pone.0083903](https://doi.org/10.1371/journal.pone.0083903)).*

Brains were dissected and immunohistochemistry was performed using an anti-GFP antibody. Anti-GFP maintains the ability to detect YFP tagged proteins, as YFP is a close genetic variant of GFP with a high sequence consensus (Veening et al., 2004). HDAC4::YFP was expressed throughout the neuropil of the brain, with high expression detected in all lobes of the mushroom body (Figure 3.2A, B). Ank2 was detected with anti-Ank2-L, an antibody specific to *Drosophila* Ank2. The anti-Ank2-L antibody has previously been shown to bind to the long isoform of Ank2 (Ank2-L) with high specificity in the neuromuscular junction of *Drosophila* (Koch et al., 2008). Ank2 is expressed highly throughout axonal tracts of the brain, in particular the surroundings of the antennal lobes. Expression is fainter but still visible in the mushroom body and can be clearly distinguished in the alpha and gamma lobes (Figure 3.2C).

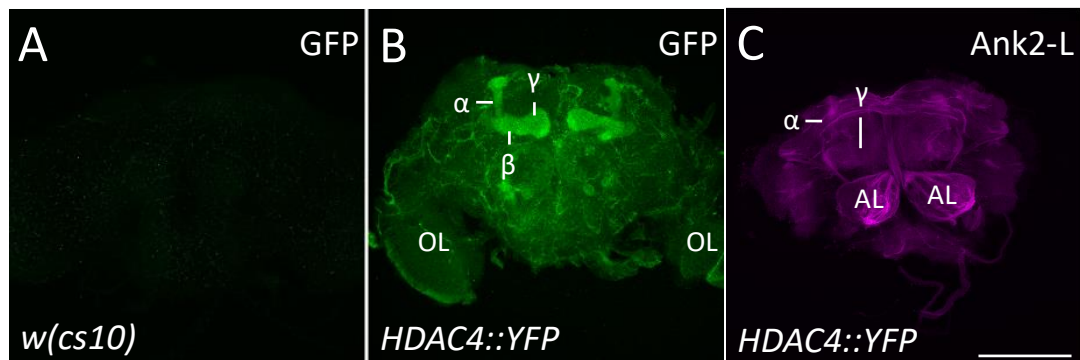


Figure 3.2. Endogenous expression of HDAC4 and Ankyrin2 in HDAC4::YFP brains. (A, B) Maximum anterior projection of (A) *w(cs10)* control and (B) *HDAC4::YFP* brains illustrating the distribution of HDAC4::YFP using an anti-GFP antibody (green). (C) Anterior projection of *HDAC4::YFP* brains illustrating endogenous Ankyrin2 distribution using an anti-Ank2-L antibody (magenta). Abbreviations: AL = antennal lobe, OL = optic lobe. Objective 40x in oil. Scale bar = 100 μ m.

These results confirm that HDAC4 and Ank2 are both endogenously expressed in the mushroom body, and both localise to the axonal bundles of the mushroom body lobes. Thus, it is possible that HDAC4 and Ank2 may physically interact in mushroom body axons.

A preliminary study by Schwartz (2016) investigated this interaction via GST pull-down to test an interaction between purified N-terminal GST-tagged HDAC4 protein that contains the putative ankyrin binding motif and a lysate from brains that carry an EGFP internal fusion in one of the smallest isoforms of Ank2. A weak interaction was detected, however, despite concerted efforts this result was unable to be reproduced (Dr H.

Fitzsimons, personal communication, 23 September, 2020), leaving it unclear as to whether HDAC4 and Ank2 interact. Rather than continue with this *in vitro* approach, a different strategy was taken in which epitope tagged Ank2 and HDAC4 were co-expressed in brains and tested for an interaction via co-immunoprecipitation (co-IP). The basis of this approach is that successful immunoprecipitation (IP) will capture and purify the specific target protein along with any other associated proteins that interact either directly or within the same complex.

For the co-IP, ideally, epitope-tagged full length *HDAC4* and *Ank2* would be co-expressed for ease of pull-down and detection. This is particularly important for *Ank2* since the Ank2-L antibody is not suitable for western blotting. *Ank2* contains at least ten transcripts, most of which are >14 kb (<http://flybase.org/reports/FBgn0261788.html>), which is prohibitively large making it difficult to amplify and subclone (Appendix 6.4). A 2268 bp N-terminal region of *Ank2* that includes the ankyrin repeat region was therefore selected with the rationale that if HDAC4 interacts through this domain, this construct should be sufficient to mediate the interaction. The 2268 bp region of *Ank2* was synthesised with a C-terminal 3x HA epitope tag and subcloned downstream of the upstream activating sequence (UAS) in the pUASTattB plasmid by Genscript (NJ, UAS) (Appendix 6.2). Transgenic flies were generated by Genetivision (Houston, TX, USA) via homologous recombination of the attB site on the plasmid into the attP landing site at chromosomal location 2R(57F5) in the VK22 strain. The strain created was hereafter termed Ank2₁₉₀₋₉₄₆-HA, indicative of the position of the amino acids based off the reference Ank2 isoform Z (<https://www.uniprot.org/uniprot/X2JC49>).

Prior to embarking on the co-IP, it was imperative to first confirm expression of the Ank2₁₉₀₋₉₄₆-HA transgene via western blotting and immunohistochemistry.

3.1.1 Confirmation of expression of Ank2₁₉₀₋₉₄₆-HA via western blot

To express Ank2₁₉₀₋₉₄₆-HA in the brain, the UAS/GAL4 system was used (Section 1.3.4.1). Female flies carrying the pan-neuronal driver *elav-GAL4* were crossed to male *UAS-Ank2₁₉₀₋₉₄₆-HA* as well as *w(cs10)* control flies. A standard crossing scheme is outlined in Figure 3.3.

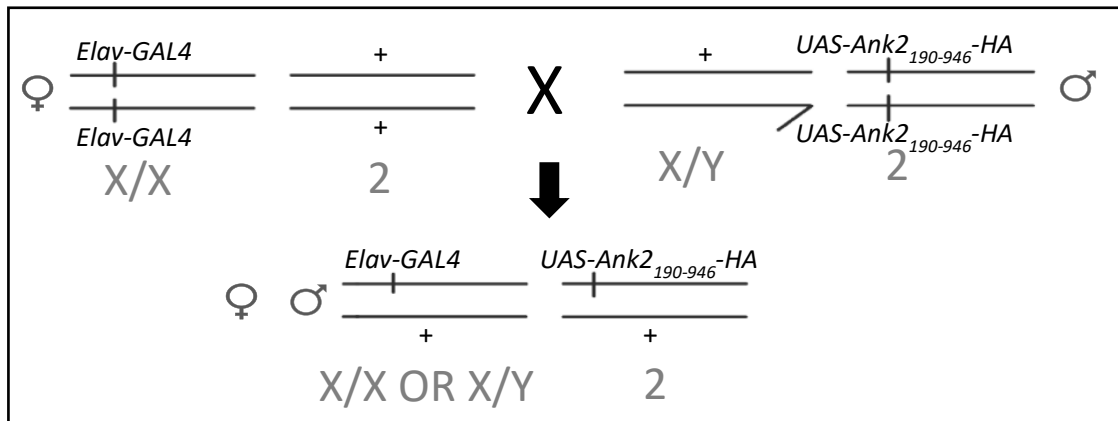


Figure 3.3. Example of a genetic crossing scheme. Chromosomes are shown in black and numbered accordingly. X/Y is chromosome 1 followed by chromosome 2. Chromosomes 3 and 4 are both wild-type and not shown. This genetic cross between *elav-GAL4* females and *UAS-Ank2₁₉₀₋₉₄₆-HA* males results in progeny that express *Ank2₁₉₀₋₉₄₆-HA* throughout the brain.

Whole cell lysates were generated from the heads of progeny and subjected to western blotting with anti-HA to detect *Ank2₁₉₀₋₉₄₆-HA* (Section 2.6). A band was produced at the expected size of 90 kDa only in the *Ank2₁₉₀₋₉₄₆-HA* lane, which was absent from the control, confirming expression of the transgene (Figure 3.4).

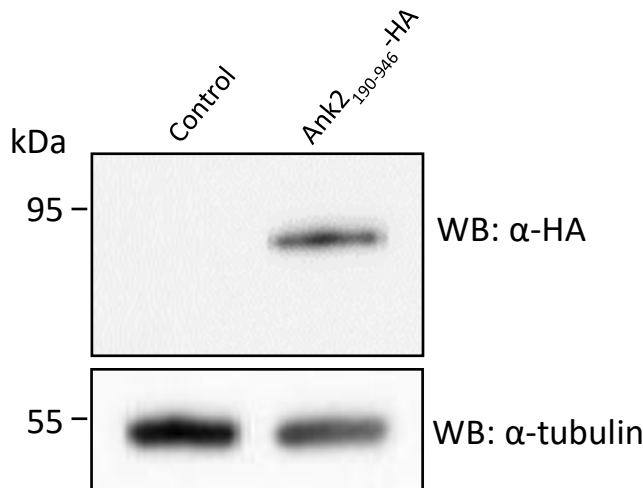


Figure 3.4. Characterising expression of *Ank2₁₉₀₋₉₄₆-HA*. Whole protein lysates extracted from fly heads were separated by SDS-PAGE and western blotted using an anti-HA antibody to probe for expression of *Ank2₁₉₀₋₉₄₆-HA*. *Ank2₁₉₀₋₉₄₆-HA* is seen at approximately 90 kDa. Protein loaded = 30 µg.

3.1.2 Confirmation of co-expression of Ank2₁₉₀₋₉₄₆-HA and DmHDAC4-Myc via immunohistochemistry

A fly line carrying *UAS-DmHDAC4* with a C-terminal 6x Myc tag was previously generated by Dr Helen Fitzsimons (Appendix 6.3). The *UAS-DmHDAC4-Myc* and *UAS-Ank2₁₉₀₋₉₄₆-HA* constructs were crossed into a single fly strain co-expressing both Ank2₁₉₀₋₉₄₆-HA and DmHDAC4-Myc (Figure 3.5).

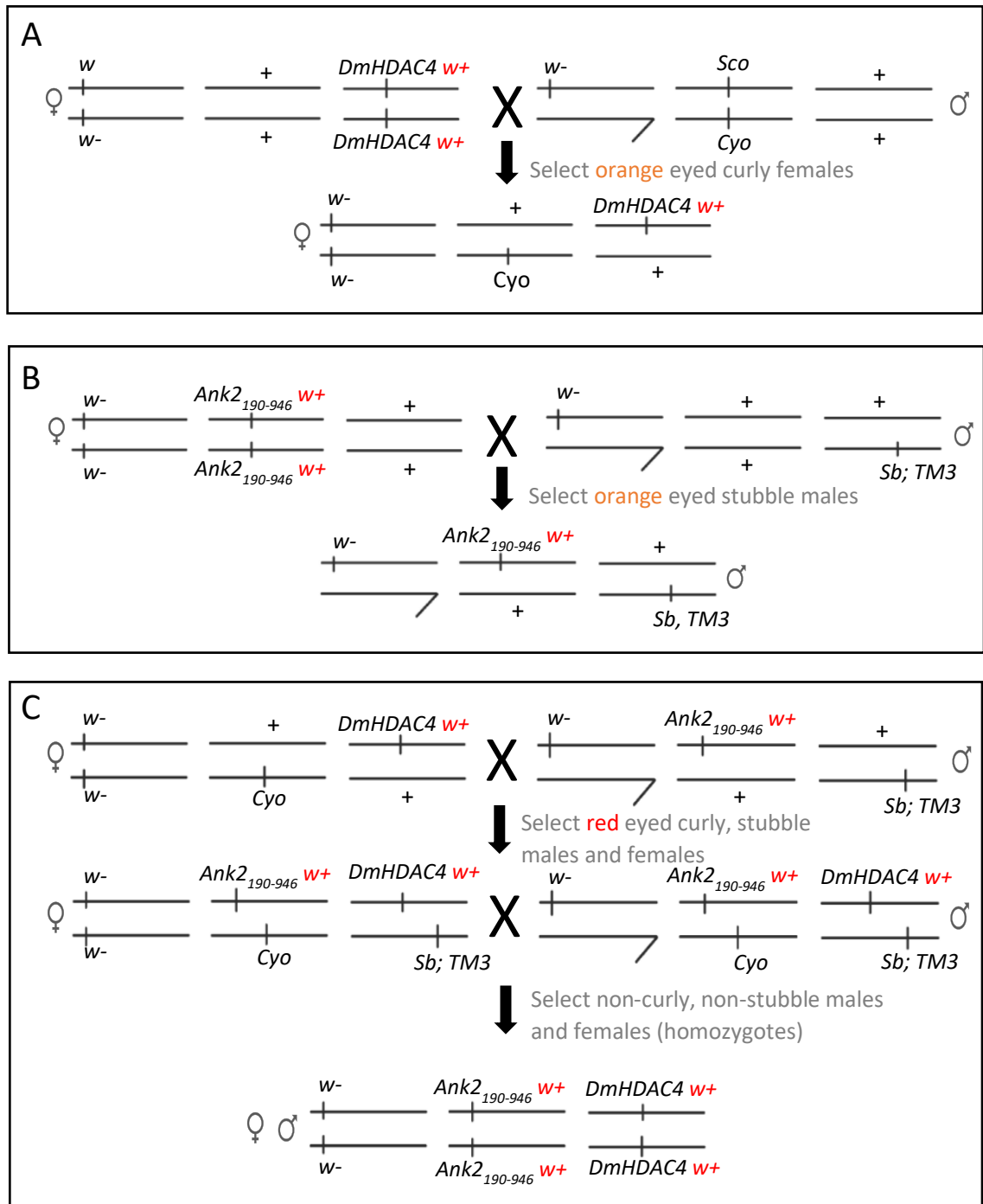


Figure 3.5. Crossing scheme to generate a *UAS-Ank2₁₉₀₋₉₄₆-HA*; *UAS-DmHDAC4-Myc* homozygous line. In order to generate a line carrying both *UAS-DmHDAC4-Myc* (denoted DmHDAC4) on the 3rd chromosome and *UAS-Ank2₁₉₀₋₉₄₆-HA* (denoted Ank2₁₉₀₋₉₄₆) on the 2nd chromosome, fly strains carrying balancer chromosomes were utilised. Balancer chromosomes are used as they provide a selectable heritable trait which can be traced through multiple crosses and prevent recombination due to multiple inversions. *w*⁻ is the background strain which has white eyes. Both the *UAS-Ank2₁₉₀₋₉₄₆-HA* and *UAS-DmHDAC4-Myc* constructs are linked to the mini-white (*w*⁺) gene which restores the red eye colour and is used as a selectable marker for presence of the transgene. *w*⁺ is dose dependent, with one copy typically conferring an orange eye colour and two copies resulting in a red eye colour. (A) Females homozygous for *UAS-DmHDAC4-Myc* on the third chromosome were crossed to males carrying the second chromosome balancer *Cyo/Sco* (curly wings). F1 orange eyed, curly winged females were selected for the cross in (C).

(B) Females homozygous for *UAS-Ank2₁₉₀₋₉₄₆-HA* on the second chromosome were crossed to males carrying the third chromosome balancer *Sb; TM3* (stubble bristles). F1 orange eyed stubble bristled males were selected for the cross in (C). (C) Orange eyed curly winged females were then crossed to orange eyed stubble bristled males from crosses (A) and (B) respectively. F1 red eyed curly winged, stubble bristled females and males were collected. These were then crossed together before non-curly, non-stubble males and females were selected and crossed together to obtain a stable fly strain homozygous for both *UAS-DmHDAC4-Myc* and *UAS-Ank2₁₉₀₋₉₄₆-HA*. Abbreviations: *Sco* = Scutoid, *CyO* = Curly of Oster balancer chromosome, *Sb* = Stubble, *TM3* = 3rd multiply-inverted balancer chromosome.

To confirm that *Ank2₁₉₀₋₉₄₆-HA* and *DmHDAC4-Myc* co-distribute in neurons, *elav-GAL4* females were then crossed to *UAS-Ank2₁₉₀₋₉₄₆-HA; UAS-DmHDAC4-Myc* males, via a standard genetic cross similar to Figure 3.3, and brains of progeny were processed by immunohistochemistry (Section 2.3.1).

Expression of *Ank2₁₉₀₋₉₄₆-HA* was observed throughout the α , β , and γ lobes of the mushroom body, as well as the antennal lobes and multiple axon tracts throughout the brain (Figure 3.6A), which is consistent with the expression pattern of endogenous *Ank2* (Figure 3.2C). *DmHDAC4-Myc* also localised at high levels in the mushroom body with a predominance of protein observed in the α , β , and γ lobes (Figure 3.6B). The expression pattern within the mushroom body did not overlap completely, which can be seen specifically within the α lobes with *Ank2₁₉₀₋₉₄₆-HA* higher at the tips (Figure 3.6C). It should also be noted that because only the N-terminus of *Ank2* is present, the expression pattern may well differ from that of endogenous *Ank2*. Nonetheless, this confirms that both proteins have been successfully expressed in neurons and can be tested for a physical interaction via co-IP.

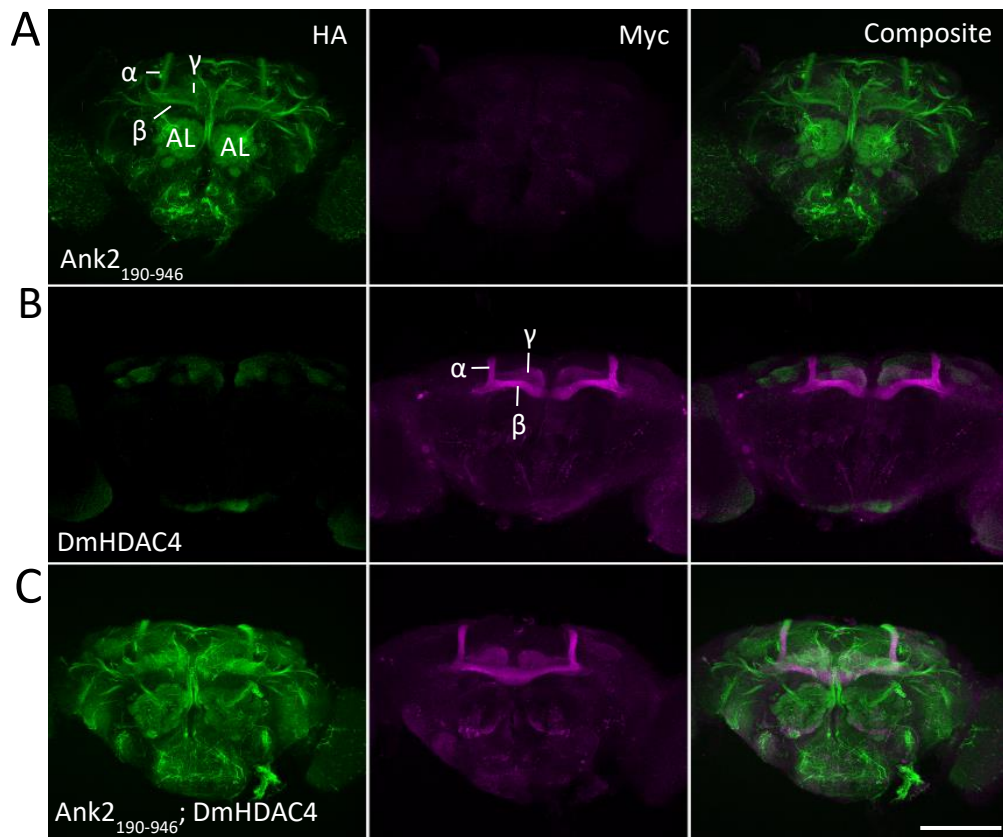


Figure 3.6. Characterizing the expression and co-distribution of Ank2₁₉₀₋₉₄₆-HA and DmHDAC4-Myc. (A) Maximum anterior projection of the brain showing distribution of Ank2₁₉₀₋₉₄₆-HA (denoted as Ank2₁₉₀₋₉₄₆) with anti-HA (green) in the mushroom body lobes, antennal lobes and axonal tracts. (B) Maximum anterior projection showing the distribution of DmHDAC4-Myc (denoted as DmHDAC4) with anti-Myc (magenta) in the mushroom body lobes. (C) Merged image showing co-distribution in the α , β and γ lobes of the mushroom body lobes. Abbreviations: AL = antennal lobe. Objective 40x in oil. Scale bar = 100 μ m.

3.1.3 Immunoprecipitation of Ank2₁₉₀₋₉₄₆-HA and DmHDAC4-Myc

To test for a physical interaction between Ank2₁₉₀₋₉₄₆-HA and DmHDAC4-Myc it was first important to demonstrate that each construct could individually be immunoprecipitated and confirm antibody specificity. Each fly strain (Ank2₁₉₀₋₉₄₆-HA and DmHDAC4-Myc) was crossed to *elav-GAL4* and whole heads of progeny were processed and subjected to IP (Section 2.7). Lysates containing Ank2₁₉₀₋₉₄₆-HA or control were immunoprecipitated with anti-HA followed by SDS-PAGE separation and western blotting (Section 2.6) with anti-HA (Figure 3.7A). A band of expected size (90 kDa) was detected in the Ank2₁₉₀₋₉₄₆-HA sample. Ank2₁₉₀₋₉₄₆-HA was not detected in negative IP controls where either the pull-down antibody (anti-HA) or the protein A/G beads had been

omitted. Inputs contain DmHDAC4-Myc as a negative control and Ank2₁₉₀₋₉₄₆-HA as a positive control for accurate anti-HA detection.

Similarly, lysates containing DmHDAC4-Myc or control were immunoprecipitated with anti-Myc and protein A/G beads before being separated by SDS-PAGE and western blotting with anti-Myc (Figure 3.7B). A band of expected size (140 kDa) was observed in the DmHDAC4-Myc sample. DmHDAC4-Myc was absent from the negative IP controls either omitting the pull-down antibody (anti-Myc) or the protein A/G beads. Inputs include Ank2₁₉₀₋₉₄₆-HA as a negative control and DmHDAC4-Myc as a positive control for accurate anti-Myc detection. A non-specific band of approximately 90 kDa is observed in all input samples which has been previously observed in this laboratory when western blotting fly head lysates with anti-Myc.

Together these IP assays confirm antibody specificity of anti-Ha and anti-Myc to the tagged constructs. Since a successful co-IP has not previously been performed in our laboratory, an initial co-IP experiment was carried out on proteins that were known to interact in order to confirm the methodology.

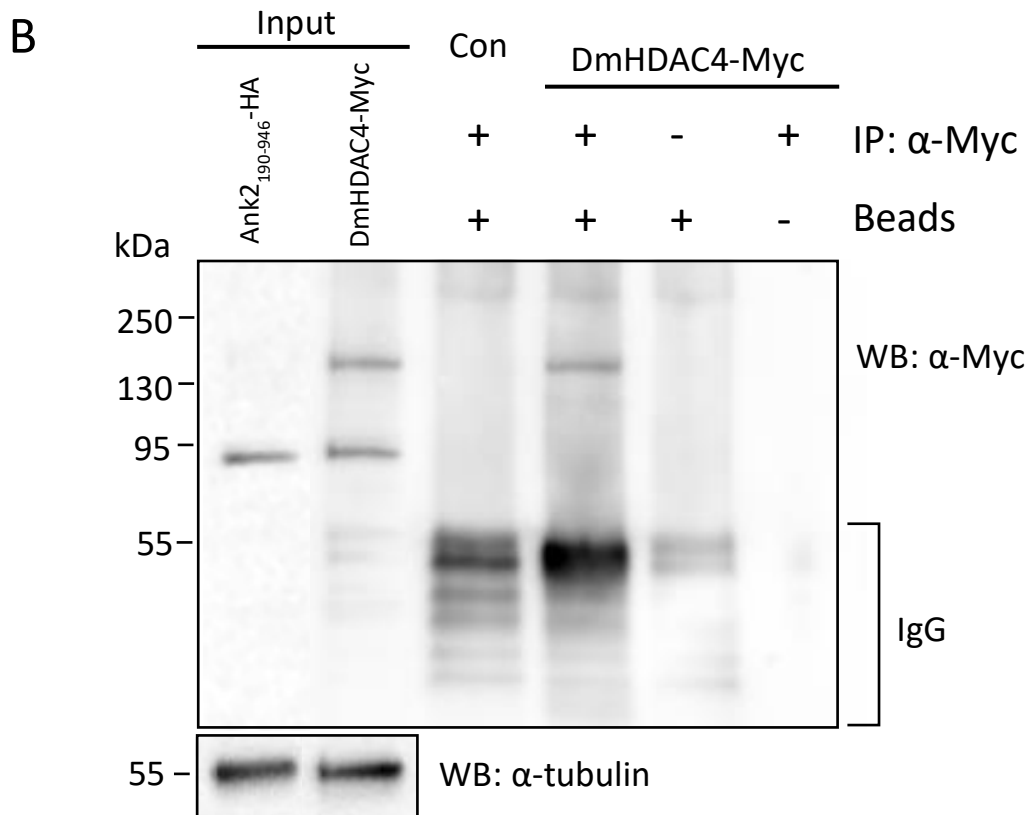
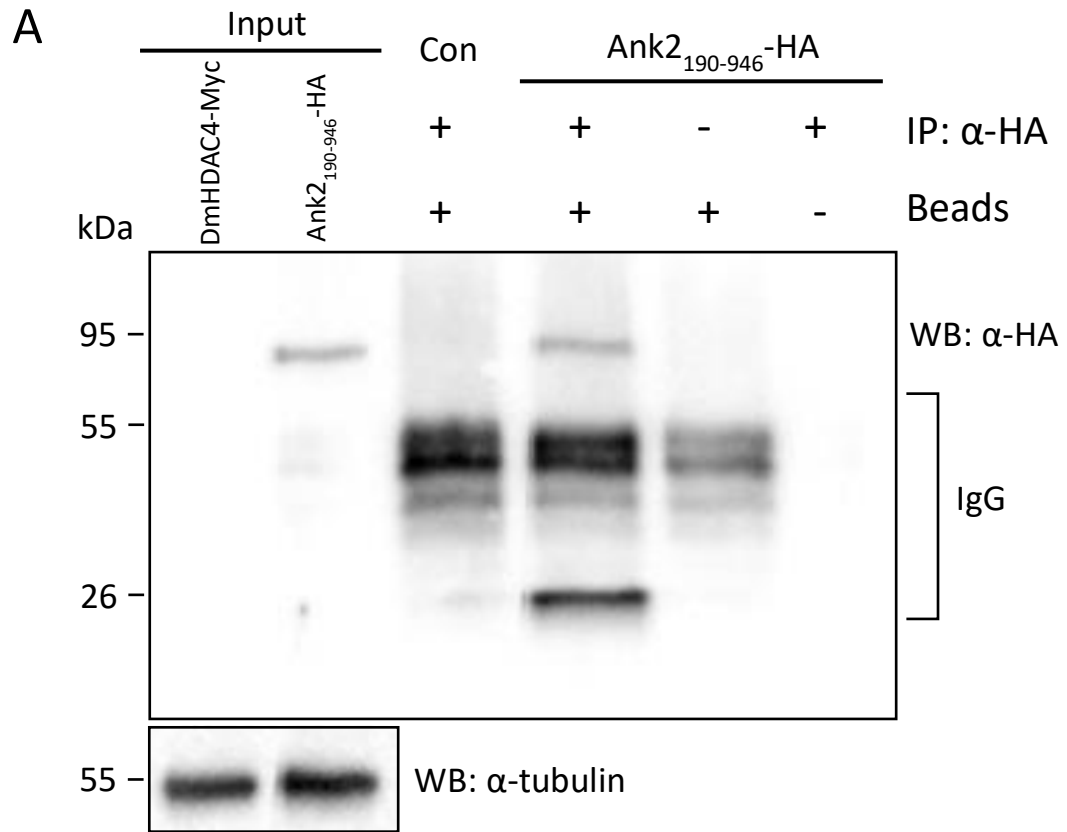


Figure 3.7. Immunoprecipitation of Ank2₁₉₀₋₉₄₆-HA and DmHDAC4-Myc. (A) Ank2₁₉₀₋₉₄₆-HA was immunoprecipitated and detected with anti-HA, whereas the negative control

DmHDAC4-Myc (denoted as con) was not immunoprecipitated. Ank2₁₉₀₋₉₄₆-HA was not detected in negative IP controls omitting either anti-HA or protein A/G beads. Input samples contain DmHDAC4-Myc as a negative control and Ank2₁₉₀₋₉₄₆-HA as a positive control. (B) DmHDAC4-Myc was immunoprecipitated and detected with anti-Myc, whereas the negative control Ank2₁₉₀₋₉₄₆-HA (denoted as con) was not immunoprecipitated. DmHDAC4-Myc was not detected in the negative IP controls omitting either anti-Myc or protein A/G beads. Ank2₁₉₀₋₉₄₆-HA and DmHDAC4-Myc were the respective negative and positive input controls. IgG bands are also observed between 25 to 55 kDa in all co-IP lanes. Proteins were measured in kDa. Abbreviations: IgG = immunoglobulin G. Input samples = 30 µg.

3.1.4 Positive co-IP control

A co-IP assay is a simple method that can be used to determine if two proteins physically interact *in vivo*. As opposed to an IP, a second antibody is used to probe a specific protein that is thought to be physically interacting with the original target protein, either as a direct physical interaction or within a complex. The N-terminal region of HDAC4 contains a glutamine-rich region that mediates homotetramerisation (Guo et al., 2007). Given that HDAC4 has the ability to tetramerise, two differentially labelled HDAC4 constructs can be co-expressed to form tetramers, and thus should co-IP with either tag. A standard genetic cross was performed between *elav-GAL4*, *HDAC4::YFP* virgin females and *UAS-DmHDAC4-Myc* males to attain progeny that co-express HDAC4::YFP and DmHDAC4-Myc in all neurons. Whole cell lysates from heads of progeny were immunoprecipitated with anti-GFP and detected with anti-Myc (Section 2.7). A band, albeit faint of approximately 140 kDa was detected, demonstrating a direct physical interaction (Figure 3.8A).

A reciprocal co-IP was also carried out in which immunoprecipitation was performed with anti-Myc before being probed with anti-GFP (Figure 3.8B). A band of similar size (140 kDa) was expected and observed for this sample but not the controls.

Together, the individual IP assays performed on Ank2₁₉₀₋₉₄₆-HA and DmHDAC4-Myc have demonstrated antibody specificity and the co-IP performed on HDAC4::YFP and DmHDAC4-Myc demonstrate that the protocol can be used successfully to detect a direct physical interaction between two proteins.

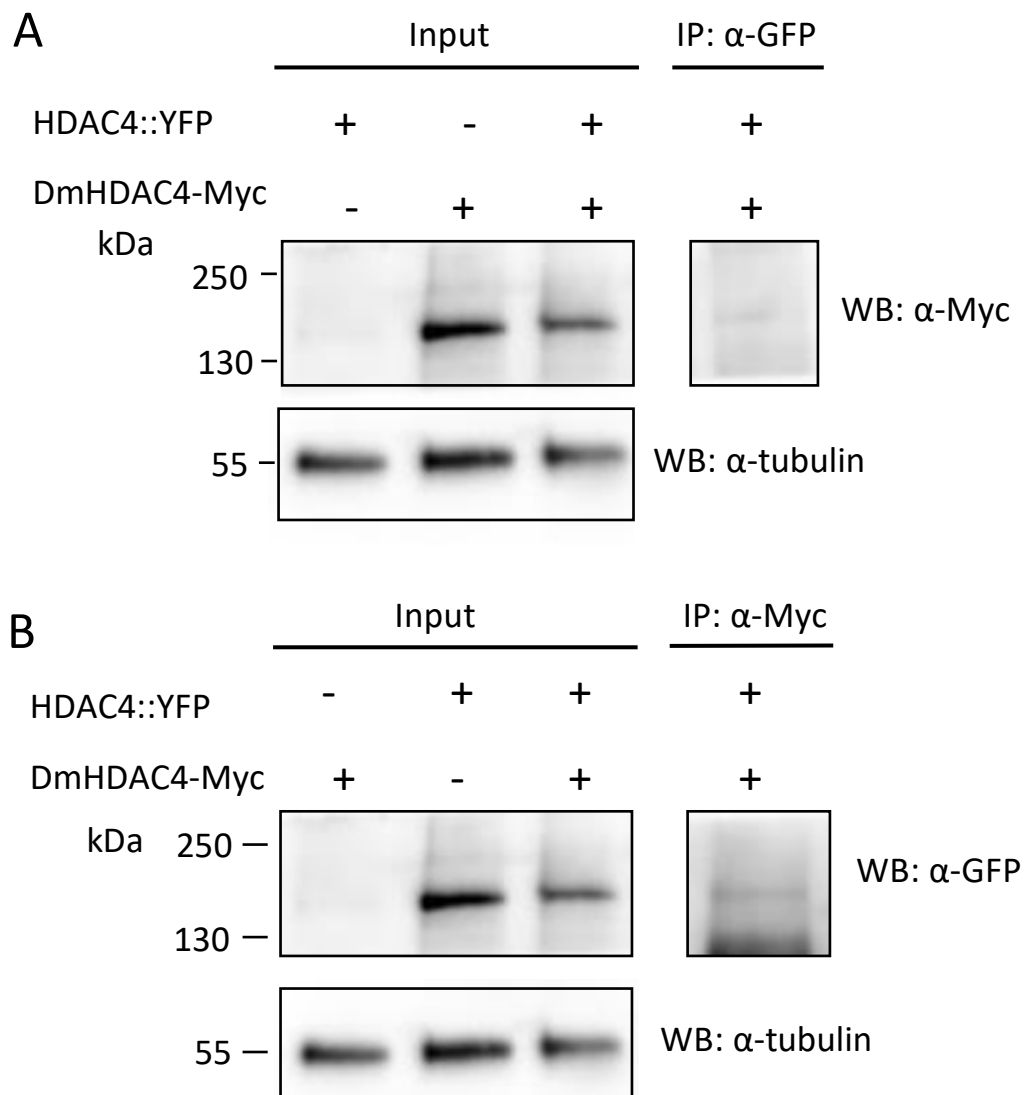


Figure 3.8. Positive co-IP control blots. Western blots demonstrating successful co-IP of HDAC4::YFP and DmHDAC4-Myc. (A) Lysates containing DmHDAC4-Myc and HDAC4::YFP were subjected to IP with anti-GFP and probed with anti-Myc. Inputs include HDAC4::YFP as a negative control and DmHDAC4-Myc and the strain containing both HDAC4::YFP and DmHDAC4-Myc as positive controls. (B) A reciprocal co-IP in which anti-Myc was used for IP followed by detection with anti-GFP. Inputs include DmHDAC4-Myc as a negative control and HDAC4::YFP and the strain containing both HDAC4::YFP and DmHDAC4-Myc as positive controls. Proteins were measured in kDa. Input samples = 30 μ g.

3.1.5 A physical interaction was not detected between Ank2₁₉₀₋₉₄₆-HA and DmHDAC4-Myc via co-IP

To determine whether there was an *in vivo* direct physical interaction between HDAC4 and Ank2, whole brain lysates from heads of flies co-expressing Ank2₁₉₀₋₉₄₆-HA and DmHDAC4-Myc were immunoprecipitated with anti-HA (Section 2.7) before being

subject to SDS-PAGE and western blotting (Section 2.6) with anti-Myc to detect Myc tagged DmHDAC4. A band of expected size (140 kDa) was not observed, even after prolonged exposure (Figure 3.9A).

A reciprocal co-IP was then performed to accurately rule out an *in vivo* physical interaction, where anti-Myc was used to immunoprecipitate DmHDAC4-Myc and anti-HA was used to detect Ank2₁₉₀₋₉₄₆-HA, and again a band of the expected size (90 kDa) was not observed (Figure 3.9B).

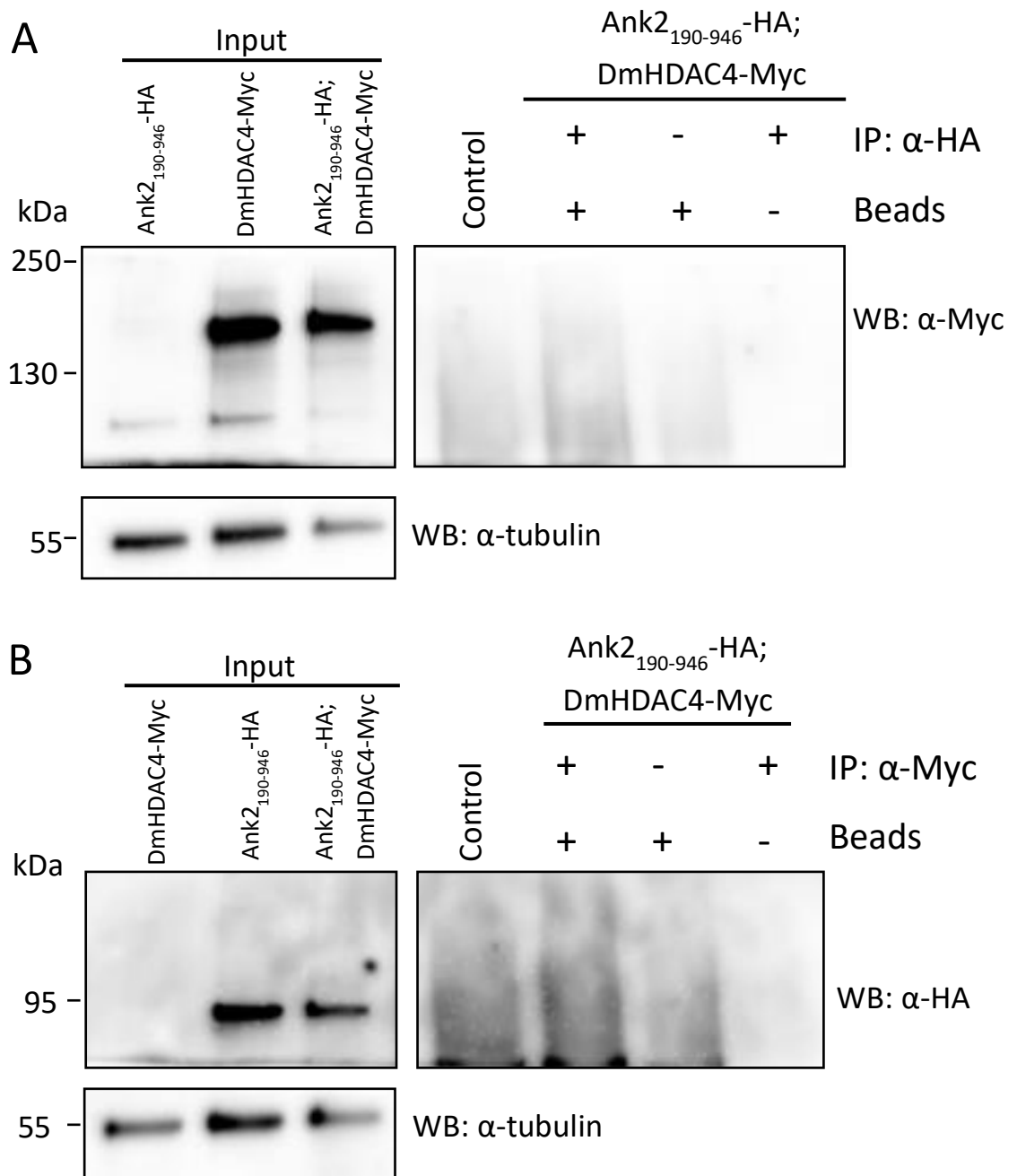


Figure 3.9. Ank2₁₉₀₋₉₄₆-HA and DmHDAC4-Myc do not physically interact via co-IP. Western blots on whole brain lysates from Ank2₁₉₀₋₉₄₆-HA, DmHDAC4-Myc and a strain containing both Ank2₁₉₀₋₉₄₆-HA and DmHDAC4-Myc following separation by SDS-PAGE. (A) Ank2₁₉₀₋₉₄₆-HA; DmHDAC4-Myc immunoprecipitated with anti-HA, however, DmHDAC4-Myc was not detected upon probing with anti-Myc. Ank2₁₉₀₋₉₄₆-HA was used as a negative control (denoted as control) and was immunoprecipitated with anti-HA before showing no detection with anti-Myc. DmHDAC4-Myc was not detected in negative IP controls where either anti-HA or protein A/G beads were omitted. Inputs include Ank2₁₉₀₋₉₄₆-HA as a negative control and DmHDAC4-Myc and Ank2₁₉₀₋₉₄₆-HA; DmHDAC4-Myc as positive controls. (B) In the reciprocal experiment, Ank2₁₉₀₋₉₄₆-HA; DmHDAC4-Myc was immunoprecipitated with anti-Myc, however Ank2₁₉₀₋₉₄₆-HA was not detected upon probing with anti-HA. DmHDAC4-Myc was used as a negative control (denoted as control) and was immunoprecipitated with anti-Myc before showing no detection with anti-HA. Negative IP controls were as stated above omitting either anti-Myc or protein A/G beads. Inputs include DmHDAC4-Myc as a negative control and Ank2₁₉₀₋₉₄₆-HA and

Ank2₁₉₀₋₉₄₆-HA; DmHDAC4-Myc as positive controls. Proteins were measured in kDa. Input samples = 30 µg.

3.2 What is the molecular basis of the genetic interaction between *HDAC4* and *Ank2*?

3.2.1 Does HDAC4 regulate *Ank2* expression?

Given the lack of evidence for a physical interaction, an alternative explanation for the genetic interaction between *HDAC4* and *Ank2* in eye development could be that HDAC4 represses expression of *Ank2*. *Ank2* is required for normal photoreceptor development, as knocking down *Ank2* to approximately 35% of wild-type expression (Schwartz, 2016) impaired normal eye development, as does overexpression of *HDAC4* (Schwartz et al., 2016). If increased expression of *HDAC4* resulted in a reduction of *Ank2* expression, then the combination of increased expression of *HDAC4* with a knockdown of *Ank2* could result in a further depletion of *Ank2* to a level low enough to result in a loss of function and severely impaired development of photoreceptors. However, previous experiments in which RNA-seq was performed on the heads of flies in which a nuclear-restricted mutant of human or *Drosophila HDAC4* was overexpressed in neurons revealed no significant change in *Ank2* expression when compared to controls of the same genetic background: human *HDAC4* vs control, log₂fold change = -0.47, padj (p-value adjusted for multiple testing) = 0.499 (Main, 2019) and *Drosophila HDAC4* vs control, log₂fold change = 0.28, padj = 0.1455 (Wei Jun Tan and Dr Helen Fitzsimons, unpublished data).

The possibility was also considered that *HDAC4* overexpression could alter the amount or stability of *Ank2* protein through an undetermined mechanism. As the *Ank2* protein is prohibitively large and the *Ank2* antibody is unsuitable for western blotting purposes, an *Ank2::EGFP* protein trap line consisting of an artificial EGFP exon inserted in frame within an *Ank2* intron was obtained (Kyoto Stock Centre). The expression of *Ank2::EGFP* has been confirmed by western blot using anti-GFP which produced a band of approximately 75 kDa which is consistent with one of the smallest *Ank2* isoforms (*Ank2-S1*) (Appendix 6.4) in which EGFP is inserted (Schwartz, 2016). This construct could therefore be used for further investigation of endogenous levels of *Ank2-S1*.

In addition to investigating whether overexpression of wild-type *HDAC4* alters the level of *Ank2* protein, several *HDAC4* mutants were also included so that if *HDAC4* does alter

Ank2 protein levels, these mutants could shed light on the specific mechanism involved. Recently, transgenic flies expressing mutant variants of human *HDAC4* (*hHDAC4*) were generated in which *hHDAC4* is restricted to the nucleus (*3SA* mutant) or cytoplasm (*L175A* mutant) in order to determine the relative roles of the nuclear and cytoplasmic pools of HDAC4 in neuronal dysfunction. Expression of *hHDAC4 3SA* was demonstrated to be detrimental to mushroom body development, eye development and long-term memory formation (Main, 2019). Transgenic flies expressing the corresponding *Drosophila* nuclear-restricted mutant named *3A* (to distinguish it from human *3SA*), has also been generated by Dr Helen Fitzsimons (Appendix 6.3). It has recently been observed that nuclear-restricted *Drosophila HDAC4 3A* also impairs eye development and mushroom body development (Wei Jun Tan, unpublished data) similarly to the *hHDAC4 3SA* mutant (Main, 2019). Other transgenic flies have also been generated, including two cytoplasmic-restricted *Drosophila* mutants Δ *MEF2*, which contains a mutation in the MEF2 binding domain, and Δ *NLS*, which contains a mutation in the nuclear localisation sequence, both of which impair HDAC4 nuclear import (Appendix 6.3). A catalytically inactive mutant *Y1142H* was also generated, which substitutes an essential tyrosine residue for a histidine residue rendering the *Drosophila HDAC4* deacetylase domain inactive as is seen in human HDAC4 (Appendix 6.3) (Lahm et al., 2007; Mielcarek et al., 2013; Sando et al., 2012). Another important component when uncovering whether HDAC4 regulates Ank2 is the ankyrin repeat binding domain on HDAC4 in which ankyrin repeat-containing proteins have been observed to interact with (Xu et al., 2012). A transgenic fly line harbouring *Drosophila HDAC4* with amino acid substitutions within the PxLPxI/L motif of the ankyrin repeat binding domain (Section 1.6) which is predicted to abolish binding to ankyrin repeats (mutation of PSLPNI to ASAANA) was generated by Dr Helen Fitzsimons and named *DmHDAC4 Δ Ank* (Appendix 6.3).

Elav-GAL4; Ank2::EGFP virgin female homozygotes were crossed to control *w(cs10)* (which is the background strain for *Ank2::EGFP*) as well as to each of the *DmHDAC4* wild-type and mutant transgenes via standard genetic crosses. Western blots were performed (Section 2.6) and probed for using anti-Myc as a control as all *DmHDAC4* transgenes have a C-terminal 6x Myc tag. Anti-GFP was used to probe for levels of *Ank2::EGFP* following crossing to the *DmHDAC4* mutants (Figure 3.10). When compared to the controls, it is difficult to determine whether increased *HDAC4* alters Ank2 protein levels or stability as the band intensity was variable. Furthermore, a pattern

was not visible when comparing the effect of nuclear vs cytoplasmic expression of *HDAC4* on *Ank2* as the two cytoplasmically restricted mutants *DmHDAC4* Δ *MEF2* and *DmHDAC4* Δ *NLS* differed in their levels of *Ank2* protein, therefore, the results of this blot remain inconclusive. Time constraints prevented this experiment from being repeated, however, these data show that each of the mutants were successfully expressed and repetition of the experiment and subsequent quantification of the bands will determine the impact of increased *HDAC4* on *Ank2* protein levels.

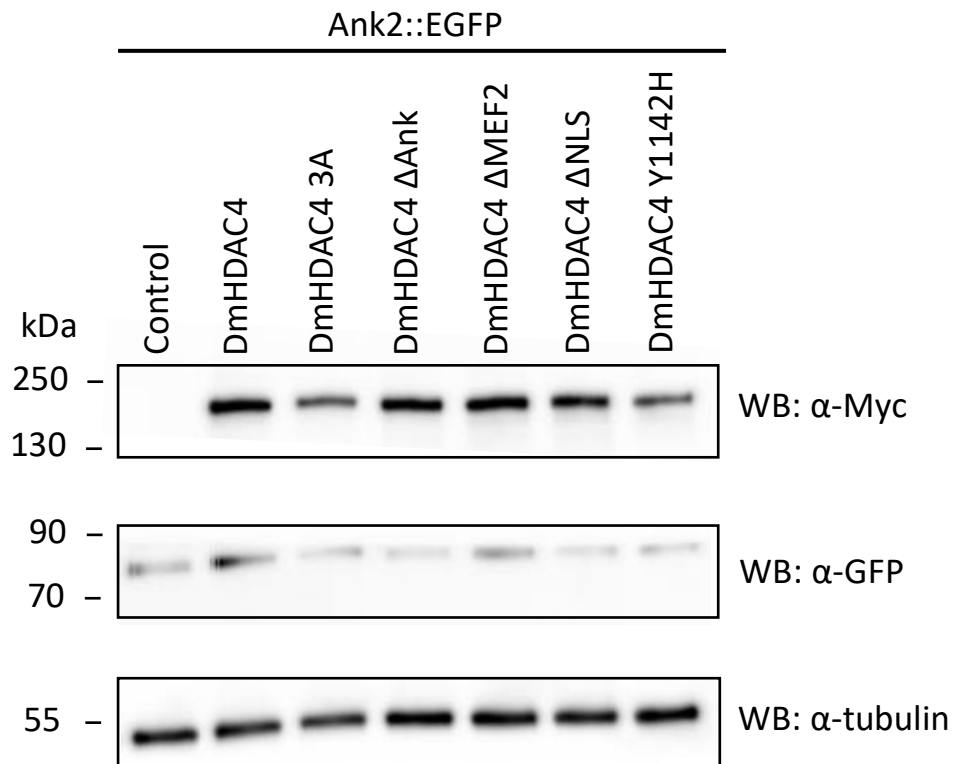


Figure 3.10. The effect of *DmHDAC4* regulation on *Ank2* protein level. Western blot of whole head lysates demonstrate the effect of expression of different *DmHDAC4* transgenes on *Ank2::EGFP* protein levels. Control consisted of *elav-GAL4* crossed to *w(cs10)*. All *DmHDAC4* transgenes are Myc tagged and crossed to *elav-GAL4; Ank2::EGFP*. Anti-Myc detected levels of *DmHDAC4* expression. Anti-GFP detected *Ank2::EGFP* protein levels. Proteins were measured in kDa. Protein loaded = 30 μ g.

3.2.2 Does *Ank2* regulate expression and/or subcellular distribution of *HDAC4* protein?

It was initially hypothesised that if *HDAC4* and *Ank2* physically interacted, that *Ank2* could potentially tether *HDAC4* in the cytoplasm, thus when *Ank2* was reduced, *HDAC4* would accumulate in the nucleus. This scenario is less likely based on the lack of detection

of a direct physical interaction between HDAC4 and Ank2. However, HDAC4 localisation is critical and disruptions in this balance leads to neurodevelopmental or neurodegenerative phenotypes (Li et al., 2012; Wu et al., 2017; Wu et al., 2016) therefore, the impact of *Ank2* knockdown on HDAC4 expression and subcellular distribution was examined. The *Ank2* RNAi that was utilised in this study was sourced from the Vienna *Drosophila* Resource Centre. This RNAi targets a portion of the C-terminal domain of the extra-long, long and medium isoforms of Ank2 (Appendix 6.4).

Firstly, it was examined whether the level of total HDAC4 protein in the cell was altered when *Ank2* RNAi was expressed, knocking down the longer Ank2 isoforms. As there is currently no *Drosophila* HDAC4 antibody suitable for detecting endogenous HDAC4 by western blotting, the previously established *HDAC4::YFP* trap line (Section 3.1) was used to detect levels of HDAC4. Virgin female flies carrying *elav-GAL4* and *HDAC4::YFP* were either crossed to *w(cs10)* (the background strain for *HDAC4::YFP*) or alleles carrying *UAS-Ank2* RNAi via standard genetic crosses. Whole cell lysates were generated and examined via western blot (Section 2.6) using an anti-GFP antibody to detect expression of *HDAC4::YFP* (Figure 3.11A). From these blots, it appears there may be a slight increase in *HDAC4::YFP* expression when *Ank2* is knocked down. To further analyse this, a normalised intensity plot was produced, where it was observed that there was a statistically significant increase in the level of HDAC4 protein when *Ank2* was reduced in the whole cell (Figure 3.11B).

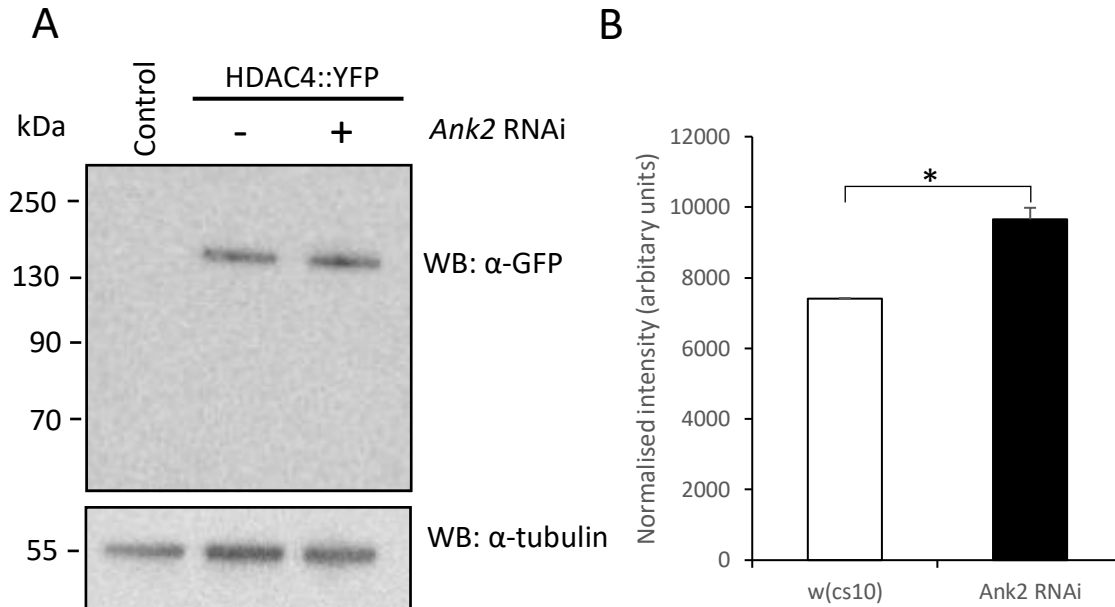


Figure 3.11. *Ank2* knockdown alters total HDAC4 protein levels. (A) Whole head lysates from negative control flies (*elav-GAL4* crossed to *w(cs10)*), positive control flies (*HDAC4::YFP* crossed to *w(cs10)*) and *HDAC4::YFP* crossed to *Ank2* RNAi flies were subjected to SDS-PAGE and western blotting using anti-GFP to detect endogenous HDAC4. Protein loaded = 30 μ g. (B) Bands were quantified from two replicate western blots to produce a normalised intensity plot showing the level of expression of HDAC4::YFP normalised to tubulin. Bars indicate +/- SEM. * = $p < 0.05$, Two-tailed unpaired Student's t-test, p -value = 0.04.

Prior to the investigation of whether knockdown of *Ank2* alters the subcellular distribution of HDAC4, the cell fractionation protocol required optimisation. In the past there has been difficulty in preparing nuclear fractions from *Drosophila* heads with minimal cytoplasmic contamination (Dr H. Fitzsimons, personal communication 22 June, 2020), therefore the NE-PER kit (Thermo) was selected as a protocol specifically detailing the use of this kit on *Drosophila* heads was available (Maitra et al., 2019). Following nuclear and cytoplasmic fractionation, western blotting was performed (Section 2.6) with antibodies to the nuclear lamin protein and the cytoplasmic alpha-tubulin protein in order to determine the purity of the fractions. Lamin was detected clearly only in the nuclear fraction, whereas tubulin was detected strongly in both the cytoplasmic and nuclear fractions (Figure 3.12A), indicating that the nuclear fraction was contaminated with cytoplasmic protein. The protocol was optimised by adding two wash steps between the collection of the cytoplasmic fraction and the final collection of the nuclear fraction as detailed in section 2.4.3. The resulting western blots were probed with anti-lamin and anti-tubulin. Lamin was again only found in the nuclear fraction, whereas tubulin was observed in all fractions, however, following the duplicate wash steps tubulin was present

at a significantly lower level in the nuclear fraction (Figure 3.12B). This optimisation allowed the impact of *Ank2* knockdown on the subcellular distribution of HDAC4 to now be assessed.

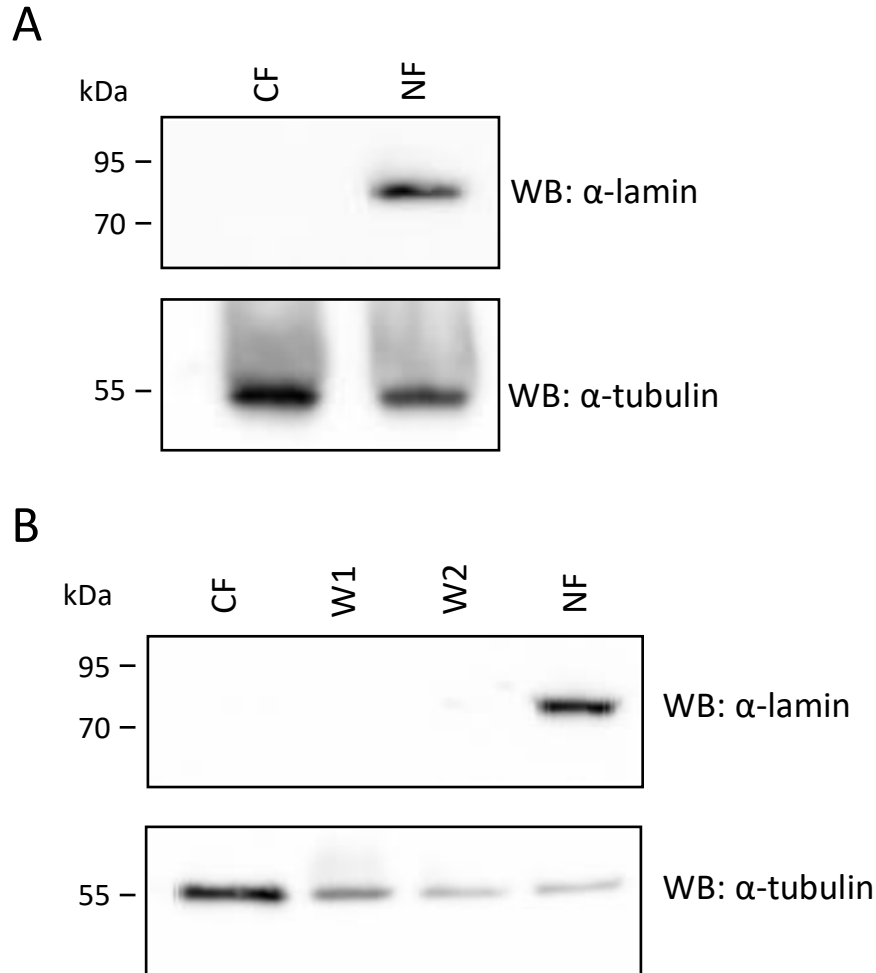


Figure 3.12. Cellular fractionation optimisation. (A) CF and NF of flies were subjected to SDS-PAGE and western blotting with anti-lamin to detect the nuclear fraction and anti-tubulin to detect the cytoplasmic fraction. (B) CF, W1, W2 and NF of flies were subjected to SDS-PAGE and western blotting using anti-lamin and anti-tubulin. Additional wash steps decreased the cytoplasmic contamination in the NF. Protein loaded = 30 μ g. Proteins were measured in kDa. Abbreviations: CF = cytoplasmic fraction, W1 = wash 1, W2 = wash 2, and NF = nuclear fraction.

To characterise the subcellular distribution of HDAC4 following knockdown of *Ank2*, virgin female flies carrying the pan-neuronal *elav-GAL4* driver and *HDAC4::YFP* were crossed to male flies harbouring the *UAS-Ank2* RNAi construct via a standard genetic cross in order to knockdown *Ank2* in all neurons during development. *elav-GAL4* flies were also crossed to *w(cs10)* flies (the background strain of *HDAC4::YFP*) as a negative

control. Nuclear and cytoplasmic fractions were isolated from heads of the progeny of each of the two crosses (Figure 3.13A).

In the cytoplasmic fraction there appeared to be a slight increase in *HDAC4::YFP* expression when *Ank2* was knocked down, but this was not significant (Figure 3.13B). In the nuclear fraction a doublet band was observed in each lane, however, as there was a single band also detected in the control, it was concluded that the topmost band was non-specific anti-GFP binding. The level of *HDAC4::YFP* expression was relatively equal between each of the nuclear fractions showing that there was no significant difference in HDAC4 protein levels in the nucleus following *Ank2* knockdown during development (Figure 3.13C).

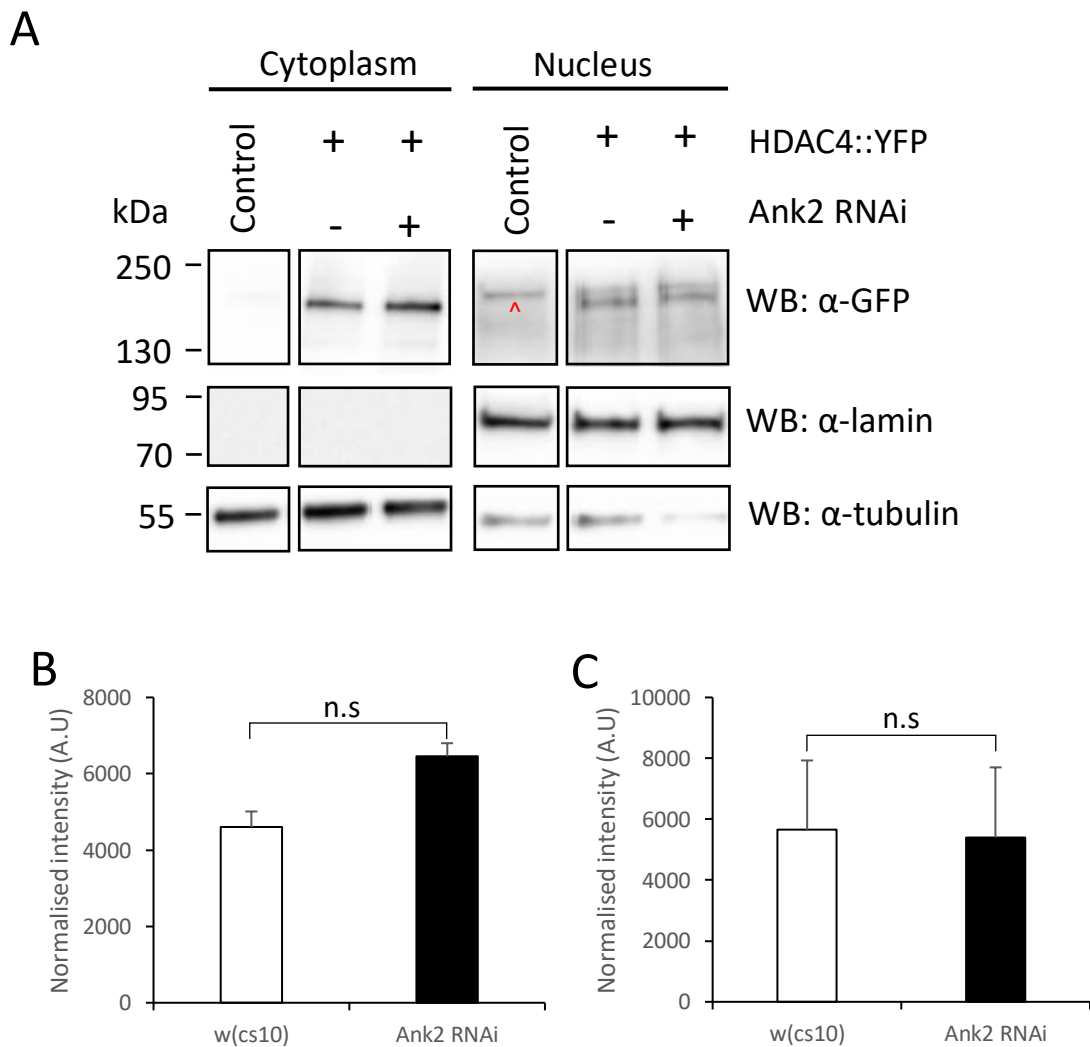


Figure 3.13. *Ank2* knockdown during development does not significantly affect *HDAC4* expression and subcellular localisation. Western blots demonstrating the nuclear and cytoplasmic subcellular distribution of HDAC4::YFP. (A) Nuclear and cytoplasmic head lysates from progeny of *elav-GAL4* flies crossed to *w(cs10)* (denoted as control), *HDAC4::YFP* crossed to *w(cs10)* and *HDAC4::YFP* crossed to *Ank2* RNAi were subjected to SDS-PAGE and western

blotting with an anti-GFP antibody. In the nuclear fraction a doublet band is present in both samples consisting of HDAC4::YFP, where the topmost band was also observed in the negative control, indicative of non-specific anti-GFP binding. Anti-lamin was used as a marker for the nuclear fraction and anti-tubulin was used as a marker for the cytoplasmic fraction. Protein loaded = 20 μ g. Proteins were measured in kDa. (B) Quantification of two replicate HDAC4::YFP bands in the cytoplasmic fraction, where no significant difference was observed on knockdown of *Ank2*. Two-tailed unpaired Student's t-test was performed, p-value = 0.132. (C) In the nuclear fraction, no significant difference was observed on knockdown of *Ank2* following quantification of two replicate bands. Two-tailed unpaired Student's t-test was performed, p-value = 0.96. n.s = not significant. Abbreviations: A.U = arbitrary units.

As *Ank2* knockdown in neurons during development results in impaired brain development (Schwartz, 2016), the TARGET system (Section 1.3.4.2) was used to restrict *Ank2* knockdown to the adult brain in case an abnormal brain structure impacted HDAC4 protein levels. *Elav-GAL4*, *HDAC4::YFP* flies were crossed to *Tub-Gal80ts* (Gal80ts under control of the alpha-tubulin promoter) as a control, and to *Tub-Gal80ts; Ank2 RNAi* to allow for temporal control of *Ank2* knockdown. Flies were raised at 18°C (at which transgene expression is inhibited) and following eclosion, adult flies were then placed at 30°C for three days to induce expression of *Ank2* RNAi. In both the cytoplasmic and nuclear fractions it appeared that the knockdown of *Ank2* in the adult brain slightly reduced the level of *HDAC4::YFP* (Figure 3.14A), however this difference was not statistically significant (Figure 3.14B, C).

These data suggest that *Ank2* may regulate the total protein level of HDAC4, as there was an overall increase in HDAC4::YFP when *Ank2* was reduced in the developing brain. There was, however, no significant alteration in the subcellular distribution of HDAC4 when *Ank2* was knocked down in the developing brain or when it was restricted to adulthood. These experiments, therefore, require repetition to determine if these results are reproducible.

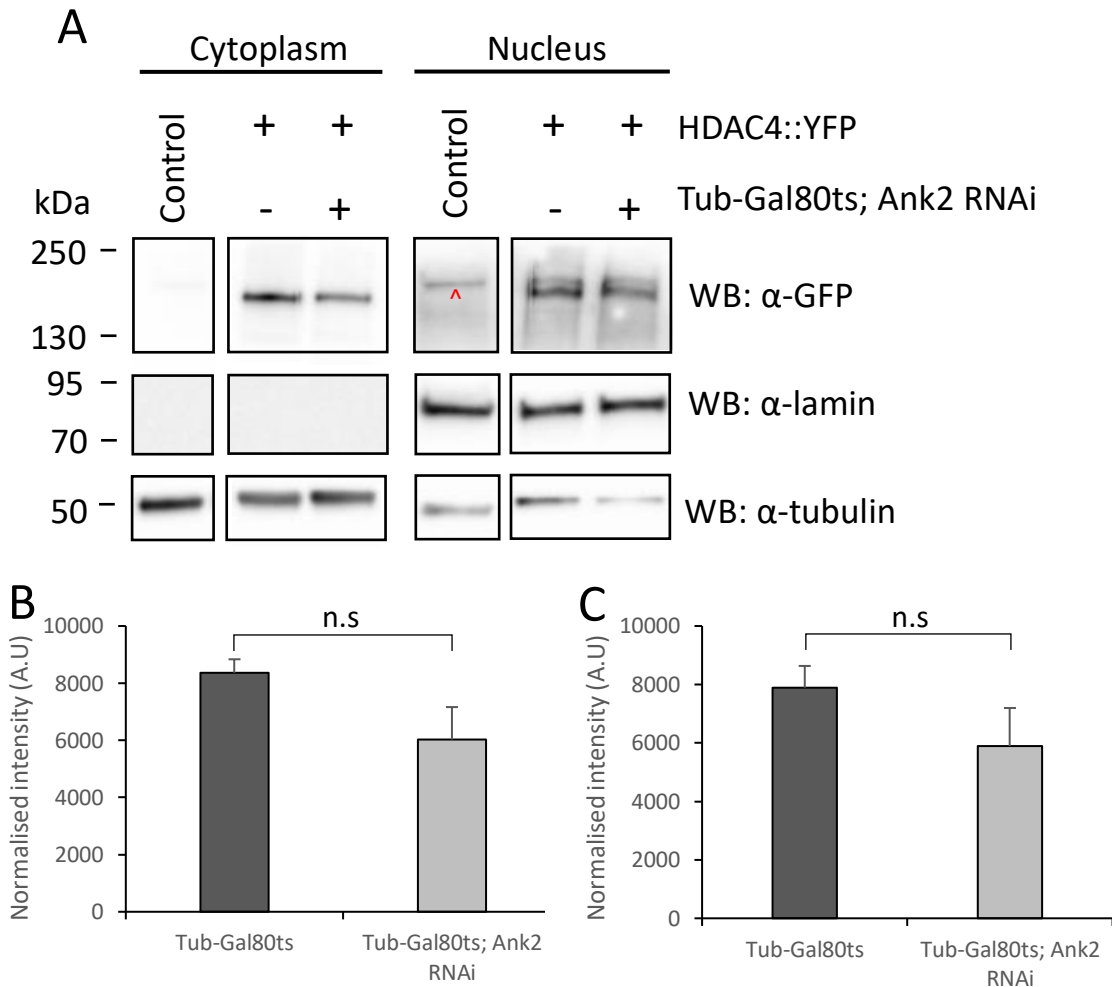


Figure 3.14. *Ank2* knockdown in the adult brain does not significantly affect *HDAC4* expression and subcellular localisation. Western blots demonstrating the nuclear and cytoplasmic subcellular distribution of HDAC4::YFP. (A) Nuclear and cytoplasmic head lysates from progeny of *elav-GAL4* crossed to *w(cs10)* (denoted as control) and HDAC4::YFP crossed to either *Tub Gal80ts* as a control or *Tub-Gal80ts; Ank2* RNAi to induce *Ank2* knockdown specifically in the adult brain. HDAC4::YFP was detected with anti-GFP, where again, in the nuclear fraction a doublet band was present, indicative of non-specific anti-GFP binding. Anti-lamin was used as a marker for the nuclear fraction and anti-tubulin was used as a marker for the cytoplasmic fraction. Protein loaded = 20 μ g. Proteins were measured in kDa. (B) In the cytoplasmic fraction, no significant difference was observed between samples following quantification of two replicate western blot bands. Two-tailed unpaired Student's t-test was performed, p-value = 0.312. (C) In the nuclear fraction, no significant difference was observed between samples following quantification of two replicate bands. Two-tailed unpaired Student's t-test was performed, p-value = 0.446. n.s = not significant, A.U = arbitrary units.

3.3 Examining the genetic interaction between *HDAC4* and *Ank2* in photoreceptors

The results generated in this study indicate that HDAC4 and Ank2 do not interact physically therefore, the previously identified genetic interaction in the *Drosophila* eye

(Schwartz, 2016) was further examined in an attempt to shed light on the nature of this interaction.

One unanswered question so far is whether the activity of HDAC4 in the nucleus or cytoplasm is required for the genetic interaction. Investigating this could aid in narrowing down the pathway through which HDAC4 and *Ank2* interact.

As the expression of nuclear-restricted human *HDAC4 3SA* displayed detrimental phenotypes in mushroom body, eye and long-term memory development (Main, 2019), investigating the role that the corresponding *Drosophila HDAC4 3A* mutant plays in conjunction with *Ank2* RNAi in eye development was of interest. Therefore, the genetic interaction between wild-type *DmHDAC4* and *Ank2* could be compared to that of *DmHDAC4 3A* and *Ank2*.

A second unanswered question is whether the genetic interaction is dependent on binding of ankyrin repeat protein(s) to HDAC4. If not, this would provide further confirmation that the genetic interaction between *HDAC4* and *Ank2* is not through direct physical binding. To this end, examining the eye phenotype resulting from expression of *DmHDAC4 ΔAnk*, a transgene which contains a mutated ankyrin repeat binding domain, would unveil whether binding of ankyrin repeat-containing proteins is essential for the *HDAC4* overexpression-induced rough eye phenotype and whether HDAC4 can retain the genetic interaction with *Ank2*.

3.3.1 A phenotypic eye screen showing the effect of *Ank2* knockdown in combination with *Drosophila HDAC4* mutants

To test for a genetic interaction between *Ank2* and the *DmHDAC4* mutants, the glass multimer reporter (GMR) driver was used to drive expression in all post mitotic cells posterior to the morphogenetic furrow in the developing eye (Freeman, 1996). The eyes of the F1 progeny were then analysed via light microscopy (Section 2.8.1) and scanning electron microscopy (SEM) (Section 2.8.2).

To provide a semi-quantitative analysis of SEM images, a rough eye phenotype scoring system was developed to categorise the severity of the rough eye phenotype. The scoring system produced a score from 0 – 1, with 0 appearing wild-type and 1 the most severe phenotype. The system was as follows; 0 (wild-type) consisted of normal ommatidia

alignment with no fusion and a wild-type array of mechanosensory bristles positioned between each ommatidium. A score of 0.25 (mild) was given if one of the following phenotypes was observed: between 5 - 10 instances of multiple bristles from one pore or missing bristles, mild ommatidia disorganisation or fusion of ommatidia in up to two areas. A score of 0.5 (moderate) was given if all mild phenotypes were collectively observed or if one of the following phenotypes was observed; between 10 – 20 instances of multiple bristles from one pore or missing bristles, moderate disorganisation or fusion of ommatidia in up to five areas. A score of 0.75 (major) was given if all moderate phenotypes were collectively observed or if one of the following phenotypes was observed: more than 20 instances of multiple bristles from one pore or missing bristles, major disorganisation, fusion of ommatidia in up to 10 areas with few large areas of fusion or up to 50 collapsed ommatidia. A score of 1 (severe) was given if all major phenotypes were collectively observed or if one of the following phenotypes was observed: severe disorganisation, fusion in more than 10 areas or multiple large patches, more than 50 collapsed ommatidia or severe collapsing of ommatidia resulting in central hole-like cavities (Table 3.1). This semi-quantitative analysis was based on observations of phenotypes resulting from overexpression of *HDAC4* in previous studies in this laboratory (Schwartz et al., 2016) as well as the more severe phenotypes resulting from expression of two copies of *HDAC4* (Schwartz, 2016).

Wild-type 0	Mild 0.25	Moderate 0.5	Major 0.75	Severe 1
Normal	1 mild	3 mild OR	4 moderate OR	4 major OR
	Between 5-10 occurrences of multiple bristles/missing bristles	Between 10-20 occurrences of multiple bristles/missing bristles	More than 20 occurrences of multiple bristles/missing bristles	
	Mild disorganisation	Moderate disorganisation	Major disorganisation	Severe disorganisation
	Fusion in up to 2 areas	Fusion in up to 5 areas	Fusion in up to 10 areas/few big areas of fusion	Fusion in more than 10/large areas of fusion
		Less than 20 ommatidia with crevices	Up to 50 ommatidia with crevices	More than 50 crevices
				Hole-like necrotic cavities in the ommatidia

Table 3.1. Semi-quantitative rough eye phenotype analysis. Scoring system developed for analysis of SEM images of fly eyes from each mutant genotype.

Control flies (*GMR-GAL4* crossed to the background *w(cs10)* strain) showed predominantly normal ommatidia alignment and no evidence of ommatidia fusion (Figure 3.15A). Knockdown of *Ank2* resulted in a moderate rough eye phenotype where collapsed ommatidia were observed in the scanning electron micrographs. Ommatidia were slightly misaligned and there were patches lacking mechanosensory bristle formation (Figure 3.15B). In a previous study overexpression of wild-type *HDAC4* resulted in a mild rough eye phenotype (Schwartz, 2016), however, in this current study, the phenotype was slightly more severe as the flies were raised at a two-degree higher temperature of 27°C. At this temperature the *GAL4* transcriptional transactivator was more active and therefore drives a higher level of transgene expression (Duffy, 2002), resulting in a moderate rough eye phenotype. This consisted of disorganised ommatidia alignment with few areas of ommatidia fusion (Figure 3.15C). Expression of the nuclear restricted *DmHDAC4 3A* mutant resulted in a slightly more severe rough eye phenotype compared to wild-type *DmHDAC4* with misaligned and fused ommatidia as well as a lack of bristle formation (Figure 3.15D). Expression of *DmHDAC4 ΔAnk* also resulted in a moderate rough eye

phenotype consisting of ommatidia fusion and misalignment (Figure 3.15E), indicating that the ankyrin binding domain is not required for the *HDAC4* overexpression-induced eye defects. It should also be noted that the phenotype analysed under light microscopy of the *DmHDAC4 ΔAnk* eyes appeared slightly more severe than wild-type *DmHDAC4* with a pronounced loss of pigmentation, which was not observable in the SEM images. When *Ank2* RNAi and either wild-type or each *DmHDAC4* transgene were co-expressed, a severe rough eye phenotype consisting of major areas of ommatidia fusion and severe misalignment was observed for all three genotypes (Figure 3.15 F, G, H), indicative of a genetic interaction.

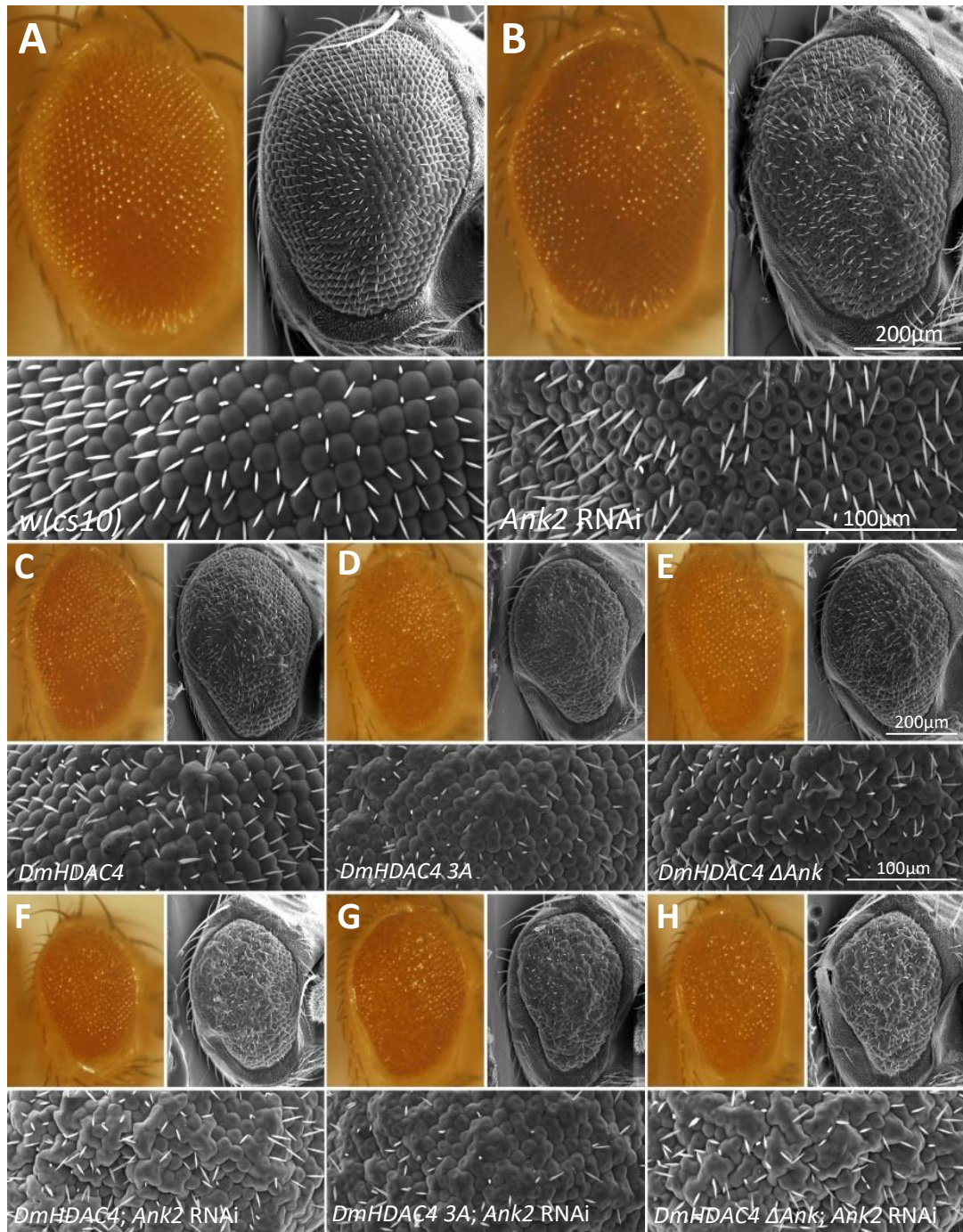


Figure 3.15. *Ank2* RNAi enhancement of the *DmHDAC4* overexpression-induced rough eye phenotype. Light and scanning electron microscope (SEM) images of the rough-eye phenotypes. *GMR-GAL4* was used to express the following UAS-fused transgenes in the eye. (A) *w(cs10)*, (B) *Ankyrin2 (Ank2)*, (C) *DmHDAC4*, (D) *DmHDAC4 3A*, (E) *DmHDAC4 ΔAnk*. (F) *DmHDAC4* and *Ank2* RNAi, (G) *DmHDAC4 3A* and *Ank2* RNAi, (H) *DmHDAC4 ΔAnk* and *Ank2* RNAi. Scale bars are as indicated in figure.

The semi-quantitative rough eye phenotype scores were calculated and averaged for each genotype (Table 3.2). These scores were taken from analyses of the SEM images.

Genotypes	Wild-type (0)	Mild (0.25)	Moderate (0.5)	Major (0.75)	Severe (1)	n
<i>w(cs10)</i>	71% (15)	29% (6)	0%	0%	0%	21
<i>Ank2 RNAi</i>	5% (1)	14% (3)	14% (3)	24% (5)	43% (9)	21
<i>DmHDAC4</i>	0%	11% (2)	47% (9)	21% (4)	21% (4)	19
<i>DmHDAC4; Ank2 RNAi</i>	0%	0%	0%	20% (4)	80% (16)	20
<i>DmHDAC4 3A</i>	0%	0%	10% (2)	50% (10)	40% (8)	20
<i>DmHDAC4 3A; Ank2 RNAi</i>	0%	0%	0%	0%	100% (13)	13
<i>DmHDAC4 ΔAnk</i>	0%	0%	50% (10)	20% (4)	30% (6)	20
<i>DmHDAC4 ΔAnk; Ank2 RNAi</i>	0%	0%	0%	11% (2)	89% (17)	19

Table 3.2. Rough eye phenotype scores. The frequency of each phenotype was denoted as a percentage with phenotypes ranging from wild-type to severe. The total number of compound eyes analysed are seen in the far-right column denoted as n.

Statistical analysis revealed that there was a significant increase in severity of the rough eye phenotype for the wild-type *DmHDAC4* and *DmHDAC4 ΔAnk* transgenes when co-expressed with *Ank2 RNAi* (Figure 3.16 A, C). Although *DmHDAC4 3A* co-expressed with *Ank2 RNAi* resulted in a severe phenotype in 100% of eyes, this was not statistically significant in comparison to the *DmHDAC4 3A* transgene expression, as expression of *DmHDAC4 3A* alone resulted in a significantly severe rough eye phenotype (Figure 3.16 B). It should be noted that this scoring system is arbitrary as the biological relevance for relative weighting of phenotypes is not known. When the phenotype scores are averaged, it appeared that the phenotypic effects were additive, however when the proportion of eyes exhibiting a severe phenotype were compared, a synergistic interaction was observed (Figure 3.16 D).

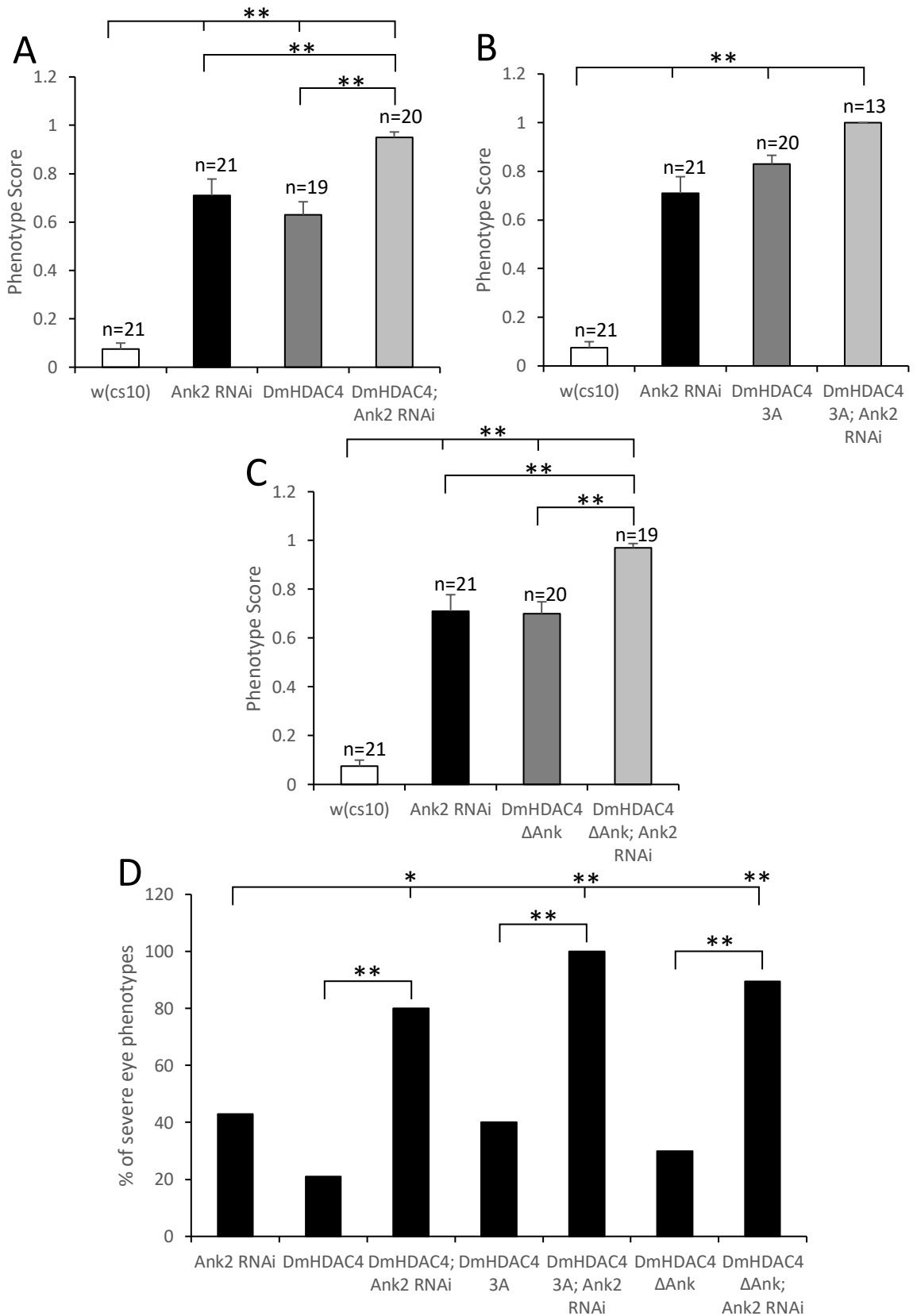


Figure 3.16. Phenotype scores for the *DmHDAC4* transgenes and *Ank2* RNAi. The average rough eye phenotype scores of each genotype are shown. Bars indicate \pm SEM. * = $p < 0.05$, ** = $p < 0.01$ following one-way ANOVA and post-hoc Tukey test for significance. (A) p-values: $w(cs10):Ank2$ RNAi = 0.001, $w(cs10):DmHDAC4$ = 0.001,

w(cs10):DmHDAC4; Ank2 RNAi = 0.001, *Ank2 RNAi:DmHDAC4* = 0.011, *DmHDAC4:DmHDAC4; Ank2 RNAi* = 0.001. (B) p-values: *w(cs10):Ank2 RNAi* = 0.001, *w(cs10):DmHDAC4 3A* = 0.001, *w(cs10):DmHDAC4 3A; Ank2 RNAi* = 0.001. (C) p-values: *w(cs10):Ank2 RNAi* = 0.001, *w(cs10):DmHDAC4 ΔAnk* = 0.001, *w(cs10):DmHDAC4 ΔAnk; Ank2 RNAi* = 0.001, *DmHDAC4 ΔAnk:DmHDAC4 ΔAnk; Ank2 RNAi* = 0.001. (D) The percentage of eyes displaying severe phenotypes are shown for each genotype. * = $p < 0.05$, ** = $p < 0.01$ following one-tailed Fisher's exact test. p-values: *Ank2 RNAi:DmHDAC4; Ank2 RNAi* = 0.247, *Ank2 RNAi:DmHDAC4 3A; Ank2 RNAi* = 0.0006, *Ank2 RNAi:DmHDAC4 ΔAnk; Ank2 RNAi* = 0.0028, *DmHDAC4:DmHDAC4; Ank2 RNAi* = 0.0004, *DmHDAC4 3A:DmHDAC4 3A; Ank2 RNAi* = 0.0005, *DmHDAC4 ΔAnk:DmHDAC4 ΔAnk2; Ank2 RNAi* = 0.0002.

In addition to the severe eye phenotypes observed above, it was also noted that the eye was physically smaller when *Ank2* RNAi was co-expressed with each *DmHDAC4* transgene compared to wild-type control eyes. This notable phenotype was therefore, investigated in more detail.

Co-expression of *Ank2* RNAi with each of the *DmHDAC4* transgenes resulted in smaller and more deformed eyes (Figure 3.17). A reduction in eye size may suggest activation or upregulation of apoptotic signalling pathways, for example, the wingless pathway, which has recently been implicated in compound eye patterning and is essential in pupal cell death (Cordero et al., 2004).

To determine the sizes of each eye for comparison between genotypes, ImageJ software was used to draw a line surrounding the eye and calculate the area in arbitrary units.

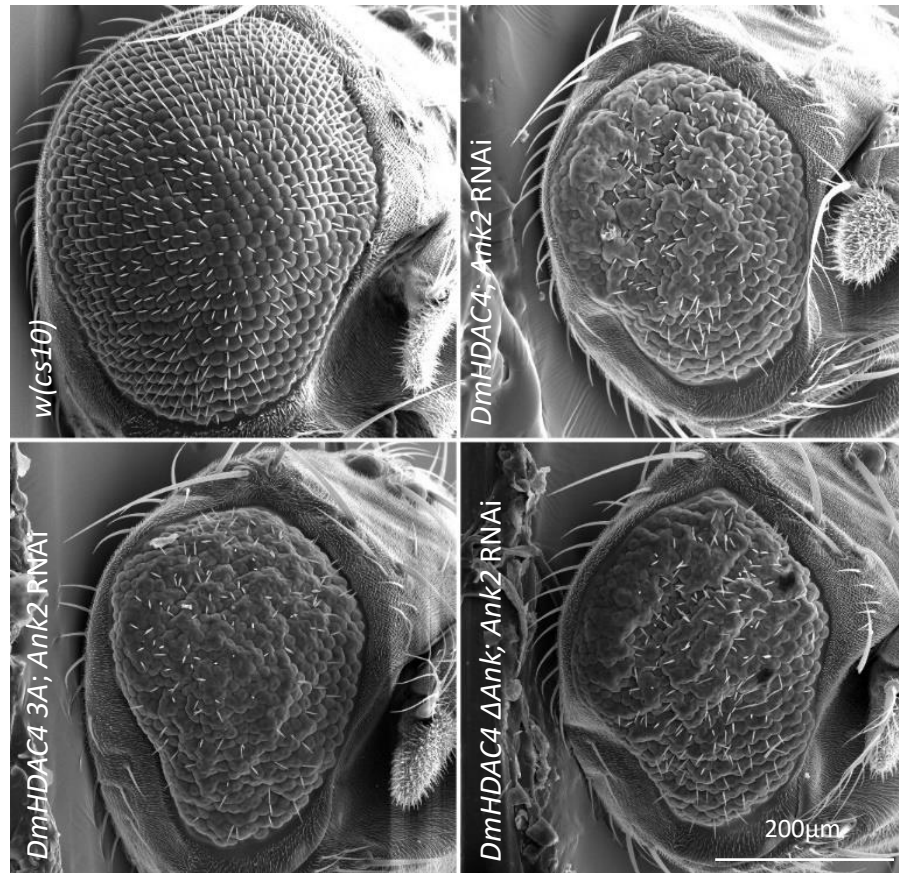


Figure 3.17. Reduced eye sizes observed when *DmHDAC4* transgenes are co-expressed with *Ank2* RNAi. Compared to *w(cs10)* control eyes, co-expression of *Ank2* RNAi with wild-type *DmHDAC4*, *DmHDAC4 3A* and *DmHDAC4 ΔAnk* resulted in physically smaller eyes. Scale bar is as indicated in the figure.

The scanning electron microscopy images that were attained for the rough eye phenotype analysis were measured for eye shape and size. Wild-type male *Drosophila* are smaller in body and head size (Mathews et al., 2017), which is not accounted for in this analysis, however, as all samples contained this combination of males and females this level of variability is controlled between samples. For this reason, all eye measurements were plotted as box and whisker graphs to demonstrate the distribution of eye sizes.

The co-expression of *Ank2* RNAi with either wild-type or mutant *DmHDAC4* resulted in significantly smaller eyes than *w(cs10)* control eyes. Co-expression of wild-type *DmHDAC4* and *DmHDAC4 ΔAnk* with *Ank2* RNAi also resulted in significantly smaller eyes than each transgene individually (Figure 3.18A, C), however, co-expression of *DmHDAC4 3A* and *Ank2* RNAi did not significantly reduce eye sizes compared to *DmHDAC4 3A* alone (Figure 3.18B).

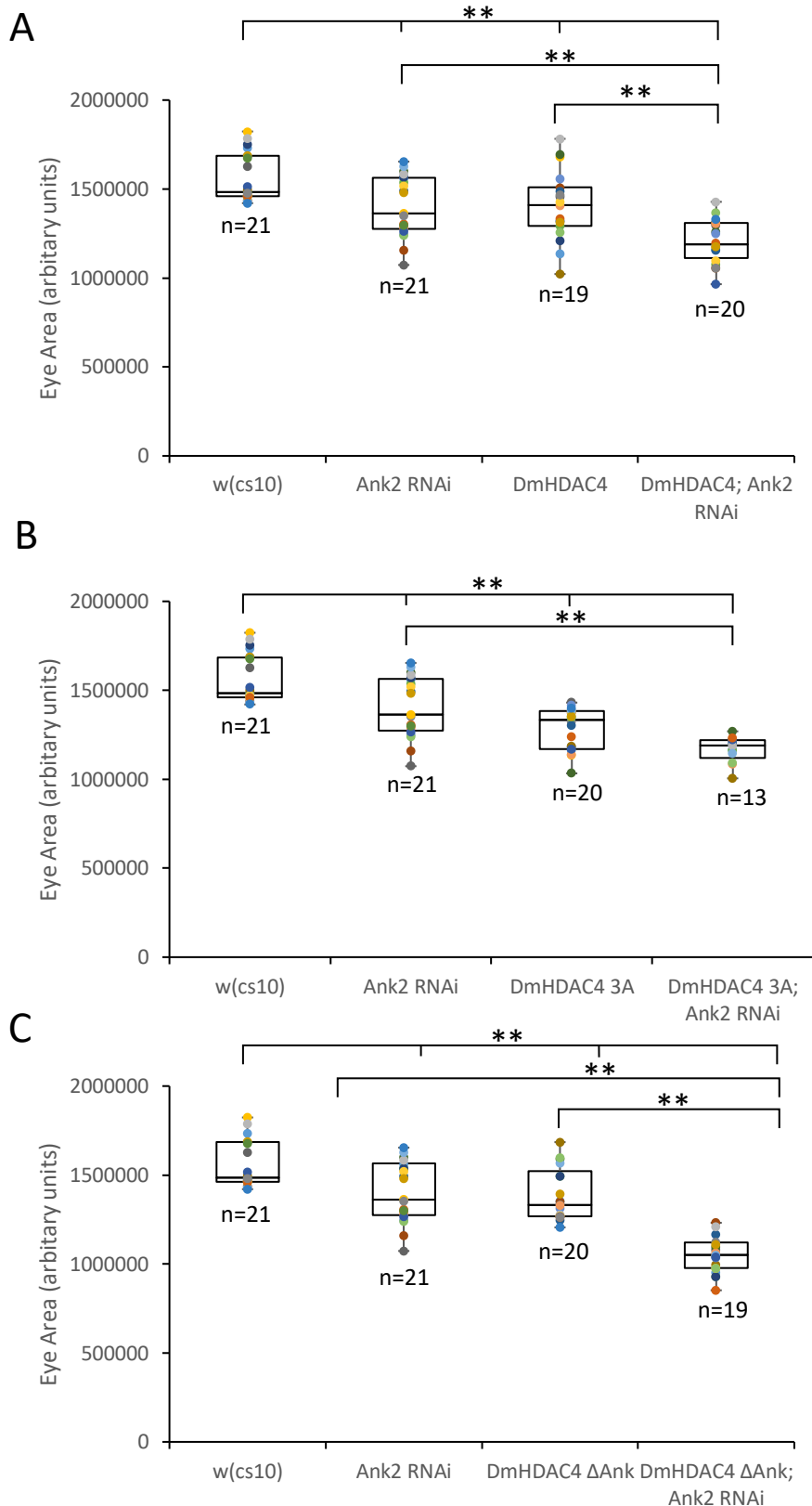


Figure 3.18. Box and whisker plot showing eye area changes observed by co-expression of *DmHDAC4* transgenes and *Ank2* RNAi. Scanning electron microscope images were analysed in ImageJ to produce area measurements of each eye within a sample. Box and whisker plots were produced with the coloured dots showing each eye measurement. ** = $p < 0.01$ following one-way ANOVA and post-hoc Tukey test for significance. (A) p-values: *w(cs10):Ank2* RNAi =

0.007, $w(cs10):DmHDAC4 = 0.009$, $w(cs10):DmHDAC4; Ank2$ RNAi = 0.001, $Ank2$ RNAi: $DmHDAC4$; $Ank2$ RNAi = 0.001, $DmHDAC4:DmHDAC4; Ank2 = 0.001$. (B) p-values: $w(cs10):Ank2$ RNAi = 0.007, $w(cs10):DmHDAC4$ 3A = 0.001, $w(cs10):DmHDAC4$ 3A; $Ank2$ RNAi = 0.001, $DmHDAC4$ 3A: $DmHDAC4$ 3A; $Ank2$ RNAi = 0.285. (C) p-values: $w(cs10):Ank2$ RNAi = 0.007, $w(cs10):DmHDAC4 \Delta Ank = 0.001$, $w(cs10):DmHDAC4 \Delta Ank; Ank2$ RNAi = 0.001, $DmHDAC4 \Delta Ank:DmHDAC4 \Delta Ank; Ank2$ RNAi = 0.001. n = number of eyes per sample.

This analysis of the reduction in eye size further confirms the genetic interaction previously observed between *Ank2* RNAi and wild-type *DmHDAC4*, and that the presence of the ankyrin repeat binding domain is not required for the genetic interaction between *HDAC4* and *Ank2*. The phenotypes observed when the *DmHDAC4* 3A transgene is co-expressed with *Ank2* RNAi in the eye becomes more severe, further suggesting that the genetic interaction with *Ank2* is mediated through nuclear *HDAC4*.

3.3.2 Characterisation of additional eye phenotypes that were observed

Knockdown of *Ank2* in the eye produced an interesting phenotype, where in over 60% of the eyes analysed, a large proportion of the ommatidia were collapsed inwards. As this was a common occurrence only within this genotype it is possible that this is a major phenotype that has not yet been reported for this gene. It appears as if the centre of each ommatidia was initially formed before collapsing in on itself (Figure 3.19A).

Co-expression of wild-type or *DmHDAC4* transgenes with *Ank2* RNAi resulted in ommatidia containing a central hole-like cavity (Figure 3.19 B, C, and D). As opposed to the phenotypes seen when *Ank2* was knocked down, these holes appear to be more severe than the collapse of an ommatidia. These hole-like structures appear as pin pricks in the centre of the ommatidia usually in large areas of ommatidia fusion and could be referred to as a previously characterised “blueberry phenotype” (Basler et al., 1990). Further analysis of this phenotype may assist in identifying the molecular pathways through which *HDAC4* and *Ank2* act to regulate neuronal development in the eye.

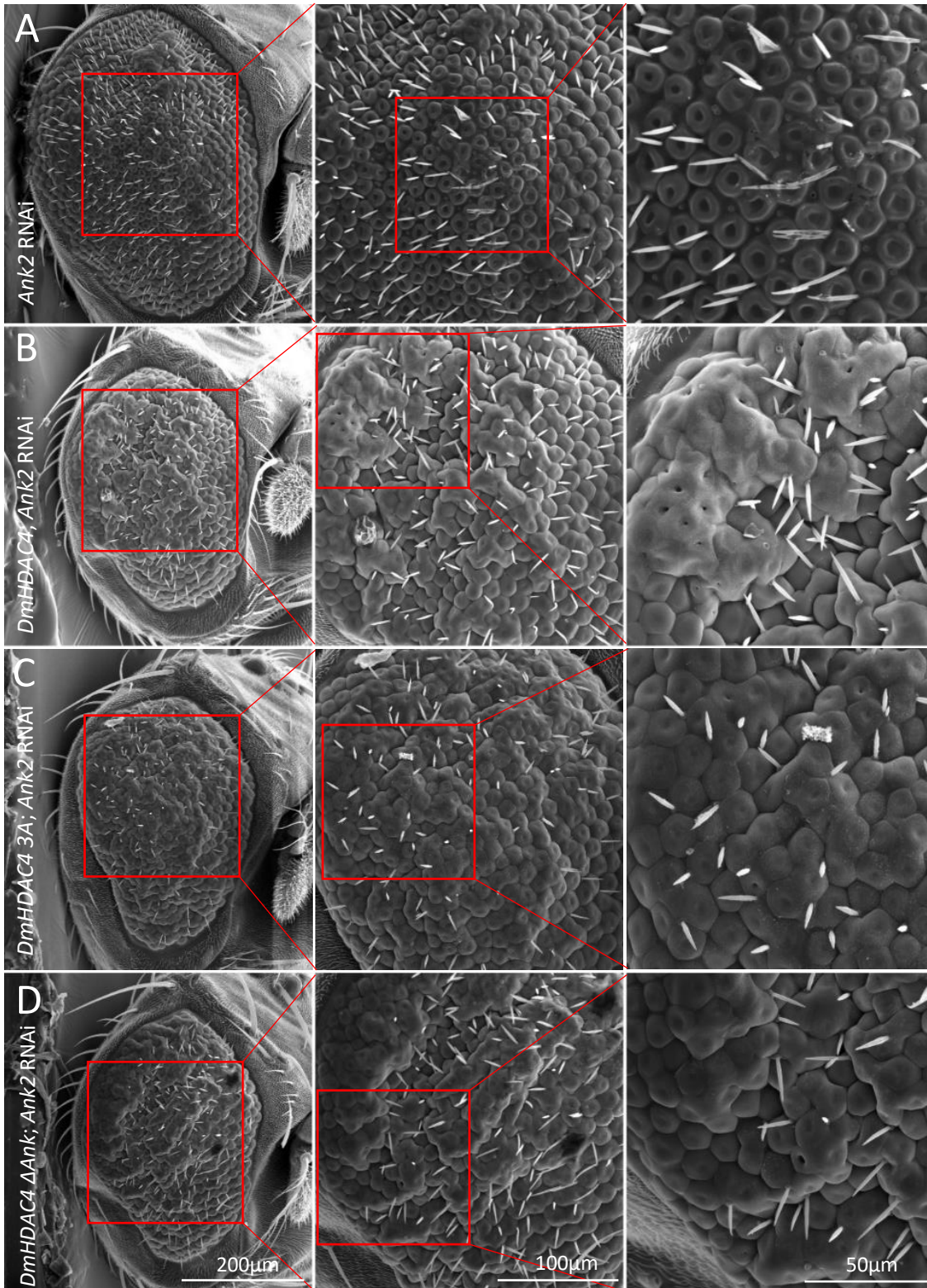


Figure 3.19. “Blueberry” phenotype observed upon *Ank2* RNAi and *DmHDAC4* transgene co-expression. Scanning electron microscopy demonstrated malformation or degenerative phenotypes when *DmHDAC4* mutants were co-expressed with *Ank2* RNAi. (A) *GMR-GAL4* induced expression of *Ank2* RNAi results in malformed or degenerated R7/8 photoreceptors in the ommatidia creating a group of collapsed ommatidia. (B, C, D) Co-expression of (B) *DmHDAC4*, (C) *DmHDAC4 3A*, (D) *DmHDAC4 ΔAnk* and *Ank2* RNAi resulted in degenerated

ommatidia resulting in necrotic craters in the centre of the ommatidia, indicative of the “blueberry” phenotype. Scale bars are as indicated in figure.

3.4 Investigation of the neurodevelopmental role of *HDAC4* and *Ank2* in dendrite morphogenesis

Following confirmation that *HDAC4* and *Ank2* interact genetically during eye development, it was investigated as to whether this interaction was also important in the morphogenesis of dendrites, since the synaptic plasticity that underlies learning and memory requires rearrangement of the actin cytoskeleton at dendritic spines (Lamprecht & LeDoux, 2004).

During *Drosophila* embryonic and larval stages, *Ank2* mutants display a reduction of dendritic branching. In *Drosophila* dopaminergic neurons, knockdown of *Ank2* resulted in decreased dendritic branching points, leading to a reduced total branch length and a lack of branching complexity (Avery et al., 2017). *Ank2* is also required for maintaining the dendritic spines in the mouse hippocampus as *Ank2* knockout mice have reduced dendritic spine complexity (Piguel et al., 2019). In addition, in the mouse hippocampus, it was observed that a double knockout of *HDAC4* and *HDAC5* resulted in an increase in dendrite arborisation, thereby increasing the complexity at the dendritic spines (Zhu et al., 2019). Interestingly, in cultured rodent hippocampal neurons increased nuclear *HDAC4* also resulted in a reduction in the complexity and length of dendritic branching, however, the number of dendritic spines remained unchanged (Litke et al., 2018). Currently, it is not yet known whether *Drosophila* *HDAC4* plays a role in dendrite morphogenesis.

This study initially aimed to investigate whether wild-type *Drosophila* *HDAC4* interacts with *Ank2* in dendrite morphogenesis similarly to the approach taken in the eye, and if an interaction was observed, it would then be of interest to investigate the previously described *DmHDAC4* mutant transgenes.

In addition, since knockdown of *HDAC4* impaired memory formation in both rodents (Kim et al., 2012) and *Drosophila* (Fitzsimons et al., 2013) (Section 1.5.2) and dendrite arborisation in the mouse as described above, it was also investigated whether there was a genetic interaction when both *HDAC4* and *Ank2* were reduced. This would suggest that

HDAC4 and *Ank2* act together to promote normal memory formation, in addition to requiring an interaction with *Ank2* to elicit the impairments resulting from increased nuclear abundance of *HDAC4*.

Branching and elongation of Kenyon cell dendrites is difficult to visualise therefore, the LPTCs of the visual system were used as a model (Section 1.3.3).

The vertical system consists of six neurons that span the dorsal-ventral axis of the lobula plate (Scott et al., 2002) and can be genetically targeted with the *3A-GAL4* driver which promotes expression predominantly in these neurons. The dendrites of the vertical system can be visualised by genetic tagging with *Lifect* which is an F-actin binding protein fused to GFP, which acts as a marker for the F-actin rich dendrites and is thus ideal for simple visualisation (Riedl et al., 2008).

Normal dendritic shaft growth differs between each of the six neurons in the visual system (VS) (Figure 3.20). The most lateral neuron (VS1) contains a main dendritic shaft that extends laterally before sweeping ventrally. This cell often contains one or more major dorsal projecting branches. The VS2 neuron is the next most laterally projecting cell, this neuron differs from the VS1 as the main shaft is less complex and often lacks branches, however, the main dendritic shaft also projects laterally before sweeping and extending ventrally. VS3 and VS4 both consist of a ventrally sweeping main shaft and a major dorsal projecting branch. VS3 appears to extend its main shaft more laterally than that of VS4. The major VS4 dorsal projecting branch extends almost as far as the ventrally projecting main shaft. VS5 and VS6 are characterised by their main dendritic shaft predominantly extending into the dorsal region of the lobula plate with smaller less complex branches extending ventrally. VS5 can be distinguished from VS6 as it often projects two major branches from the main dendritic shaft. One of the branches extends ventrally, while the other extends into the lateral region of the lobula plate. VS6 however contains one major branch which extends ventrally and is observed to be the closest branch to the medial region of the lobula plate (Scott et al., 2002).

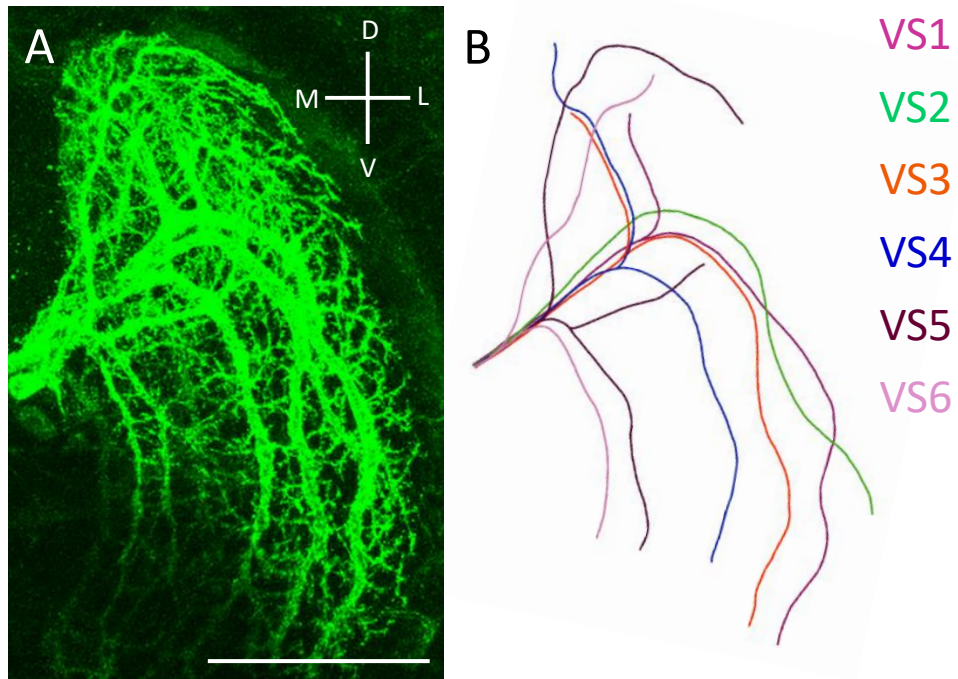


Figure 3.20. Characteristic normal dendrite growth in the visual system LPTCs. (A) Confocal micrograph demonstrating the characteristic branching pattern in the LPTCs. (B) Cartoon trace of the confocal micrograph showing the dendritic branching of each of the six vertical system neurons (VS1-6). Abbreviations: D = dorsal, V = ventral, M = medial and L = lateral, VS = vertical system. Scale bar = 50 μ m.

Image stacks produced from confocal microscopy were analysed, and a semi-quantitative scoring system was employed to distinguish a normal from an abnormal phenotype. An abnormal phenotype included shortened, thinned and a total loss of one or more of the main dendritic shafts as compared to a wild-type representative control image. Representative images of normal and abnormal phenotypes are shown in Figure 3.21.

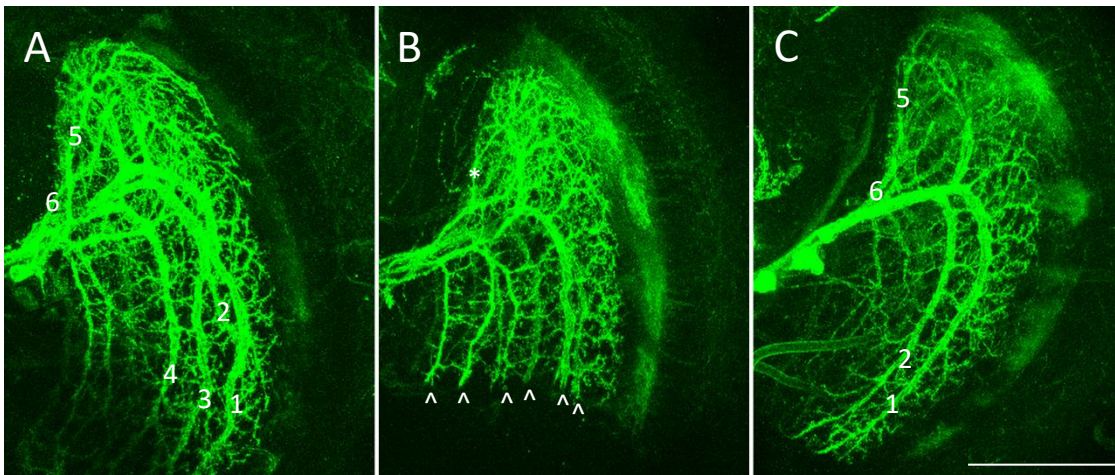


Figure 3.21. Representative images of the phenotypes observed in the LPTCs. (A) Characteristic normal phenotype, all six vertical system neurons are present and labelled 1-6. (B) Abnormal phenotype resulting in shortened vertical system neurons (white arrows) and a thinned VS5 dendrite (white asterisk). (C) Abnormal phenotype resulting in a total loss of two vertical system neurons, the remaining neurons are numbered. Scale bar = 50 μ m.

A normal phenotype consisted of the wild-type organisation of LPTCs in a single hemisphere and was scored as 0. An abnormal phenotype consisted of one or more of the main LPTC dendritic shafts being shortened, thinned or entirely missing, resulting in a phenotype different from the normal wild-type, and was scored as 1. Brain hemispheres were therefore scored as normal or abnormal compared to the stereotypic control. It should however be noted that a significant proportion of wild-type brains also differed from the stereotypic control as there was a large amount of variability in all samples. This was due to difficulty in the staining technique and subsequent confocal imaging; therefore, further optimisation is required. In a proportion of brains, it was difficult to identify and differentiate individual branches due to a high level of staining, whereas in other brains the LPTCs were not visible due to weak staining. Due to these difficulties the LPTCs were too variable to analyse each of the abnormal phenotypes individually as there were a large proportion of LPTCs which consisted of a combination of shortened, thinned and missing dendrites. Scores were then calculated as a percentage of normal to abnormal within a single genotype before being displayed in a bar graph to demonstrate the proportion of normal to abnormal dendrite morphogenesis observed in the vertical system LPTCs.

The total shaft and major branch length inclusive of all six neuronal shafts and their major visible branches were also measured to provide a quantitative assessment of dendritic

branching. The ImageJ plugin, NeuroAnatomy contains a programme called SNT where branching trace plots can be reproduced from the dendritic arborizations (Avery et al., 2017). Total shaft and branch lengths were traced and calculated before being plotted into a box and whisker graph.

A static confocal projection of a wild-type LPTC branching dendrite was traced using the SNT tracer programme to produce a tracing plot containing branches of all six neurons and their visible associated major branches. These measurements were then added together to produce a total sum branch length. This traced plot proved difficult to visually interpret; therefore, an overlay image was traced to produce a plot where all dendrites were easily defined (Figure 3.22).

This dendritic tracing was then performed on each confocal projection for each genotype to produce box and whisker plots.

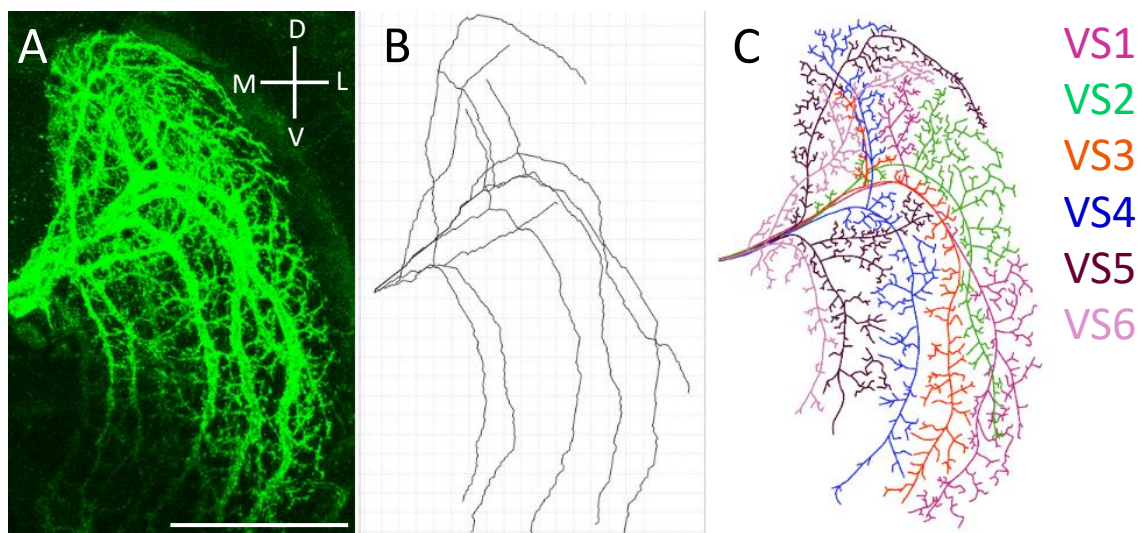


Figure 3.22. Tracing plot of a characteristic LPTC dendritic arbour. (A) Confocal micrograph of the characteristic LPTCs. (B) Dendritic trace using the SNT tracer programme in ImageJ. (C) A simplified coloured diagram of the characteristic dendrite trace displaying all six vertical system neurons. Scale bar = 50 μ m.

3.4.1 Characterisation of the genetic interaction between *HDAC4* and *Ank2* in dendrite morphogenesis

Female flies carrying the *3A-GAL4; UAS Lifect* driver were crossed to *w(cs10)* as a control and individually to *UAS-Ank2 RNAi*, *UAS-HDAC4*, and *UAS-HDAC4 RNAi*

flies, then also flies carrying both *UAS-HDAC4* and *UAS-Ank2* RNAi, as well as *UAS-HDAC4* RNAi and *UAS-Ank2* RNAi via standard genetic crosses. F1 progeny were then dissected (Section 2.3), subjected to immunohistochemistry (Section 2.3.1) and imaged via confocal microscopy. Each genotype was then assessed and the proportion of normal to abnormal phenotypes were detailed in Table 3.3.

Genotype	Normal Phenotype	Abnormal Phenotype	n
<i>w(cs10)</i>	60%	40%	20
<i>Ank2</i> RNAi	16.7%	83.3%	18
<i>HDAC4</i>	29.4%	70.6%	17
<i>HDAC4; Ank2</i> RNAi	18.7%	81.3%	16
<i>HDAC4</i> RNAi	52.6%	47.4%	19
<i>HDAC4</i> RNAi; <i>Ank2</i> RNAi	29.4%	70.6%	17

Table 3.3. Proportion of normal vs abnormal phenotypes induced by *HDAC4* mutants and *Ank2* RNAi in the visual system LPTCs. Each proportion is expressed as a percentage with the number of LPTCs analysed for each sample in the far-right column denoted as n.

Individual knockdown of *Ank2* resulted in a significant increase in the proportion of thinned, shortened and missing dendritic shafts compared to control brains, indicating that *Ank2* is required for normal dendritic branching in the adult visual system. Overexpression of *HDAC4* had a similar phenotype, but not significantly different compared to control brains. The combination of both *Ank2* RNAi and *HDAC4* resulted in a similar number of abnormalities as each mutation individually, suggesting that *HDAC4* and *Ank2* do not interact genetically in dendrite morphogenesis (Figure 3.23A).

HDAC4 knockdown did not result in a significantly different level of dendritic abnormalities compared to control LPTCs and the number of defects resulting from the co-expression of *Ank2* RNAi and *HDAC4* RNAi was similar to that of *Ank2* knockdown alone (Figure 3.23B).

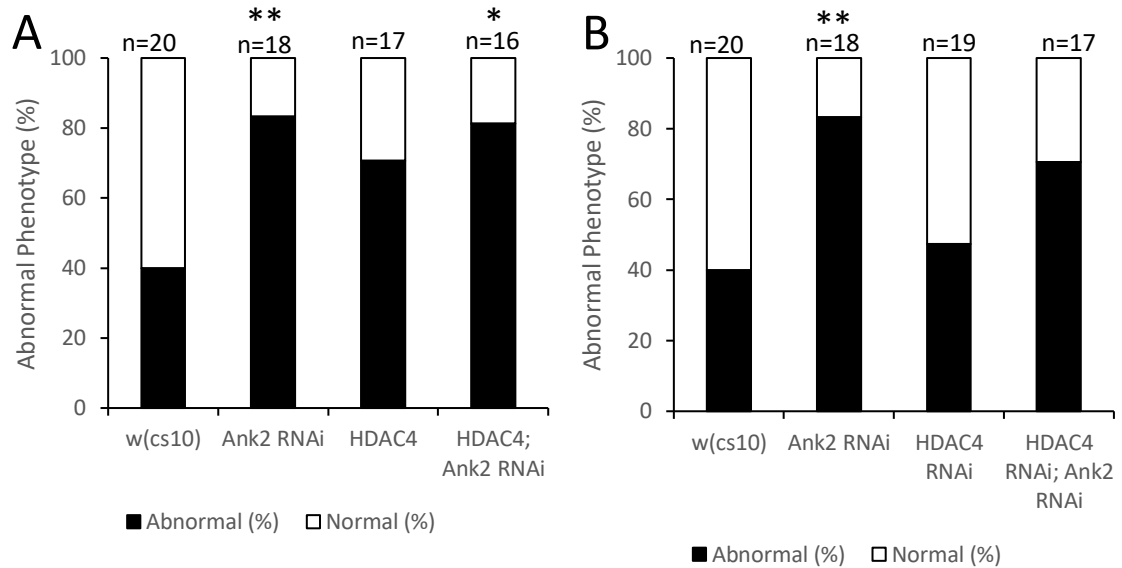


Figure 3.23. The percentage of abnormal phenotypes in LPTCs induced by *HDAC4* mutants and *Ank2* RNAi. Each bar represents the percentage of abnormal phenotypes observed with the genotype. *w(cs10)* LPTCs were used as a control in which the LPTCs resulting from each *HDAC4* and *Ank2* mutant were compared to. (A) *HDAC4* and *Ank2* RNAi were expressed individually and together. Statistical significance for each genotype compared to control is denoted as (*), * = $p < 0.05$, ** = $p < 0.01$. Statistical significance was determined using one-tailed Fisher's exact test. p-values: *w(cs10):Ank2* RNAi = 0.0089, *w(cs10):HDAC4; Ank2* RNAi = 0.0186. (B) *HDAC4* RNAi and *Ank2* RNAi were expressed individually and together. Statistical significance for each genotype compared to control is denoted as (*), ** = $p < 0.01$ following one-tailed Fisher's exact test. p-values: *w(cs10):Ank2* RNAi = 0.0089. n = total number in the sample.

The LPTCs were then traced using the ImageJ SNT tracer programme to measure the total length of all LPTC dendrites per optic lobe to demonstrate whether alterations in the level of *HDAC4* or *Ank2* result in growth and extension defects. The total length of the LPTCs included the six main dendritic shafts and all major distinguishable branches.

Although the wild-type control sample consisted of some of the longest total LPTC dendrite lengths there was a large amount of variability across all samples due to inconsistencies in staining and imaging. From these data, although there is a significant difference in dendrite morphology, the growth and extension of LPTC dendrites show no significant difference between the wild-type control group and the *Ank2* and *HDAC4* mutants, therefore it is unable to be definitively concluded whether alterations in the level of *HDAC4* and *Ank2* alter growth and extension of dendrites in the LPTCs (Figure 3.24).

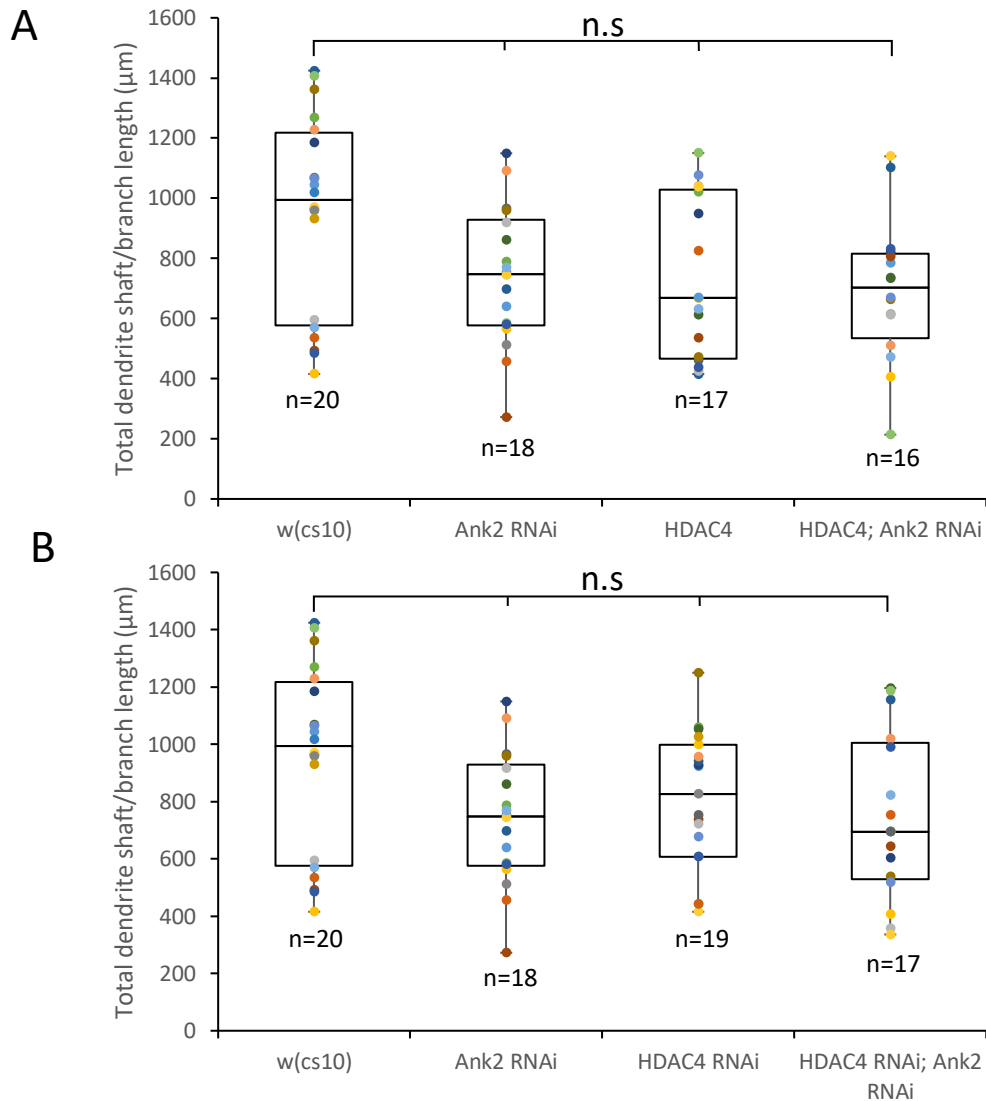


Figure 3.24. Alterations in the level of *HDAC4* and *Ank2* do not affect the growth and extension of the visual system LPTCs. Dendrite branching reconstruction plots and measurements were produced using ImageJ software NeuroAnatomy (SNT). Total branch lengths were displayed as box and whisker plots with the coloured dots detailing each individual sum of the six dendritic shafts and major branches in each optic lobe within a genotype. *w(cs10)* LPTCs were used as a control in which the LPTCs resulting from each *HDAC4* and *Ank2* mutant were compared to. (A) *HDAC4* and *Ank2* RNAi were expressed individually and together. A one-way ANOVA was performed with post-hoc Tukey test and determined that there was no significant difference in total dendrite length between each genotype. (B) *HDAC4* RNAi and *Ank2* RNAi were expressed individually and together. A one-way ANOVA was performed with post-hoc Tukey test and determined that there was no significant difference in total dendrite length between each genotype. n = total number in sample, n.s = not significant.

3.5 Investigation of the neurodevelopmental role of *Ank2* and *HDAC4* in axon morphogenesis in the mushroom body

Both overexpression of *HDAC4* (Main, 2019) and knockdown of *Ank2* (Schwartz, 2016) result in significant mushroom body developmental deficits including impaired axon elongation and termination. Given the importance of the mushroom body in long-term memory, the final investigation of this thesis was to determine whether *HDAC4* and *Ank2* genetically interact during axon morphogenesis in the mushroom body. Firstly, *Ank2* RNAi was expressed in all neurons with the *elav-GAL4* driver. The resulting phenotype displayed characteristics of developmental defects in mushroom body lobe formation, growth and extension. There was a wide range of different defects observed, from wild-type (Figure 3.25A), to thinned lobe formation, indicative of a subset of axons not elongating (Figure 3.25B) to missing lobes, indicative of a complete lack of axon elongation in all axons of a cell subtype (Figure 3.25C) and axonal guidance defects (Figure 3.25D, E). The most extreme phenotype observed in this genotype was a combination of thinned lobes, missing lobes, axon bundling, guidance and growth defects (Figure 3.25F).

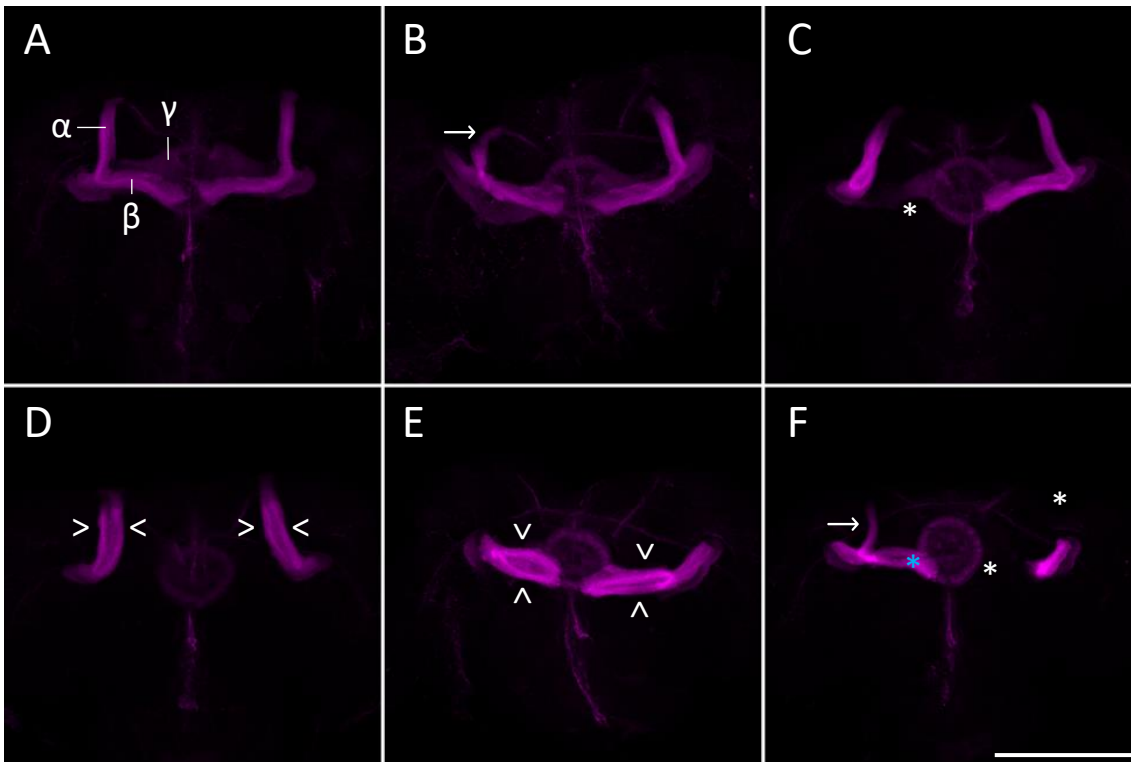


Figure 3.25. Mushroom body phenotypes resulting from *Ank2* RNAi at 25°C. Immunohistochemistry on whole mount brains using anti-FasII to label the mushroom body revealed a range of morphological defects in development. *elav-GAL4* driven *Ank2* RNAi flies were raised at 25°C. Static confocal projections from z-stacked images were produced and resulted in (A) a characteristic normal phenotype, (B) thinned α -lobe, (C) missing β -lobe, (D) guidance deficit in which the β -lobes are extending vertically rather than medially, (E) guidance deficit in which the α -lobes are extending medially rather than vertically, and (F) a combination of defects. White arrow = thinned lobe, white asterisk = missing lobe, white arrowhead = guidance defect, blue asterisk = axon bundling defect. Objective 40x in oil. Scale bar = 100 μ m.

Overexpression of *HDAC4* resulted in a much more severe phenotype in which the mushroom body lobes were entirely absent (Figure 3.26B) compared to the wild-type control (Figure 3.25A). As expected, co-expression of *Ank2* RNAi and *HDAC4* produced the same phenotype (Figure 3.26C), thus it could not be determined as to whether the *HDAC4* and *Ank2* interact under these experimental conditions.

Due to the severity of the *HDAC4* overexpression phenotype, a semi-quantitative scoring analysis was unable to be performed to determine whether *Ank2* knockdown rescues the *HDAC4*-induced mushroom body phenotype.

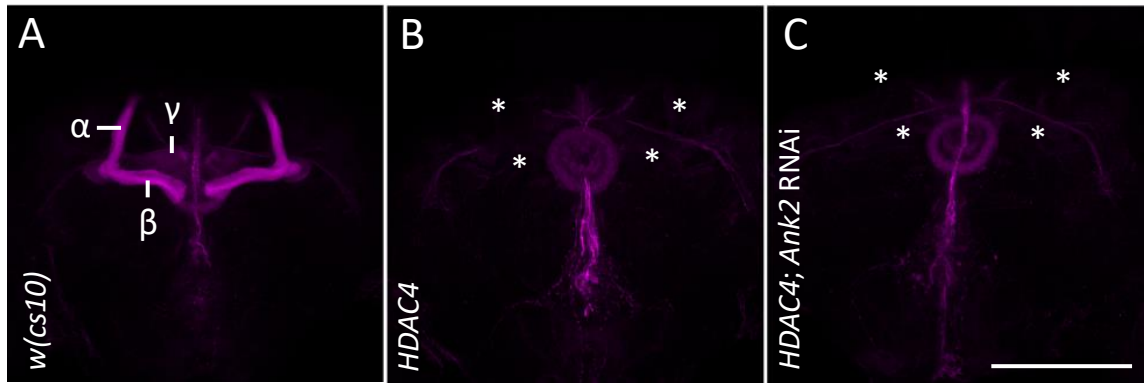


Figure 3.26. Mushroom body phenotypes from *HDAC4* overexpression and *Ank2* RNAi at 25°C. Immunohistochemistry on whole mount brains using anti-FasII to label the mushroom body. Static confocal projections from z-stacked images were produced. *elav-GAL4* was crossed to each transgene and *w(cs10)* as a control. (A) Control brains displayed a normal mushroom body phenotype. (B) *HDAC4* overexpression resulted in a lack of mushroom body morphogenesis. (C) *HDAC4* overexpression co-expressed with *Ank2* RNAi also prevented mushroom body formation. White asterix = missing lobe. Objective 40x in oil. Scale bar = 100 μ m.

4 Discussion and Future Directions

The data presented in this thesis furthers the understanding of the relationship between *HDAC4* and *Ank2*. A direct physical interaction was not detected; however, it was identified that the genetic interaction was mediated through nuclear *HDAC4* and does not require the presence of the ankyrin repeat binding domain on *HDAC4*. It was also identified that *Ank2* is required for dendrite morphogenesis in the visual system LPTCs and increased expression of *HDAC4* disrupts their normal development, however, *Ank2* and *HDAC4* do not appear to interact in LPTC branching. A novel observation was also made where knockdown of *Ank2* combined with overexpression of *HDAC4* impaired photoreceptor development and resulted in the “blueberry” phenotype that has not previously been characterised for these genes.

4.1 There is not a direct physical interaction between HDAC4 and Ank2

In an effort to further examine the nature of the interaction between HDAC4 and Ank2 a strategy was adopted in which co-immunoprecipitation was carried out on brain lysates co-expressing HDAC4 and the N-terminal portion of Ank2 in order to determine whether a physical interaction occurs between these two proteins.

Reciprocal co-IPs were performed alongside appropriate controls and it was concluded that there is either no direct physical interaction between HDAC4 and the ankyrin repeat-containing region of Ank2, or the interaction is present albeit too weak to be detected using this experimental approach.

The co-IP that was used as a positive control interaction is transient as HDAC4 monomers interact via weak interactions in which they tetramerise to form a four-helix bundle. The equilibrium between the monomer and tetramer species undergoes rapid changes in solution, implying that the tetrameric interactions are weak and unstable (Guo et al., 2007). This suggests that the co-IP is sensitive enough to detect the unstable HDAC4 tetramer interaction therefore, even if the interaction between HDAC4 and Ank2 is a weak one, it should be readily detected. This does however provide an opportunity to further optimise the co-IP protocol for detection of weaker interactions. It would also be ideal to use the full length Ank2 protein as there is the possibility that other regions of the Ank2 protein may be essential in stabilising the interaction.

In a previous study in this laboratory, a GST pull-down assay was employed where purified GST-tagged HDAC4 was combined with a cytoplasmic lysate from whole bodies of flies containing an EGFP-tagged short isoform of Ank2. A weak band indicating a physical interaction was detected, however this band was not clearly defined and this result was unable to be replicated, therefore it was not clear if it was “real” or an artefact (Schwartz, 2016).

Similarly, a second modified *in vitro* GST pull-down experiment combining both purified GST-tagged HDAC4 and purified Ank2, as opposed to a cytoplasmic lysate, would conclude whether HDAC4 and Ank2 have the ability to interact. However, this still would not provide insight into whether HDAC4 and Ank2 interact *in vivo*.

To further the results from this study, FRET could be used as another method for investigating a direct physical interaction between two proteins *in vivo*. FRET is fluorescence resonance energy transfer, which demonstrates the transfer of energy between two molecules (Sekar & Periasamy, 2003). This methodology could be used to determine whether HDAC4 and Ank2 are in close enough proximity to one another for FRET to occur. HDAC4 would be tagged with a donor chromophore, while Ank2 would be tagged with an acceptor chromophore, if the two proteins reside in close proximity the changes in fluorescence of the donor chromophore can be monitored using fluorescence confocal microscopy to detect a protein-protein interaction (Sekar & Periasamy, 2003).

Although the results in this study demonstrate that HDAC4 and Ank2 do not interact via a direct physical interaction, the possibility of an indirect interaction cannot be ruled out as HDAC4 may be acting on Ank2 through mechanisms such as histone and non-histone deacetylation, gene expression or SUMOylation.

4.2 Ank2 may regulate the level of HDAC4 protein

As a physical interaction between HDAC4 and Ank2 was not observed, it was next investigated whether *HDAC4* regulates the level of Ank2 protein.

This was considered feasible as HDAC4 has been shown to promote deacetylation of non-histone targets (Gaughan et al., 2002; Glozak et al., 2005) and has been implicated in promoting SUMOylation (Zhao et al., 2005) which can alter protein stability (Müller et al., 2001). HDAC4 has also been demonstrated to interact with Ubc9, a SUMO E2

conjugation enzyme, during long term memory formation (Schwartz et al., 2016) and HDAC4 itself is also regulated by SUMOylation (Kirsh et al., 2003).

The results from this analysis were inconclusive due to variability in protein loading and there was no correlation between the subcellular distribution of HDAC4 and Ank2 protein levels. Incomplete lysis of nuclei may account for such a result. As *DmHDAC4 3A* resides solely in the nucleus, incomplete lysis may appear to reduce *DmHDAC4 3A* levels. It is, therefore, unlikely that there would be a significant difference in the level of Ank2 between wild-type and nuclear-restricted *DmHDAC4* overexpression. This experiment requires at least an additional two repetitions with bands quantified in order to draw any conclusions; however, this was not possible due to time constraints, therefore, no firm conclusion could be drawn as to whether overexpression of *HDAC4* alters Ank2 protein levels.

An early hypothesis, when it was unknown whether HDAC4 and Ank2 physically interact was that Ank2 may tether HDAC4 in the cytoplasm, which would prevent the detrimental mutant phenotypes associated with nuclear-restricted HDAC4. Although it was subsequently determined that there was not a detectable physical interaction present between HDAC4 and Ank2, this does not rule out the possibility that *Ank2* somehow regulates the subcellular distribution of HDAC4 in an indirect manner. Knockdown of *Ank2* during development resulted in a higher level of total HDAC4 protein, however this result requires confirmation. In addition, to avoid potential confounding developmental effects, an experiment is yet to be carried out in which knockdown of *Ank2* is restricted to the adult brain, to determine whether the total HDAC4 protein levels are also increased, similarly to that observed during development. There was no significant change in subcellular distribution of HDAC4 on knockdown of *Ank2*, however these blots were only repeated twice due to time constraints and further optimisation and repetition with band quantification is required to confirm these data and determine whether the subcellular distribution correlates with the total level of HDAC4 from whole cell lysates.

Although as yet there is no definitive conclusion as to whether *Ank2* regulates HDAC4 subcellular distribution, the protocol for nuclear and cytoplasmic fractionation of *Drosophila* brain lysates has now been significantly optimised for future experiments. Further optimisations may include the addition of a third wash step and the use of a

different antibody to remove the non-specific band that was detected in the nuclear fraction with anti-GFP to obtain a more clearly defined, pure nuclear fraction.

The importance of these future experiments are that they will aid in understanding the nature of the genetic interaction between *HDAC4* and *Ank2*; if a knockdown of *Ank2* reduces HDAC4 protein levels, it is difficult to elucidate how the genetic interaction occurs as HDAC4 would be reduced back to wild-type levels, which should result in a less severe phenotype.

4.3 Nuclear HDAC4 interacts genetically with *Ank2*

In an effort to understand the nature of the interaction between *HDAC4* and *Ank2*, the genetic interaction previously detailed was further examined with the use of a range of *Drosophila HDAC4* mutants. The aim of this experiment was to determine the subcellular pool of HDAC4 that is important for the genetic interaction with *Ank2*, as well as whether this interaction is dependent on the presence of the ankyrin repeat binding domain. Wild-type *DmHDAC4*, *DmHDAC4 ΔAnk*, and nuclear restricted *DmHDAC4 3A* were expressed in *Drosophila* photoreceptors individually and in conjunction with *Ank2* RNAi. As previously observed by Schwartz (2016), individual *HDAC4* overexpression and *Ank2* knockdown resulted in a mild rough eye phenotype. These phenotypes were however more pronounced in this study as the flies were raised at a two-degree higher temperature (27°C compared to 25°C). The GAL4 transactivator is more active at higher temperatures and thus promotes higher expression of the transgenes (Duffy, 2002). The more efficient knockdown of *Ank2* uncovered a unique phenotype best understood as a mild “blueberry” phenotype that was not readily observed at 25°C (Section 4.5.2).

When *DmHDAC4 3A* was co-expressed with *Ank2* RNAi, a much more severe phenotype was observed than with either construct alone, suggesting that the genetic interaction between HDAC4 and *Ank2* may be mediated through the presence of nuclear HDAC4. This suggests that in the nucleus, the activity of HDAC4 may be impairing a pathway involved in eye development in which *Ank2* acts in, such that when *Ank2* is also reduced, this specific molecular pathway breaks down, resulting in eye deficiencies.

The regulatory role that HDAC4 plays in eye development is currently unknown, therefore there are many possible mechanisms in which overexpressing wild-type and

nuclear-restricted *HDAC4* alters the affected developmental pathways. As opposed to human HDAC4, *Drosophila* HDAC4 retains its catalytic activity by having a functional deacetylase domain. This may mean that nuclear HDAC4 may be deacetylating non-histone proteins and altering their activity in eye development pathways. As previously mentioned, HDAC4 has also been proposed to play a role in SUMOylation (Schwartz et al., 2016; Zhao et al., 2005), which can alter the activity, stability and/or subcellular distribution of a protein, such that its normal role in the cell may be altered (Müller et al., 2001). These could possibly be proteins that activate or repress *Ank2* activity, resulting in impaired development or defects of the spectrin-actin cytoskeleton due to a lack of ion channel and cell adhesion molecule recruitment.

Although few changes in gene expression were observed between nuclear and cytoplasmically restricted HDAC4 (Main, 2019; Schwartz, 2016), the possibility that HDAC4 could be altering gene expression in a small subset of cells which would not have been detected by RNA-seq could not be ruled out. Thus far the genetic interaction between *HDAC4* and *Ank2* has been restricted to the photoreceptors in the eye. RNA-seq was performed on whole heads of flies which is inclusive of the eye, therefore photoreceptor cells were present in the lysate subjected to RNA-seq. However, these photoreceptor cells would make up a small subset of the total number of cells in the lysate. If the interaction was only present in the eye, this small number of photoreceptor cells would not induce a large change in gene expression, therefore, would not have been detected by RNA-seq.

4.3.1 The genetic interaction does not depend on the presence of the ankyrin binding domain on HDAC4

Co-expression of *DmHDAC4 ΔAnk* and *Ank2* RNAi induced a significantly more severe rough eye phenotype compared to each transgene individually, indicative of a genetic interaction. Thus, the genetic interaction observed in the previous study by Schwartz (2016) was not mediated through *Ank2* binding to the PxLPxI/L motif of the ankyrin repeat binding domain on HDAC4. These results are consistent with the finding that there was no detectable physical interaction between HDAC4 and *Ank2*.

Ankyrin binding does however play a role in the *HDAC4* overexpression-induced eye phenotype, as it was observed that the *DmHDAC4 ΔAnk* phenotype was more severe than wild-type *DmHDAC4*. In the light microscopy images, it was seen that the *DmHDAC4 ΔAnk* mutant resulted in a particularly more pronounced loss of pigmentation. In an experiment carried out in parallel to this study by Dr Helen Fitzsimons, the eye phenotypes of flies homozygous for wild-type *DmHDAC4* or *DmHDAC4 ΔAnk* revealed an even more significant difference between wild-type *DmHDAC4* and the *DmHDAC4 ΔAnk* mutant with respect to pigmentation loss (Dr H. Fitzsimons, personal communication, 18 December, 2020).

It would, therefore, be useful to perform fractionation experiments on wild-type *DmHDAC4* and the *DmHDAC4 ΔAnk* mutant to determine the subcellular distribution of HDAC4. This would show whether there is an increased level of nuclear HDAC4 when the *DmHDAC4 ΔAnk* mutant is expressed, which could account for the more severe rough eye phenotype observed. These results could also suggest whether there are any additional ankyrin repeat-containing proteins binding to HDAC4 and regulating its subcellular distribution. This could be of interest as it has recently been demonstrated that mutations of L351 and L354 of human HDAC4 abolishes binding of the ankyrin repeat containing protein ANKRA2 (Xu et al., 2012), therefore, it is possible that other ankyrin repeat-containing proteins are being displaced in the *DmHDAC4 ΔAnk* mutant.

The original rough eye enhancer screen (Schwartz, 2016) also identified that *RFXANK* interacts genetically with *HDAC4*. *RFXANK* encodes an ankyrin repeat-containing protein. Mammalian *RFXANK* is a paralogue of ANKRA2 and has also been demonstrated to bind to HDAC4 via the PxLPxI/L motif (Xu et al., 2012). This suggests that *Drosophila* *RFXANK* may also interact with HDAC4 via this binding motif to regulate the subcellular distribution of HDAC4, however analyses such as a GST pulldown or co-IP are still required to determine whether *RFXANK* interacts physically with nuclear HDAC4 and whether the interaction is mediated through the PxLPxI/L motif.

To determine additional candidate proteins which may interact with nuclear HDAC4 via the PxLPxI/L motif, immunoprecipitation mass spectrometry (IP-MS) (ten Have et al., 2011) could be performed. Wild-type *DmHDAC4*, nuclear-restricted *DmHDAC4 3A* and *DmHDAC4 ΔAnk* would be subject to IP-MS where HDAC4 would be pulled down in

order to identify associated proteins. These can then be compared to determine what proteins interact with nuclear HDAC4 and whether this interaction is mediated through the PxLPxI/L motif in the ankyrin repeat binding domain. As nuclear accumulated HDAC4 has been implicated in numerous neurodevelopmental and neurodegenerative diseases, it is hypothesised that if interactions with any ankyrin repeat-containing proteins alter the subcellular distribution or stability of HDAC4, these proteins may be useful targets for the development of treatments (Figure 4.1).

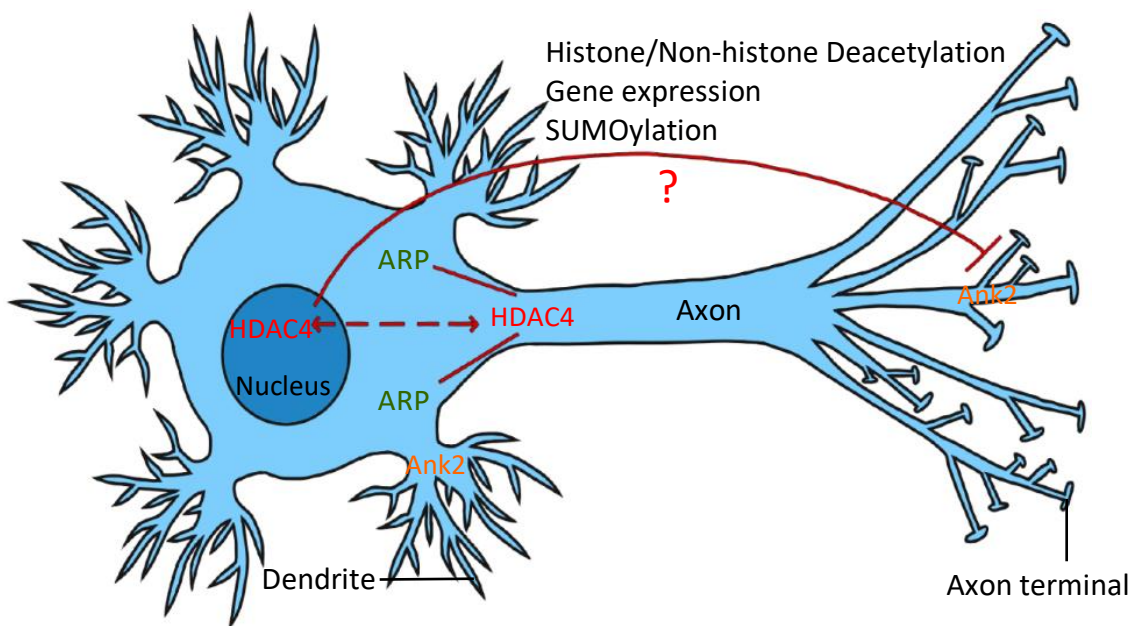


Figure 4.1. Model of the proposed genetic interaction between *HDAC4*, *Ank2* and unidentified ankyrin repeat-containing protein(s). In a normal neuron, HDAC4 shuttles between the nucleus and cytoplasm and Ank2 is localised to the axons, axon terminals and the dendrites. The genetic interaction between *Ank2* and *HDAC4* remains undetermined but relies on nuclear HDAC4 and does not require the ankyrin repeat binding domain. The interaction could therefore potentially be through histone or non-histone deacetylation pathways, gene expression alterations or SUMOylation. It is also proposed that other unidentified ankyrin repeat-containing protein(s) bind via the ankyrin repeat binding domain on HDAC4 and restrict its nuclear entry. Disruption to this interaction i.e. in the *DmHDAC4 ΔAnk* mutant, HDAC4 may then accumulate in the nucleus, exacerbating the developmental deficits observed in the *Drosophila* eye. Abbreviations: ARP = ankyrin repeat-containing protein.

4.4 What is the nature of the interaction between HDAC4 and Ank2?

One hypothesis is that both HDAC4 and Ank2 may influence each other in an indirect manner in specific cellular regions known to be important in neurodevelopment, synaptic activation/remodelling and long-term memory formation.

4.4.1 The role in the mushroom body

Previous studies of mushroom body axon morphogenesis showed that overexpression of *HDAC4* (Main, 2019) and knockdown of *Ank2* (Schwartz, 2016) resulted in mushroom body defects. This study replicated these findings with knockdown of *Ank2* resulting in a variety of different mushroom body defects including axon elongation and termination defects. Overexpression of *HDAC4* however resulted in complete loss of the mushroom body lobes. In order to be able to determine whether there is a genetic interaction between *HDAC4* and *Ank2* in the mushroom body axons, the severity of the *HDAC4* overexpression phenotype would need to be reduced. In a parallel study in the laboratory, a strain in which the *UAS-HDAC4* construct is inserted at a different genomic location was used to examine mushroom body development. This strain resulted in a lower level of *HDAC4* expression and less severe phenotypes which include defects in axon elongation and termination (Wei Jun Tan, unpublished data). Alternatively, the TARGET system provides precise control of gene expression as the level of expression can be increased or decreased by changing the temperature, where the level of expression is proportional to temperature, with minimal expression at 18°C and maximal expression at 30°C (Schwartz, 2016). A temperature could then be identified at which *HDAC4* expression produces a minimal phenotype, thus allowing investigation of whether co-expression of *Ank2* RNAi enhances the *HDAC4* overexpression-induced phenotype.

In the mushroom body axons *Ank2* binds the cell adhesion molecule Neuroglian which is the sole *Drosophila* orthologue of the L1-CaM family of proteins (Bieber et al., 1989). Similarly to *Ank2*, Neuroglian is required for normal axon growth and guidance in the mushroom body (Siegenthaler et al., 2015). Aside from binding to *Ank2*, Neuroglian has also recently been shown to bind to a second cytoskeletal regulator protein, Moesin, creating a ternary complex between *Ank2*, Neuroglian and Moesin (Siegenthaler et al., 2015) (Figure 4.2).

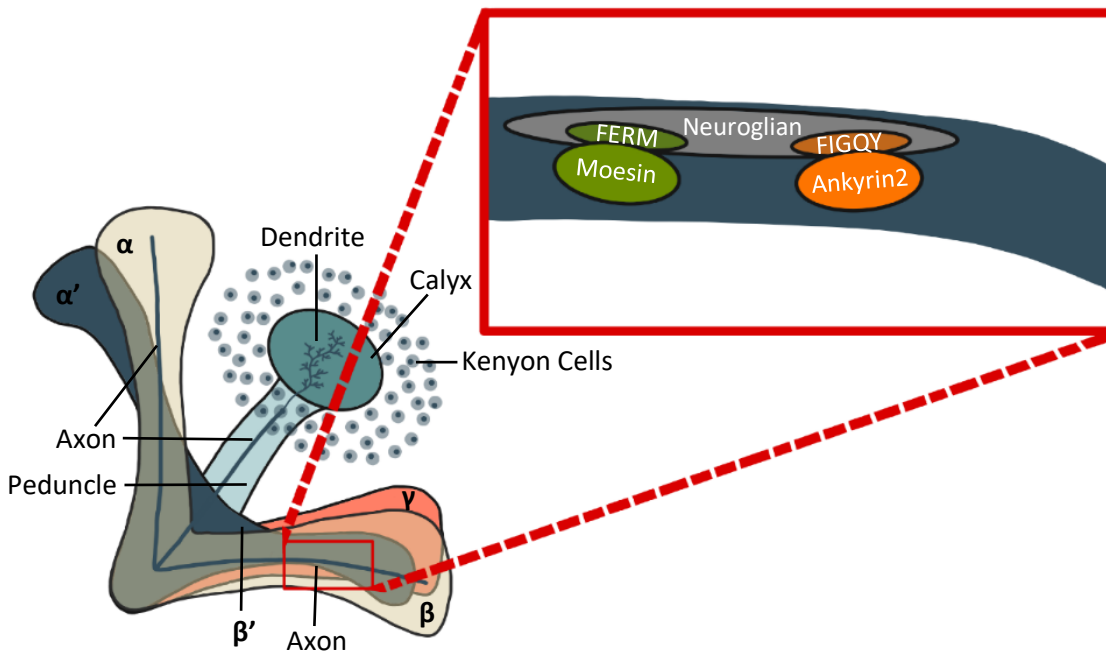


Figure 4.2. The ternary complex found in *Drosophila* mushroom body axons. The Kenyon cell dendrites project into the calyx and the axon travels down through the peduncle where the axon bifurcates forming the vertical α lobe and the medial β lobe. Ank2 is localised in the axons where it binds to the L1-CaM Neuroglial through the FIGQY motif. Moesin, another ankyrin repeat-containing protein also binds to Neuroglial through the FERM motif, therefore, producing a ternary complex structure in the axons of the mushroom body. *Original artwork with reference to the following literature, Lee et al. (1999), Siegenthaler et al. (2015), and Technau and Heisenberg (1982).*

Moesin plays an essential role in modifying the membrane cytoskeleton in neuronal morphogenesis (Karagiannis & Ready, 2004) and it has recently been discovered to genetically interact with *HDAC4* in the previously performed rough eye phenotype screen (Schwartz, 2016). As with *Ank2* and *Neuroglial*, reduction of *Moesin* also shows similar disruption to mushroom body development, resulting in defects in axon elongation and termination (Freymuth, 2016; Freymuth & Fitzsimons, 2017).

Given the striking similarity of these phenotypes with *HDAC4* overexpression, it is hypothesised that *HDAC4* may influence the complex formed between *Ank2*, *Neuroglial*, and *Moesin*. This, however, does not imply that *HDAC4* acts in a complex with these proteins. It would be interesting to determine whether protein levels (by western blot) and the subcellular distribution (by cell fractionation) of each of these proteins is altered when *HDAC4* is overexpressed and analyse whether the binding abilities within the complex are disrupted via co-IP. If these binding abilities and

processes are disrupted by *HDAC4* overexpression, it can then be ascertained as to whether overexpression of *Ank2*, *Neuroglian* and/or *Moesin* improves these phenotypes.

As the cell adhesion molecule L1 is SUMOylated in mouse neurons (Lutz et al., 2012), it is possible that the *Drosophila* L1-CaM orthologue Neuroglian may also be SUMOylated. This SUMOylation may be a process by which HDAC4 indirectly interacts with Ank2. To investigate this, a co-IP approach could be taken whereby a Neuroglian-specific antibody would be used to pull down Neuroglian, followed by detection with a SUMO specific antibody in the presence and absence of *HDAC4* overexpression.

4.4.2 The role in memory formation

Fitzsimons et al. (2013) identified that overexpression of *HDAC4* throughout the α/β , α'/β' and γ neurons of the mushroom body resulted in impairments in long-term courtship memory formation, whereas short-term memory remained intact. To narrow down the specific neurons responsible for inducing this memory impairment, *HDAC4* overexpression was restricted to each lobe independently, where it was seen that overexpression of *HDAC4* specifically in the γ neurons was responsible for the long-term memory deficit (Fitzsimons et al., 2013).

Interestingly, knockdown of *Ank2* specifically in the γ -neurons also impaired the formation of long-term courtship memory (Schwartz, 2016) and strikingly, in accordance with the similarity in mushroom body defects, knockdown of *Moesin* resulted in the same phenotype (Freymuth, 2016; Freymuth & Fitzsimons, 2017) as *Ank2* knockdown (Schwartz, 2016) and *HDAC4* overexpression (Fitzsimons et al., 2013). Thus far, the role of Neuroglian in memory formation remains undetermined. As Neuroglian is a cell adhesion molecule rather than a cytoskeletal adaptor protein like Ank2 and Moesin, it would be beneficial to understand whether it is also required for long-term memory formation. Knockdown of *Ank2* (Schwartz, 2016), *Moesin* (Freymuth & Fitzsimons, 2017), and *Neuroglian* (Siegenthaler et al., 2015) all result in mushroom body deficits, therefore, it is hypothesised that knockdown of *Neuroglian* would also result in long-term memory formation defects similar to what was observed when *Ank2* and *Moesin* were knocked down (Freymuth & Fitzsimons, 2017; Schwartz, 2016).

The γ -lobe of the mushroom body is a site of long-term memory formation in *Drosophila* (Zhao et al., 2018), and interestingly, there is an axon initial segment-like domain in the γ -lobe of adult flies (Trunova et al., 2011). In mammals, the axon initial segment is an essential component of the neuron as it is the site of action potential initiation. The human homologue of Ank2, ANK-G, is an essential component of the axon initial segment as it stabilises the axon through recruitment of ion channels and L1-CaMs to maintain cell polarity (Garrido et al., 2003; Huang & Rasband, 2018; Pan et al., 2006; Zhou et al., 1998). It can therefore be hypothesised that in *Drosophila*, binding and clustering of wild-type levels of Ank2, Moesin and potentially Neuroglian at the axon initial segment-like domain in the γ -lobe of the mushroom body is essential for long-term memory formation. As wild-type levels of HDAC4 are also required in the γ -lobe for normal memory formation (Fitzsimons et al., 2013), it can be speculated that through some indirect mechanism HDAC4 may be regulating this complex formed between Ank2, Neuroglian, and Moesin at the axon initial segment-like domain in order to maintain cytoskeletal stability and long-term memory formation. To further examine the relationship between these proteins, it would be of interest to also determine whether the overexpression of *Ank2* or *Moesin* could improve the long-term memory impairments induced by the overexpression of *HDAC4*.

4.5 What is the molecular basis of the observed rough eye phenotypes?

4.5.1 Reduction of eye sizes attributed to apoptosis

The co-expression of nuclear-restricted *DmHDAC4 3A* and *Ank2* RNAi resulted in significantly smaller eyes compared to the wild-type control, suggesting an upregulation of apoptosis.

The wingless signalling pathway is required for normal *Drosophila* eye patterning in which apoptosis of specific ommatidial cells is triggered during pupation (Cordero et al., 2004). Notch signalling is also important in eye development for promotion and inhibition of neural differentiation, which is required for successive steps of R8 determination (Baker et al., 1990; Cagan & Ready, 1989). It is possible that there could be an interaction occurring between HDAC4, Notch, and Ank2 in the wingless signalling pathway,

whereby apoptosis becomes upregulated leading to a reduction in the size of the *Drosophila* eye. Interestingly, Notch is also required for long-term memory formation (Presente et al., 2003), and contains an ankyrin repeat domain consisting of six ankyrin repeats that are each 33 amino acids long (Zweifel et al., 2003). It would therefore be worthwhile to determine whether there is an interaction between Notch and the PxLPxI/L motif in the ankyrin repeat binding domain of HDAC4, and if this interaction occurs in photoreceptors and/or Kenyon cells in the mushroom body.

In contrast to the current study, HDAC4 has been reported to protect cells from endoplasmic reticulum (ER) stress-induced apoptosis by an interaction with the activating transcription factor 4 (ATF4) (Zhang et al., 2014). Overexpression of *HDAC4* in HEK293T cells resulted in retention of ATF4 in the cytoplasm, thereby inhibiting the transcriptional activity of ATF4 which induces apoptosis. Overexpression of *HDAC4* therefore appears to confer a protective role against ER stress-induced apoptosis, which could be attributed to the recently identified neuroprotective role of cytoplasmic HDAC4 (Li et al., 2012).

In order to determine whether cytoplasmic *HDAC4* has a neuroprotective role in *Drosophila* eye development it would be necessary to test the effect that the cytoplasmically restricted *DmHDAC4* mutants (*DmHDAC4* Δ MEF2 and *DmHDAC4* Δ NLS) have on the development of the eye. If cytoplasmic *DmHDAC4* has a neuroprotective role it is hypothesised that expression of these mutants in the eye may improve the detrimental phenotypes observed when nuclear-restricted *DmHDAC4* 3A is overexpressed.

4.5.2 The “blueberry” phenotype

It was observed that when *Ank2* RNAi was co-expressed with wild-type *DmHDAC4*, nuclear-restricted *DmHDAC4* 3A and *DmHDAC4* Δ *Ank*, hole-like cavities were produced in large groupings of ommatidia. These holes were not observed in specific patterns and were not seen in all eyes within the samples, however, a common feature that was observed was that these cavities only formed in ommatidia that were fused to at least one other neighbouring ommatidia. The observed phenotype is known as the “blueberry” phenotype which is a severe lens defect (Basler et al., 1990). This is speculated to be a result of dysregulation in the development and terminal differentiation of cone cells and

surrounding primary pigment cells (Charlton-Perkins & Cook, 2010) and has been associated with mutation in the *Bar* gene. *Bar* mutants display cavity-like holes in the ommatidium where several layers of the lens becomes damaged forming a cavity in the centre of the ommatidia (Higashijima et al., 1991). It is therefore possible that a knockdown of *Ank2* is affecting the development of cone cells by impairing the ability to secrete lens matter. If so, when paired with overexpression of *HDAC4*, this phenotype is exacerbated resulting in severe lens damage and hole-like cavities in the centre of the ommatidia. This could be further investigated by examining whether *HDAC4* overexpression and/or *Ank2* knockdown alters the expression of *Bar* and whether this could be rescued by increasing the expression of *Bar*.

4.6 Wild-type levels of HDAC4 and Ank2 are required for normal dendrite morphogenesis in the optic lobes

Both *HDAC4* and *Ank2* appear to interact genetically in the *Drosophila* eye. It was therefore investigated as to whether this interaction also occurred during morphogenesis of dendrites. The LPTCs of the *Drosophila* visual system were chosen as a model system to investigate dendrite morphogenesis as they have a stereotypical well-characterised structure, are actin enriched for simple visualisation and produce and grow dendritic spine-like protrusions which are an underlying essential process in learning and memory (Leiss et al., 2009; Scott et al., 2002).

Ank2 was found to be required for normal dendritic morphogenesis of LPTCs and *HDAC4* overexpression resulted in a high proportion of dendritic abnormalities, however, there was no evidence of a genetic interaction between *HDAC4* and *Ank2* in the morphogenesis of LPTC dendrites.

To further these findings, nuclear and cytoplasmic mutants of *HDAC4* could also be examined to demonstrate whether nuclear *DmHDAC4 3A* is also responsible for the morphological defects observed from overexpressing wild-type *DmHDAC4*, as was observed in the *Drosophila* eye (Section 4.3).

The overall branch length measurements taken from the LPTCs would have demonstrated differences in the growth and extension of dendrites. In this study however, these measurements were difficult to produce and quantify even in the wild-type LPTCs.

Therefore, an alternative method would be to examine the rearrangement of the actin cytoskeleton at dendritic spines as this is an important process in the formation of new memories (Lamprecht & LeDoux, 2004). This rearrangement involves the transition of monomeric globular G-actin to filamentous F-actin, where the distribution of F-actin can be visualised using the F-actin GFP marker Lifeact (Riedl et al., 2008). To further elucidate the roles that HDAC4 and Ank2 play in actin rearrangement co-IP assays could be performed on whole head lysates of flies expressing different *DmHDAC4* mutants and *Ank2* RNAi. F-actin bound to Lifeact would be pulled down and detected with an optimised anti-Actin antibody. If a relationship is observed in a co-IP assay, this would provide further evidence that HDAC4 and Ank2 interact to regulate the rearrangement of the actin cytoskeleton leading to the formation of new memories.

4.7 Conclusion

It has been well documented that alteration in expression and subcellular distribution of HDAC4 is associated with neurodevelopmental and neurodegenerative diseases, and loss of Ank2 also results in similar neurodevelopmental deficits. In addition, both HDAC4 and Ank2 are required for normal memory formation in animal models. As *HDAC4* and *Ank2* were shown to genetically interact in *Drosophila*, the aim of this study was to determine the nature of this interaction to provide further understanding of their involvement in normal memory formation and neuronal development.

It was discovered that there is not a direct physical interaction present between the ankyrin repeat region of Ank2 and HDAC4, however, further insight into the genetic interaction was revealed. It was determined that nuclear *HDAC4* is responsible for the genetic interaction observed in the *Drosophila* eye, and that the ankyrin repeat binding domain on *HDAC4* is not necessary for this interaction to occur. A novel discovery was made where *Ank2* RNAi co-expressed with wild-type *DmHDAC4* overexpression resulted in a rare “blueberry” phenotype that has not yet been associated with either HDAC4 or Ank2. It was also demonstrated that both Ank2 and HDAC4 are required for normal dendrite morphogenesis in the *Drosophila* visual system, and when HDAC4 is in excess, morphological defects ensue.

To conclude, an understanding of the relationship between HDAC4 and Ank2 by investigation of other genes that may be involved would aid in understanding the mechanisms of the molecular pathway that these genes act in and how these pathways are implicated in neurodevelopmental and neurodegenerative disease and memory disorders. Unravelling these pathways could lead to an expansion of studies into mammalian models where an understanding of the proteins involved, and the effects of dysregulation could, in the future, aid in potential therapeutic approaches to assist in neurodevelopmental and neurodegenerative disease and memory disorders.

5 References

- Alberini, C. M. (2011). The role of reconsolidation and the dynamic process of long-term memory formation and storage. *Frontiers in Behavioral Neuroscience*, 5(12), 1-10. <https://doi.org/10.3389/fnbeh.2011.00012>
- Alonso, A. D. C., Grundke-Iqbal, I., & Iqbal, K. (1996). Alzheimer's disease hyperphosphorylated tau sequesters normal tau into tangles of filaments and disassembles microtubules. *Nature Medicine*, 2(7), 783-787. <https://doi.org/10.1038/nm0796-783>
- Arancibia-Carcamo, I. L., & Attwell, D. (2014). The node of ranvier in CNS pathology. *Acta Neuropathologica*, 128(2), 161-175. <https://doi.org/10.1007/s00401-014-1305-z>
- Athanasou, L., Mattingsdal, M., Kahler, A. K., Brown, A., Gustafsson, O., Agartz, I., Giegling, I., Muglia, P., Cichon, S., Rietschel, M., Pietilainen, O. P., Peltonen, L., Bramon, E., Collier, D., Clair, D. S., Sigurdsson, E., Petursson, H., Rujescu, D., Melle, I., Steen, V. M., Djurovic, S., & Andreassen, O. A. (2010, Sep). Gene variants associated with schizophrenia in a Norwegian genome-wide study are replicated in a large European cohort. *Journal of Psychiatric Research*, 44(12), 748-753. <https://doi.org/10.1016/j.jpsychires.2010.02.002>
- Avery, A. W., Thomas, D. D., & Hays, T. S. (2017, Oct 31). β -III-spectrin spinocerebellar ataxia type 5 mutation reveals a dominant cytoskeletal mechanism that underlies dendritic arborization. *Proceedings of the National Academy of Sciences of the United States of America*, 114(44), E9376-E9385. <https://doi.org/10.1073/pnas.1707108114>
- Bailey, C., & Kandel, E. R. (1993). Structural changes accompanying memory storage. *Annual Review of Physiology*, 55, 397-426. <https://doi.org/10.1146/annurev.ph.55.030193.002145>
- Baker, N. E., Mlodzik, M., & Rubin, G. M. (1990). Spacing differentiation in the developing *Drosophila* eye: a fibrinogen-related lateral inhibitor encoded by *scabrous*. *Science*, 250(4986), 1370-1377. <https://doi.org/10.1126/science.2175046>
- Basler, K., Yen, D., Tomlinson, A., & Hafen, E. (1990). Reprogramming cell fate in the developing *Drosophila* retina: transformation of R7 cells by ectopic expression of *rough*. *Genes & Development*, 4(5), 728-739. <https://doi.org/10.1101/gad.4.5.728>
- Bertos, N. R., Wang, A. H., & Yang, X.-J. (2001). Class II histone deacetylases: Structure, function, and regulation. *Biochemistry and Cell Biology*, 79(3), 243-252. <https://doi.org/10.1139/bcb-79-3-243>

- Bi, C., Wu, J., Jiang, T., Liu, Q., Cai, W., Yu, P., Cai, T., Zhao, M., Jiang, Y. H., & Sun, Z. S. (2012). Mutations of ANK3 identified by exome sequencing are associated with autism susceptibility. *Human Mutation*, 33(12), 1635-1638. <https://doi.org/10.1002/humu.22174>
- Bieber, A. J., Snow, P. M., Hortsch, M., Patel, N. H., Jacobs, J. R., Traquina, Z. R., Schilling, J., & Goodman, C. S. (1989). *Drosophila* neuroglian: A member of the immunoglobulin superfamily with extensive homology to the vertebrate neural adhesion molecule L1. *Cell*, 59(3), 447-460. [https://doi.org/10.1016/0092-8674\(89\)90029-9](https://doi.org/10.1016/0092-8674(89)90029-9)
- Birkenmeier, C. S., White, R. A., Peters, L. L., Hall, E. J., Lux, S. e., & Barker, J. E. (1993). Complex patterns of sequence variation and multiple 5' and 3' ends are found among transcripts of the erythroid ankyrin gene. *Journal of Biological Chemistry*, 268(13), 9533-9540. [https://doi.org/10.1016/S0021-9258\(18\)98384-5](https://doi.org/10.1016/S0021-9258(18)98384-5)
- Borczyk, M., Sliwinska, M. A., Caly, A., Bernas, T., & Radwanska, K. (2019, Feb 8). Neuronal plasticity affects correlation between the size of dendritic spine and its postsynaptic density. *Scientific Reports*, 9(1), 1693. <https://doi.org/10.1038/s41598-018-38412-7>
- Bouley, M., Tian, M. Z., Paisley, K. L., Shen, Y.-C., Malhotra, J. D., & Hortsch, M. (2000). The L1-type cell adhesion molecule neuroglian influences the stability of neural ankyrin in the *Drosophila* embryo but not its axonal localization. *Journal of Neuroscience*, 20(12), 4515-4523. <https://doi.org/10.1523/JNEUROSCI.20-12-04515.2000>
- Brand, A. H., & Perrimon, N. (1993). Targeted gene expression as a means of altering cell fates and generating dominant phenotypes. *Development*, 118(2), 401-415. <https://dev.biologists.org/content/develop/118/2/401.full.pdf>
- Cagan, R. L., & Ready, D. F. (1989). *Notch* is required for successive cell decisions in the developing *Drosophila* retina. *Genes & Development*, 3(8), 1099-1112. <https://doi.org/10.1101/gad.3.8.1099>
- Campos-Ortega, J. A., Jurgens, G., & Hofbauer, A. (1979). Cell clones and pattern formation: Studies on *sevenless*, a mutant of *Drosophila melanogaster*. *Wilhelm Roux's archives of Developmental Biology*, 186(1), 27-50. <https://doi.org/10.1007/BF00848106>
- Cantrell, A. R., Scheuer, T., & Catterall, W. A. (1999). Voltage-dependent neuromodulation of Na⁺ channels by D1-like dopamine receptors in rat hippocampal neurons. *Journal of Neuroscience*, 19(13), 5301-5310. <https://doi.org/10.1523/JNEUROSCI.19-13-05301.1999>

- Charlton-Perkins, M., & Cook, T. A. (2010). Building a fly eye: Terminal differentiation events of the retina, corneal lens, and pigmented epithelia. *Current Topics in Developmental Biology*, 93, 129-173. <https://doi.org/10.1016/B978-0-12-385044-7.00005-9>
- Chawla, S., Vanhoutte, P., Arnold, F. J. L., Huang, C. L. H., & Bading, H. (2003). Neuronal activity-dependent nucleocytoplasmic shuttling of HDAC4 and HDAC5. *Journal of Neurochemistry*, 85(1), 151-159. <https://doi.org/10.1046/j.1471-4159.2003.01648.x>
- Chiang, A. S., Lin, C. Y., Chuang, C. C., Chang, H. M., Hsieh, C. H., Yeh, C. W., Shih, C. T., Wu, J. J., Wang, G. T., Chen, Y. C., Wu, C. C., Chen, G. Y., Ching, Y. T., Lee, P. C., Lin, C. Y., Lin, H. H., Wu, C. C., Hsu, H. W., Huang, Y. A., Chen, J. Y., Chiang, H. J., Lu, C. F., Ni, R. F., Yeh, C. Y., & Hwang, J. K. (2011). Three-dimensional reconstruction of brain-wide wiring networks in *Drosophila* at single-cell resolution. *Current Biology*, 21(1), 1-11. <https://doi.org/10.1016/j.cub.2010.11.056>
- Cho, Y., Griswold, A., Campbell, C., & Min, K. T. (2005). Individual histone deacetylases in *Drosophila* modulate transcription of distinct genes. *Genomics*, 86(5), 606-617. <https://doi.org/10.1016/j.ygeno.2005.07.007>
- Cline, H. T. (2001). Dendritic arbor development and synaptogenesis. *Current Opinion in Neurobiology*, 11(1), 118-126. [https://doi.org/10.1016/s0959-4388\(00\)00182-3](https://doi.org/10.1016/s0959-4388(00)00182-3)
- Cohen, T. J., Waddell, D. S., Barrientos, T., Lu, Z., Feng, G., Cox, G. A., Bodine, S. C., & Yao, T. P. (2007). The histone deacetylase HDAC4 connects neural activity to muscle transcriptional reprogramming. *The Journal of Biological Chemistry*, 282(46), 33752-33759. <https://doi.org/10.1074/jbc.M706268200>
- Cordero, J., Jassim, O., Bao, S., & Cagan, R. (2004). A role for *wingless* in an early pupal cell death event that contributes to patterning the *Drosophila* eye. *Mechanisms of Development*, 121(12), 1523-1530. <https://doi.org/10.1016/j.mod.2004.07.004>
- Cunha, S. R., & Mohler, P. J. (2009). Ankyrin protein networks in membrane formation and stabilization. *Journal of Cellular and Molecular Medicine*, 13(11-12), 4364-4376. <https://doi.org/10.1111/j.1582-4934.2009.00943.x>
- Darcy, M. J., Calvin, K., Cavnar, K., & Ouimet, C. C. (2010). Regional and subcellular distribution of HDAC4 in mouse brain. *The Journal of Comparative Neurology*, 518(5), 722-740. <https://doi.org/10.1002/cne.22241>

Dementia economic impact report 2016. (2017). D. T. T. Ltd.

- Devarajan, P., Stabach, P. R., Mann, A. S., Ardito, T., Kashgarian, M., & Morrow, J. S. (1996). Identification of a small cytoplasmic ankyrin (AnkG119) in the kidney and muscle binds β I Σ^* spectrin and associates with the golgi apparatus. *Journal of Cell Biology*, 133(4), 819-830. <https://doi.org/10.1083/jcb.133.4.819>
- Dietzl, G., Chen, D., Schnorrer, F., Su, K. C., Barinova, Y., Fellner, M., Gasser, B., Kinsey, K., Oettel, S., Scheiblaue, S., Couto, A., Marra, V., Keleman, K., & Dickson, B. J. (2007). A genome-wide transgenic RNAi library for conditional gene inactivation in *Drosophila*. *Nature*, 448(7150), 151-156. <https://doi.org/10.1038/nature05954>
- Duffy, J. B. (2002). GAL4 system in *Drosophila*: a fly geneticist's Swiss army knife. *Genesis*, 34(1-2), 1-15. <https://doi.org/10.1002/gene.10150>
- Dukas, R. (2008). Evolutionary biology of insect learning. *Annual Review Entomology*, 53, 145-160. <https://doi.org/10.1146/annurev.ento.53.103106.093343>
- Dvorak, D. R., Bishop, L. G., & Eckert, H. E. (1975). On the identification of movement detectors in the fly optic lobe. *Journal of Comparative Physiology*, 100, 5-23. <https://doi.org/10.1007/BF00623928>
- Ejima, A., & Griffith, L. C. (2011). Assay for courtship suppression in *Drosophila*. *Cold Spring Harbor Protocols*, 2011(2), 250-255. <https://doi.org/10.1101/pdb.prot5575>
- Enneking, E. M., Kudumala, S. R., Moreno, E., Stephan, R., Boerner, J., Godenschwege, T. A., & Pielage, J. (2013). Transsynaptic coordination of synaptic growth, function, and stability by the L1-type CAM neuroglian. *PLoS Biology*, 11(4), e1001537. <https://doi.org/10.1371/journal.pbio.1001537>
- Fischer, J. A., Giniger, E., Maniatis, T., & Ptashne, M. (1988). GAL4 activates transcription in *Drosophila*. *Nature*, 332(6167), 853-856. <https://doi.org/10.1038/332853a0>
- Fischle, W., Kiermer, V., Dequiedt, F., & Verdin, E. (2001). The emerging role of class II histone deacetylases. *Biochemistry and Cell Biology*, 79(3), 337-348. <https://doi.org/10.1139/bcb-79-3-337>
- Fitzsimons, H. L., Schwartz, S., Given, F. M., & Scott, M. J. (2013). The histone deacetylase HDAC4 regulates long-term memory in *Drosophila*. *PLoS One*, 8(12), e83903. <https://doi.org/10.1371/journal.pone.0083903>

- Fitzsimons, H. L., & Scott, M. J. (2011). Genetic modulation of Rpd3 expression impairs long-term courtship memory in *Drosophila*. *PLoS One*, 6(12), e29171. <https://doi.org/10.1371/journal.pone.0029171>
- Foglietti, C., Filocamo, G., Cundari, E., De Rinaldis, E., Lahm, A., Cortese, R., & Steinkuhler, C. (2006, Jun 30). Dissecting the biological functions of *Drosophila* histone deacetylases by RNA interference and transcriptional profiling. *Journal of Biological Chemistry*, 281(26), 17968-17976. <https://doi.org/10.1074/jbc.M511945200>
- Foust, A., Popovic, M., Zecevic, D., & McCormick, D. A. (2010, May 19). Action potentials initiate in the axon initial segment and propagate through axon collaterals reliably in cerebellar purkinje neurons. *The Journal of Neuroscience*, 30(20), 6891-6902. <https://doi.org/10.1523/JNEUROSCI.0552-10.2010>
- Freeman, M. (1996). Reiterative use of the EGF receptor triggers differentiation of all cell types in the *Drosophila* eye. *Cell*, 87(4), 651-660. [https://doi.org/10.1016/S0092-8674\(00\)81385-9](https://doi.org/10.1016/S0092-8674(00)81385-9)
- Freeman, M. (1997). Cell determination strategies in the *Drosophila* eye. *Development*, 124(2), 261-270. <https://dev.biologists.org/content/develop/124/2/261.full.pdf>
- Freymuth, P. S. (2016). *The actin-binding protein moesin and memory formation in Drosophila : a thesis presented in partial fulfilment of the requirements for the degree of Master of Science in Biochemistry at Massey University, Manawatu, New Zealand* Palmerston North.
- Freymuth, P. S., & Fitzsimons, H. L. (2017, Aug 29). The ERM protein moesin is essential for neuronal morphogenesis and long-term memory in *Drosophila*. *Molecular Brain*, 10(1), 41. <https://doi.org/10.1186/s13041-017-0322-y>
- Gallagher, P. G., Tse, W. T., Scarpa, A. L., Lux, S. E., & Forget, B. G. (1997). Structure and organization of the human ankyrin-1 gene. *The Journal of Biological Chemistry*, 272(31), 19220-19228. <https://doi.org/10.1074/jbc.272.31.19220>
- Garrido, J. J., Giraud, P., Carlier, E., Fernandes, F., Moussif, A., Fache, M.-P., Debanne, D., & Dargent, B. (2003). A targeting motif involved in sodium channel clustering at the axonal initial segment. *Science*, 300(5628), 2091-2094. <https://doi.org/10.1126/science.1085167>
- Gaughan, L., Logan, I. R., Cook, S., Neal, D. E., & Robson, C. N. (2002). Tip60 and histone deacetylase 1 regulate androgen receptor activity through changes to the acetylation status of the receptor. *The Journal of Biological Chemistry*, 277(29), 25904-25913. <https://doi.org/10.1074/jbc.M203423200>

- Glozak, M. A., Sengupta, N., Zhang, X., & Seto, E. (2005, Dec 19). Acetylation and deacetylation of non-histone proteins. *Gene*, 363, 15-23. <https://doi.org/10.1016/j.gene.2005.09.010>
- Gregoretta, I. V., Lee, Y. M., & Goodson, H. V. (2004, Apr 16). Molecular evolution of the histone deacetylase family: functional implications of phylogenetic analysis. *Journal of Molecular Biology*, 338(1), 17-31. <https://doi.org/10.1016/j.jmb.2004.02.006>
- Grozinger, C. M., Hassig, C. A., & Schreiber, S. L. (1999). Three proteins define a class of human histone deacetylases related to yeast Hda1p. *Proceedings of the National Academy of Sciences of the United States of America*, 96(9), 4868-4873. <https://doi.org/10.1073/pnas.96.9.4868>
- Grozinger, C. M., & Schreiber, S. L. (2000). Regulation of histone deacetylase 4 and 5 and transcriptional activity by 14-3-3 dependent cellular localization. *Proceedings of the National Academy of Sciences of the United States of America*, 97(14), 7835-7840. <https://doi.org/10.1073/pnas.140199597>
- Grozinger, C. M., & Schreiber, S. L. (2002). Deacetylase enzymes: biological functions and the use of small-molecule inhibitors. *Chemistry & Biology*, 9(1), 3-16. [https://doi.org/10.1016/s1074-5521\(02\)00092-3](https://doi.org/10.1016/s1074-5521(02)00092-3)
- Guan, Z., Giustetto, M., Lomvardas, S., Kim, J.-H., Miniaci, M. C., Schwartz, J., H., Thanos, D., & Kandel, E. R. (2002). Integration of long-term-memory-related synaptic plasticity involves bidirectional regulation of gene expression and chromatin structure. *Cell*, 111(4), 483-493. [https://doi.org/10.1016/s0092-8674\(02\)01074-7](https://doi.org/10.1016/s0092-8674(02)01074-7)
- Guo, L., Han, A., Bates, D. L., Cao, J., & Chen, L. (2007). Crystal structure of a conserved N-terminal domain of histone deacetylase 4 reveals functional insights into glutamine-rich domains. *Proceedings of the National Academy of Sciences of the United States of America*, 104(11), 4297-4302. <https://doi.org/10.1073/pnas.0608041104>
- Halassa, M. M., Fellin, T., Takano, H., Dong, J. H., & Haydon, P. G. (2007). Synaptic islands defined by the territory of a single astrocyte. *The Journal of Neuroscience*, 27(24), 6473-6477. <https://doi.org/10.1523/JNEUROSCI.1419-07.2007>
- Harris, W. A., Stark, W. S., & Walker, J. A. (1976). Genetic dissection of the photoreceptor system in the compound eye of *Drosophila melanogaster*. *The Journal of Physiology*, 256(2), 415-439. <https://doi.org/10.1113/jphysiol.1976.sp011331>

- Herrup, K., Li, J., & Chen, J. (2013, Aug). The role of ATM and DNA damage in neurons: upstream and downstream connections. *DNA Repair (Amst)*, 12(8), 600-604. <https://doi.org/10.1016/j.dnarep.2013.04.012>
- Heslop-Harrison, J. S., & Schwarzacher, T. (2013). Nucleosomes and centromeric DNA packaging. *Proceedings of the National Academy of Sciences of the United States of America*, 110(50), 19974-19975. <https://doi.org/10.1073/pnas.1319945110>
- Higashijima, S., Kojima, T., Michiue, T., Ishimaru, S., Emori, Y., & Saigo, K. (1991). Dual *Bar* homeo box genes of *Drosophila* required in two photoreceptor cells, R1 and R6, and primary pigment cells for normal eye development. *Genes & Development*, 6(1), 50-60. <https://doi.org/10.1101/gad.6.1.50>
- Hildmann, C., Wegener, D., Riester, D., Hempel, R., Schober, A., Merana, J., Giurato, L., Guccione, S., Nielsen, T. K., Ficner, R., & Schwienhorst, A. (2006). Substrate and inhibitor specificity of class 1 and class 2 histone deacetylases. *Journal of Biotechnology*, 124(1), 258-270. <https://doi.org/10.1016/j.jbiotec.2006.01.030>
- Hortsch, M., Paisley, K. L., Tian, M. Z., Qian, M., Bouley, M., & Chandler, R. (2002, May). The axonal localization of large *Drosophila* ankyrin2 protein isoforms is essential for neuronal functionality. *Molecular and Cellular Neuroscience*, 20(1), 43-55. <https://doi.org/10.1006/mcne.2002.1113>
- Huang, C. Y., & Rasband, M. N. (2018). Axon initial segments: structure, function, and disease. *Annals of the New York Academy of Sciences*, 1420(1), 46-61. <https://doi.org/10.1111/nyas.13718>
- Huang, Y. C., Wang, C. T., Su, T. S., Kao, K. W., Lin, Y. J., Chuang, C. C., Chiang, A. S., & Lo, C. C. (2018). A single-cell level and connectome-derived computational model of the *Drosophila* brain. *Frontiers in Neuroinformatics*, 12, 99. <https://doi.org/10.3389/fninf.2018.00099>
- Iqbal, Z., Vandeweyer, G., van der Voet, M., Waryah, A. M., Zahoor, M. Y., Besseling, J. A., Roca, L. T., Vulto-van Silfhout, A. T., Nijhof, B., Kramer, J. M., Van der Aa, N., Ansar, M., Peeters, H., Helsmoortel, C., Gilissen, C., Vissers, L. E., Veltman, J. A., de Brouwer, A. P., Frank Kooy, R., Riazuddin, S., Schenck, A., van Bokhoven, H., & Rooms, L. (2013). Homozygous and heterozygous disruptions of ANK3: at the crossroads of neurodevelopmental and psychiatric disorders. *Human Molecular Genetics*, 22(10), 1960-1970. <https://doi.org/10.1093/hmg/ddt043>
- Ito, K., Suzuki, K., Estes, P., Ramaswami, M., Yamamoto, D., & Strausfeld, N. J. (1998). The organization of extrinsic neurons and their implications in the functional roles of the mushroom bodies in *Drosophila melanogaster* meigen. *Learning & Memory*, 5(1-2), 52-77. <https://doi.org/10.1101/lm.5.1.52>

- Jaenisch, R., & Bird, A. (2003). Epigenetic regulation of gene expression: how the genome integrates intrinsic and environmental signals. *Nature Genetics*, *33*, 245-254. <https://doi.org/10.1038/ng1089>
- Jayathilaka, N., Han, A., Gaffney, K. J., Dey, R., Jarusiewicz, J. A., Noridomi, K., Philips, M. A., Lei, X., He, J., Ye, J., Gao, T., Petasis, N. A., & Chen, L. (2012). Inhibition of the function of class IIa HDACs by blocking their interaction with MEF2. *Nucleic Acids Research*, *40*(12), 5378-5388. <https://doi.org/10.1093/nar/gks189>
- Jenett, A., Rubin, G. M., Ngo, T.-T. B., Shepherd, D., Murphy, C., Dionne, H., Pfeiffer, B. D., Cavallaro, A., Hall, D., Jeter, J., Iyer, N., Fetter, D., Hausenfluck, J. H., Peng, H., Trautman, E. T., Svirskas, R., Myers, E. W., Iwinski, Z. R., Aso, Y., DePasquale, G. M., Enos, A., Hulamm, P., Lam, S. C. B., Li, H.-H., Laverly, T. R., Long, F., Qu, L., Murphy, S. D., Rokicki, K., Safford, T., Shaw, K., Simpson, J. H., Sowell, A., Tae, S., Yu, Y., & Zugates, C. T. (2012). A GAL4-driver line resource for *Drosophila* neurobiology. *Cell Reports*, *2*(4), 991-1001. <https://doi.org/10.1016/j.celrep.2012.09.011>
- Kandel, E. R., Dudai, Y., & Mayford, M. R. (2014). The molecular and systems biology of memory. *Cell*, *157*(1), 163-186. <https://doi.org/10.1016/j.cell.2014.03.001>
- Kao, H.-Y., Downes, M., Ordentlich, P., & Evans, R. M. (1999). Isolation of a novel histone deacetylase reveals that class I and class II deacetylases promote SMRT-mediated repression. *Genes & Development*, *14*(1), 55-66. <https://www.ncbi.nlm.nih.gov/pmc/articles/PMC316336/pdf/x11.pdf>
- Karagiannis, S. A., & Ready, D. F. (2004). Moesin contributes an essential structural role in *Drosophila* photoreceptor morphogenesis. *Development*, *131*(4), 725-732. <https://doi.org/10.1242/dev.00976>
- Kennedy, M. B. (2013). Synaptic signaling in learning and memory. *Cold Spring Harbor Perspective Biology*, *8*(2), a016824. <https://doi.org/10.1101/cshperspect.a016824>
- Kim, M. S., Akhtar, M. W., Adachi, M., Mahgoub, M., Bassel-Duby, R., Kavalali, E. T., Olson, E. N., & Monteggia, L. M. (2012). An essential role for histone deacetylase 4 in synaptic plasticity and memory formation. *The Journal of Neuroscience*, *32*(32), 10879-10886. <https://doi.org/10.1523/JNEUROSCI.2089-12.2012>
- Kim, Y. C., Lee, H. G., & Han, K. A. (2007). D1 dopamine receptor dDA1 is required in the mushroom body neurons for aversive and appetitive learning in *Drosophila*. *The Journal of Neuroscience*, *27*(29), 7640-7647. <https://doi.org/10.1523/JNEUROSCI.1167-07.2007>

- Kirsh, O., Seeler, J. S., Pichler, A., Gast, A., Muller, S., Miska, E., Mathieu, M., Harel-Bellan, A., Kouzarides, T., Melchior, F., & Dejean, A. (2003). The SUMO E3 ligase RanBP2 promotes modification of the HDAC4 deacetylase. *The EMBO Journal*, 21(11), 2682-2691. <https://doi.org/10.1093/emboj/21.11.2682>
- Koch, I., Schwarz, H., Beuchle, D., Goellner, B., Langegger, M., & Aberle, H. (2008). *Drosophila* ankyrin 2 is required for synaptic stability. *Neuron*, 58(2), 210-222. <https://doi.org/10.1016/j.neuron.2008.03.019>
- Kordeli, E., Lambert, S., & Bennett, V. (1995). AnkyrinG. A new ankyrin gene with neural-specific isoforms localized at the axonal initial segment and node of ranvier. *The Journal of Biological Chemistry*, 270(5), 2352-2359. <https://doi.org/10.1074/jbc.270.5.2352>
- Kumar, A., Kumar Singh, S., Kumar, V., Kumar, D., Agarwal, S., & Rana, M. K. (2015). Huntington's disease: an update of therapeutic strategies. *Gene*, 556(2), 91-97. <https://doi.org/10.1016/j.gene.2014.11.022>
- Kumar, J. P. (2012). Building an ommatidium one cell at a time. *Developmental Dynamics*, 241(1), 136-149. <https://doi.org/10.1002/dvdy.23707>
- Lahm, A., Paolini, C., Pallaoro, M., Nardi, M. C., Jones, P., Neddermann, P., Sambucini, S., Bottomley, S., Surdo, P. L., Carfi, A., Koch, U., Francesco, R. D., Steinkuler, C., & Gallinari, P. (2007). Unraveling the hidden catalytic activity of vertebrate class IIa histone deacetylases. *Proceedings of the National Academy of Sciences of the United States of America*, 104(44). <https://doi.org/10.1073/pnas.0706487104>
- Lambert, S., Yu, H., Prchal, J. T., Lawler, J., Ruff, P., Speicher, D., Cheung, M. C., Kan, Y. W., & Palek, J. (1990). cDNA sequence for human erythrocyte ankyrin. *Proceedings of the National Academy of Sciences of the United States of America*, 87(5), 1730-1734. <https://doi.org/10.1073/pnas.87.5.1730>
- Lamprecht, R., & LeDoux, J. (2004). Structural plasticity and memory. *Nature Reviews Neuroscience*, 5(1), 45-54. <https://doi.org/10.1038/nrn1301>
- Lee, T., Lee, A., & Luo, L. (1999). Development of the *Drosophila* mushroom bodies: Sequential generation of three distinct types of neurons from a neuroblast. *Development*, 126, 4065-4076. <https://doi.org/10.1242/dev.00466>
- Leiss, F., Koper, E., Hein, I., Fouquet, W., Lindner, J., Sigrist, S., & Tavosanis, G. (2009, Mar). Characterization of dendritic spines in the *Drosophila* central nervous system. *Developmental Neurobiology*, 69(4), 221-234. <https://doi.org/10.1002/dneu.20699>

- Leterrier, C., Clerc, N., Rueda-Boroni, F., Montersino, A., Dargent, B., & Castets, F. (2017). Ankyrin G membrane partners drive the establishment and maintenance of the axon initial segment. *Frontiers in Cellular Neuroscience*, *11*, 6. <https://doi.org/10.3389/fncel.2017.00006>
- Li, J., Chen, J., Ricupero, C. L., Hart, R. P., Schwartz, M. S., Kusnecov, A., & Herrup, K. (2012, May). Nuclear accumulation of HDAC4 in ATM deficiency promotes neurodegeneration in ataxia telangiectasia. *Nature Medicine*, *18*(5), 783-790. <https://doi.org/10.1038/nm.2709>
- Libersat, F., & Duch, C. (2004). Mechanisms of dendritic maturation. *Molecular Neurobiology*, *29*(3), 303-320. <https://doi.org/10.1385/MN:29:3:303>
- Litke, C., Bading, H., & Mauceri, D. (2018). Histone deacetylase 4 shapes neuronal morphology via a mechanism involving regulation of expression of vascular endothelial growth factor D. *Journal of Biological Chemistry*, *293*(21), 8196-8207. <https://doi.org/10.1074/jbc.RA117.001613>
- Lloyd, T. E., & Taylor, J. P. (2010). Flightless flies: *Drosophila* models of neuromuscular disease. *Annals of the New York Academy of Sciences*, *1184*(1). <https://doi.org/10.1111/j.1749-6632.2010.05432.x>
- Lu, J., McKinsey, T. A., Nicol, R. L., & Olson, E. N. (2000). Signal-dependent activation of the MEF2 transcription factor by dissociation from histone deacetylases. *Proceedings of the National Academy of Sciences of the United States of America*, *97*(8), 4070-4075. <https://doi.org/10.1073/pnas.080064097>
- Lutz, D., Wolters-Eisfeld, G., Joshi, G., Djogo, N., Jakovcevski, I., Schachner, M., & Kleene, R. (2012). Generation and nuclear translocation of sumoylated transmembrane fragment of cell adhesion molecule L1. *The Journal of Biological Chemistry*, *287*(21), 17161-17175. <https://doi.org/10.1074/jbc.M112.346759>
- Main, P. (2019). *Investigating the role of HDAC4 subcellular distribution in Drosophila : a thesis presented in partial fulfilment of the requirements for the degree of Doctor of Philosophy in Genetics at Massey University, Manawatu, New Zealand Palmerston North.*
- Maitra, U., Scaglione, M. N., Chtarbanova, S., & O'Donnell, J. M. (2019). Innate immune responses to paraquat exposure in a *Drosophila* model of Parkinson's disease. *Scientific Reports*, *9*(1), 12714. <https://doi.org/10.1038/s41598-019-48977-6>
- Margulies, C., Tully, T., & Dubnau, J. (2005). Deconstructing memory in *Drosophila*. *Current Biology*, *15*(17), 700-713. <https://doi.org/10.1016/j.cub.2005.08.024>

- Maslah, E., Rockenstein, E., Adame, A., Alford, M., Crews, L., Hashimoto, M., Seubert, P., Lee, M., Goldstein, J., Chilcote, T., Games, D., & Schenk, D. (2005). Effects of α -synuclein immunization in a mouse model of Parkinson's disease. *Neuron*, *46*(6), 857-868. <https://doi.org/10.1016/j.neuron.2005.05.010>
- Mathews, K. W., Cavegn, M., & Zwicky, M. (2017). Sexual dimorphism of body size Is controlled by dosage of the X-chromosomal gene *Myc* and by the sex-determining gene *tra* in *Drosophila*. *Genetics*, *205*(3), 1215-1228. <https://doi.org/10.1534/genetics.116.192260>
- McBride, S. M. J., Giuliani, G., Choi, C., Krause, P., Correale, D., Watson, K., Baker, G., & Siwicki, K. K. (1999). Mushroom body ablation impairs short-term and long-term memory of courtship conditioning in *Drosophila melanogaster*. *Neuron*, *24*(4), 967-977. [https://doi.org/10.1016/s0896-6273\(00\)81043-0](https://doi.org/10.1016/s0896-6273(00)81043-0)
- McGuire, S. E., Mao, Z., & Davis, R. L. (2004). Spatiotemporal gene expression targeting with the TARGET and gene-switch systems in *Drosophila*. *Sci STKE*, *2004*(220), pl6. <https://doi.org/10.1126/stke.2202004pl6>
- McKinsey, T. A., Kuwahara, K., Bezprozvannaya, S., & Olson, E. N. (2006). Class II histone deacetylases confer signal responsiveness to the ankyrin-repeat proteins ANKRA2 and RFXANK. *Molecular Biology of the Cell*, *17*(1), 438-447. <https://doi.org/10.1091/mbc.e05-07-0612>
- Mielcarek, M., Seredenina, T., Stokes, M. P., Osborne, G. F., Landles, C., Inuabasi, L., Franklin, S. A., Silva, J. C., Luthi-Carter, R., Beaumont, V., & Bates, G. P. (2013). HDAC4 does not act as a protein deacetylase in the postnatal murine brain *in vivo*. *PLoS One*, *8*(11), e80849. <https://doi.org/10.1371/journal.pone.0080849>
- Miska, E. A., Karlsson, C., Langley, E., Nielson, S. J., Pines, J., & Kouzarides, T. (1999). HDAC4 deacetylase associates with and represses the MEF2 transcription factor. *The EMBO Journal*, *18*(18), 5099-5107. <https://doi.org/10.1093/emboj/18.18.5099>
- Mohler, P. J., Gramolini, A. O., & Bennett, V. (2002). Ankyrins. *Journal of Cell Science*, *115*(8), 1565-1566. <https://jcs.biologists.org/content/joces/115/8/1565.full.pdf>
- Morgan, A. R., Hamilton, G., Turic, D., Jehu, L., Harold, D., Abraham, R., Hollingworth, P., Moskvina, V., Brayne, C., Rubinsztein, D. C., Lynch, A., Lawlor, B., Gill, M., O'Donovan, M., Powell, J., Lovestone, S., Williams, J., & Owen, M. J. (2008). Association analysis of 528 intra-genic SNPs in a region of chromosome 10 linked to late onset Alzheimer's disease. *American Journal of Medical Genetics Part B (Neuropsychiatric Genetics)*, *147B*(6), 727-731. <https://doi.org/10.1002/ajmg.b.30670>

- Morris, B., Etoubleau, C., Bourthoumieu, S., Reynaud-Perrine, S., Laroche, C., Lebbar, A., Yardin, C., & Elsea, S. H. (2012). Dose dependent expression of HDAC4 causes variable expressivity in a novel inherited case of brachydactyly mental retardation syndrome. *American Journal of Medical Genetics A*, 158A(8), 2015-2020. <https://doi.org/10.1002/ajmg.a.35463>
- Morris, M. J., & Monteggia, L. M. (2013, Oct). Unique functional roles for class I and class II histone deacetylases in central nervous system development and function. *Int J Dev Neurosci*, 31(6), 370-381. <https://doi.org/10.1016/j.ijdevneu.2013.02.005>
- Mosavi, L. K., Minor, D. L., & Peng, Z.-Y. (2002). Consensus-derived structural determinants of the ankyrin repeat motif. *Proceedings of the National Academy of Sciences of the United States of America*, 99(25), 16029-16034. <https://doi.org/10.1073/pnas.252537899>
- Müller, S., Hoegge, C., Pyrowolakis, G., & Jentsch, S. (2001). Sumo, ubiquitin's mysterious cousin. *Nature Reviews Molecular Cell Biology*, 2(202-210). <https://doi.org/10.1038/35056591>
- Neugroschl, J., & Wang, S. (2011). Alzheimer's disease: diagnosis and treatment across the spectrum of disease severity. *Mt Sinai Journal of Medicine*, 78(4), 596-612. <https://doi.org/10.1002/msj.20279>
- Nickel, M., & Gu, C. (2018). Regulation of central nervous system myelination in higher brain functions. *Neural Plasticity*, 2018(3), 6436453. <https://doi.org/10.1155/2018/6436453>
- Nowak, S. J., & Corces, V. G. (2004). Phosphorylation of histone H3: a balancing act between chromosome condensation and transcriptional activation. *Trends in Genetics*, 20(4), 214-220. <https://doi.org/10.1016/j.tig.2004.02.007>
- Pan, Z., Kao, T., Horvath, Z., Lemos, J., Sul, J. Y., Cranstoun, S. D., Bennett, V., Scherer, S. S., & Cooper, E. C. (2006). A common ankyrin-G-based mechanism retains KCNQ and NaV channels at electrically active domains of the axon. *The Journal of Neuroscience*, 26(10), 2599-2613. <https://doi.org/10.1523/JNEUROSCI.4314-05.2006>
- Pandey, U. B., & Nichols, C. D. (2011). Human disease models in *Drosophila melanogaster* and the role of the fly in therapeutic drug discovery. *Pharmacological Reviews*, 63(2), 411-436. <https://doi.org/10.1124/pr.110.003293>

- Patterson, C. (2018). *World Alzheimer report 2018. The state of the art of dementia research: New frontiers*. A. D. International.
- Perez-Perez, J. M., Candela, H., & Micol, J. L. (2009). Understanding synergy in genetic interactions. *Trends in Genetics*, 25(8), 368-376. <https://doi.org/10.1016/j.tig.2009.06.004>
- Pielage, J., Cheng, L., Fetter, R. D., Carlton, P. M., Sedat, J. W., & Davis, G. W. (2008). A presynaptic giant ankyrin stabilizes the NMJ through regulation of presynaptic microtubules and transsynaptic cell adhesion. *Neuron*, 58(2), 195-209. <https://doi.org/10.1016/j.neuron.2008.02.017>
- Piguel, N. H., Yoon, S., DeSimone, F. I., Sanders, S. S., Gao, R., Horan, K. E., Dionisio, L. E., Garza, J. C., Petryshen, T. L., Thomas, G. M., Smith, K. R., & Penzes, P. (2019). Ankyrin-G-190 palmitoylation mediates dendrite and spine morphogenesis and is altered in response to lithium. *bioRxiv*. <https://doi.org/10.1101/620708>
- Polymeropoulos, M. H., Lavedan, C., Leroy, E., Ide, S. E., Dehejia, A., Dutra, A., Pike, B., Root, H., Rubenstein, J., Boyer, R., Stenroos, E. S., Chandrasekharappa, S., Athanassiadou, A., Papapetropoulos, T., Johnson, W. G., Lazzarini, A. M., Duvoisin, R. C., Di Iorio, G., Golbe, L. I., & Nussbaum, R. L. (1997). Mutation in the α -synuclein gene identified in families with Parkinson's disease. *Science*, 276(5321), 2045-2047. <https://doi.org/10.1126/science.276.5321.2045>
- Presente, A., Boyles, R. S., Serway, C. N., de Belle, J. S., & Andres, A. J. (2003). Notch is required for long-term memory in *Drosophila*. *Proceedings of the National Academy of Sciences of the United States of America*, 101(6), 1764-1768. <https://doi.org/10.1073/pnas.0308259100>
- Przedborski, S. (2017). The two-century journey of Parkinson disease research. *Nature Reviews Neuroscience*, 18(4), 251-259. <https://doi.org/10.1038/nrn.2017.25>
- Rattner, J. B., & Hamkalo, B. A. (1978). Higher order structure in metaphase chromosomes. II. The relationship between the 250 A fiber, superbands and beads-on-a-string. *Chromosoma*, 69(3), 373-379. <https://doi.org/10.1007/BF00332140>
- Ready, D. F., Hanson, T. E., & Benzer, S. (1976). Development of the *Drosophila* retina, a neurocrystalline lattice. *Developmental Biology*, 53(2), 217-240. [https://doi.org/10.1016/0012-1606\(76\)90225-6](https://doi.org/10.1016/0012-1606(76)90225-6)
- Reece, J. B., Meyers, N., Urry, L. A., Cain, M. L., Wasserman, S. A., Minorsky, P. V., Jackson, R. B., & Cooke, B. N. (2014). Animal form and function. In *Campbell biology* (10 ed., pp. 1090-1103). Pearson Education Inc.

- Reiter, L. T., Potocki, L., Chien, S., Gribskov, M., & Bier, E. (2001). A systematic analysis of human disease-associated gene sequences in *Drosophila melanogaster*. *Genome Research*, 11(6), 1114-1125. <https://doi.org/10.1101/gr.169101>
- Richmond, T. J., & Davey, C. A. (2003). The structure of DNA in the nucleosome core. *Nature*, 423(6936), 145-150. <https://doi.org/10.1038/nature01595>
- Riedl, J., Crevenna, A. H., Kessenbrock, K., Yu, J. H., Neukirchen, D., Bista, M., Bradke, F., Jenne, D., Holak, T. A., Werb, Z., Sixt, M., & Wedlich-Soldner, R. (2008). Lifeact: a versatile marker to visualize F-actin. *Nature Methods*, 5(7), 605-607. <https://doi.org/10.1038/nmeth.1220>
- Rundlett, S. E., Carmen, A. A., Kobayashi, R., Bavykin, S., Turner, B. M., & Grunstein, M. (1996). HDAC1 and RPD3 are members of distinct yeast histone deacetylase complexes that regulate silencing and transcription. *Proceedings of the National Academy of Sciences of the United States of America*, 93(25), 14503-14508. <https://doi.org/10.1073/pnas.93.25.14503>
- Sando, R., 3rd, Gounko, N., Pieraut, S., Liao, L., Yates, J., 3rd, & Maximov, A. (2012). HDAC4 governs a transcriptional program essential for synaptic plasticity and memory. *Cell*, 151(4), 821-834. <https://doi.org/10.1016/j.cell.2012.09.037>
- Schlumm, F., Mauceri, D., Freitag, H. E., & Bading, H. (2013). Nuclear calcium signaling regulates nuclear export of a subset of class IIa histone deacetylases following synaptic activity. *The Journal of Biological Chemistry*, 288(12), 8074-8084. <https://doi.org/10.1074/jbc.M112.432773>
- Schwartz, S. (2016). *Investigating the role of histone deacetylase HDAC4 in long-term memory formation : a thesis presented in partial fulfilment of the requirements for the degree of Doctor of Philosophy in Genetics at Massey University, Manawatu, New Zealand* [Doctoral, Palmerston North. <http://hdl.handle.net/10179/11504>
- Schwartz, S., Truglio, M., Scott, M. J., & Fitzsimons, H. L. (2016). Long-term memory in *Drosophila* is influenced by histone deacetylase HDAC4 interacting with SUMO-conjugating enzyme Ubc9. *Genetics*, 203(3), 1249-1264. <https://doi.org/10.1534/genetics.115.183194>
- Scott, E. K., Raabe, T., & Luo, L. (2002). Structure of the vertical and horizontal system neurons of the lobula plate in *Drosophila*. *The Journal of Comparative Neurology*, 454(4), 470-481. <https://doi.org/10.1002/cne.10467>

- Sekar, R. B., & Periasamy, A. (2003). Fluorescence resonance energy transfer (FRET) microscopy imaging of live cell protein localizations. *The Journal of Cell Biology*, *160*(5), 629-633. <https://doi.org/10.1083/jcb.200210140>
- Shen, X., Chen, J., Li, J., Kofler, J., & Herrup, K. (2016). Neurons in vulnerable regions of the Alzheimer's disease brain display reduced ATM signaling. *eNeuro*, *3*(1), 1-18. <https://doi.org/10.1523/ENEURO.0124-15.2016>
- Sidiropoulou, K., Pissadaki, E. K., & Poirazi, P. (2006). Inside the brain of a neuron. *EMBO Reports*, *7*(9), 886-892. <https://doi.org/10.1038/sj.embor.7400789>
- Siegenthaler, D., Enneking, E. M., Moreno, E., & Pielage, J. (2015). L1CAM/neuroglial controls the axon-axon interactions establishing layered and lobular mushroom body architecture. *The Journal of Cell Biology*, *208*(7), 1003-1018. <https://doi.org/10.1083/jcb.201407131>
- Somoza, J. R., Skene, R. J., Katz, B. A., Mol, C., Ho, J. D., Jennings, A. J., Luong, C., Arvai, A., Buggy, J. J., Chi, E., Tang, J., Sang, B. C., Verner, E., Wynands, R., Leahy, E. M., Dougan, D. R., Snell, G., Navre, M., Knuth, M. W., Swanson, R. V., McRee, D. E., & Tari, L. W. (2004). Structural snapshots of human HDAC8 provide insights into the class I histone deacetylases. *Structure*, *12*(7), 1325-1334. <https://doi.org/10.1016/j.str.2004.04.012>
- Starkman, B. G., Sakharkar, A. J., & Pandey, S. C. (2012). Epigenetics - Beyond the genome in alcoholism. *Alcohol Research Current Reviews*, *34*(3), 293-305. <https://www.ncbi.nlm.nih.gov/pmc/articles/PMC3860414/pdf/arcr-34-3-293.pdf>
- Stephan, R., Goellner, B., Moreno, E., Frank, C. A., Hugenschmidt, T., Genoud, C., Aberle, H., & Pielage, J. (2015). Hierarchical microtubule organization controls axon caliber and transport and determines synaptic structure and stability. *Developmental Cell*, *33*(1), 5-21. <https://doi.org/10.1016/j.devcel.2015.02.003>
- Sterner, D. E., & Berger, S. L. (2000). Acetylation of histones and transcription-related factors. *Microbiology and molecular biology reviews*, *64*(2), 435-459. <https://doi.org/10.1128/mnbr.64.2.435-459.2000>
- Sudhof, T. C., & Malenka, R. C. (2008). Understanding synapses: past, present, and future. *Neuron*, *60*(3), 469-476. <https://doi.org/10.1016/j.neuron.2008.10.011>
- Suster, M. L., Seugnet, L., Bate, M., & Sokolowski, M. B. (2004). Refining GAL4-driven transgene expression in *Drosophila* with a GAL80 enhancer-trap. *Genesis*, *39*(4), 240-245. <https://doi.org/10.1002/gene.20051>

- Technau, G., & Heisenberg, M. (1982). Neural reorganization during metamorphosis of the corpora pedunculata in *Drosophila melanogaster*. *Nature*, 295(5848), 405-407. <https://doi.org/10.1038/295405a0>
- ten Have, S., Boulon, S., Ahmad, Y., & Lamond, A. I. (2011). Mass spectrometry-based immuno-precipitation proteomics - the user's guide. *Proteomics*, 11(6), 1153-1159. <https://doi.org/10.1002/pmic.201000548>
- Tesli, M., Koefoed, P., Athanasiu, L., Mattingsdal, M., Gustafsson, O., Agartz, I., Rimol, L. M., Brown, A., Wirgenes, K. V., Smorr, L. L., Kahler, A. K., Werge, T., Mors, O., Mellerup, E., Jonsson, E. G., Melle, I., Morken, G., Djurovic, S., & Andreassen, O. A. (2011). Association analysis of ANK3 gene variants in nordic bipolar disorder and schizophrenia case-control samples. *American Journal of Medical Genetics. Part B Neuropsychiatric Genetics*, 156B(8), 969-974. <https://doi.org/10.1002/ajmg.b.31244>
- Thevananther, S., Kolli, A. H., & Devarajan, P. (1998). Identification of a novel ankyrin isoform (AnkG190) in kidney and lung that associates with the plasma membrane and binds a-Na,K-ATPase. *Journal of Biological Chemistry*, 273(37), 23952-23958. <https://doi.org/10.1074/jbc.273.37.23952>
- Tomlinson, A., & Ready, D. F. (1987). Neuronal differentiation in the *Drosophila* ommatidium. *Developmental Biology*, 120(2), 366-376. [https://doi.org/10.1016/0012-1606\(87\)90239-9](https://doi.org/10.1016/0012-1606(87)90239-9)
- Trunova, S., Baek, B., & Giniger, E. (2011). Cdk5 regulates the size of an axon initial segment-like compartment in mushroom body neurons of the *Drosophila* central brain. *The Journal of Neuroscience*, 31(29), 10451-10462. <https://doi.org/10.1523/JNEUROSCI.0117-11.2011>
- Turner, G. C., Bazhenov, M., & Laurent, G. (2008). Olfactory representations by *Drosophila* mushroom body neurons. *Journal of Neurophysiology*, 99(2), 734-746. <https://doi.org/10.1152/jn.01283.2007>
- van der Kloot, W., & Kita, H. (1974). Mechanisms for neurotransmitter release. *Oxford Journals*, 24(1), 13-17. <https://www.jstor.org/stable/1296654>
- Veening, J. W., Smits, W. K., Hamoen, L. W., Jongbloed, J. D., & Kuipers, O. P. (2004). Visualization of differential gene expression by improved cyan fluorescent protein and yellow fluorescent protein production in *Bacillus subtilis*. *Applied and Environmental Microbiology*, 70(11), 6809-6815. <https://doi.org/10.1128/AEM.70.11.6809-6815.2004>
- Verreault, A. (2000). De novo nucleosome assembly: new pieces in an old puzzle. *Genes & Development*, 14(12), 1430-1438. <https://doi.org/10.1101/gad.14.12.1430>

- Villavicencio-Lorini, P., Klopocki, E., Trimborn, M., Koll, R., Mundlos, S., & Horn, D. (2013). Phenotypic variant of Brachydactyly-mental retardation syndrome in a family with an inherited interstitial 2q37.3 microdeletion including *HDAC4*. *European Journal of Human Genetics*, 21(7), 743-748. <https://doi.org/10.1038/ejhg.2012.240>
- Wang, A. H., Bertos, N. R., Vezmar, M., Pelletier, N., Crosato, M., Heng, H. H., Th'ng, J., Han, J., & Yang, X.-J. (1999). HDAC4, a human histone deacetylase related to yeast HDA1, is a transcriptional corepressor. *Molecular and Cellular Biology*, 19(11), 7816-7827. <https://doi.org/10.1128/mcb.19.11.7816>
- Wang, A. H., Gregoire, S., Zika, E., Xiao, L., Li, C. S., Li, H., Wright, K. L., Ting, J. P., & Yang, X. J. (2005). Identification of the ankyrin repeat proteins ANKRA and RFXANK as novel partners of class IIa histone deacetylases. *The Journal of Biological Chemistry*, 280(32), 29117-29127. <https://doi.org/10.1074/jbc.M500295200>
- Wang, A. H., & Yang, X. J. (2001). Histone deacetylase 4 possesses intrinsic nuclear import and export signals. *Molecular and Cellular Biology*, 21(17), 5992-6005. <https://doi.org/10.1128/mcb.21.17.5992-6005.2001>
- Wang, C., Wei, Z., Chen, K., Ye, F., Yu, C., Bennett, V., & Zhang, M. (2014). Structural basis of diverse membrane target recognitions by ankyrins. *Elife*, 3, e04353. <https://doi.org/10.7554/eLife.04353>
- Wang, Z., Qin, G., & Zhao, T. C. (2014). Histone deacetylase 4 (HDAC4): mechanism of regulation and biological functions. *Epigenomics*, 6(1), 139-150. <https://doi.org/10.2217/epi.13.73>
- Weber, T., Stephan, R., Moreno, E., & Pielage, J. (2019). The ankyrin repeat domain controls presynaptic localization of *Drosophila* ankyrin2 and is essential for synaptic stability. *Frontiers in Cell and Developmental Biology*, 7, 148. <https://doi.org/10.3389/fcell.2019.00148>
- Weller, J., & Budson, A. (2018). Current understanding of Alzheimer's disease diagnosis and treatment. *F1000Research*, 7, 1161. <https://doi.org/10.12688/f1000research.14506.1>
- Williams, S. R., Aldred, M. A., Der Kaloustian, V. M., Halal, F., Gowans, G., McLeod, D. R., Zondag, S., Toriello, H. V., Magenis, R. E., & Elsea, S. H. (2010). Haploinsufficiency of HDAC4 causes brachydactyly mental retardation syndrome, with brachydactyly type E, developmental delays, and behavioral problems. *The American Journal of Human Genetics*, 87(2), 219-228. <https://doi.org/10.1016/j.ajhg.2010.07.011>

- Wu, Q., Yang, X., Zhang, L., Zhang, Y., & Feng, L. (2017). Nuclear accumulation of histone deacetylase 4 (HDAC4) exerts neurotoxicity in models of Parkinson's disease. *Molecular Neurobiology*, 54(9), 6970-6983. <https://doi.org/10.1007/s12035-016-0199-2>
- Wu, Y., Hou, F., Wang, X., Kong, Q., Han, X., & Bai, B. (2016). Aberrant expression of histone deacetylases 4 in cognitive disorders: molecular mechanisms and a potential target. *Frontiers in Molecular Neuroscience*, 9, 114. <https://doi.org/10.3389/fnmol.2016.00114>
- Xu, C., Jin, J., Bian, C., Lam, R., Tian, R., Weist, R., You, L., Nie, J., Bochkarev, A., Tempel, W., Tan, C. S., Wasney, G. A., Vedadi, M., Gish, G. D., Arrowsmith, C. H., Pawson, T., Yang, X.-J., & Min, J. (2012). Sequence-specific recognition of a PxLPxI/L motif by an ankyrin repeat tumbler lock. *Science Signaling*, 5(226), ra39. <https://doi.org/10.1126/scisignal.2002979>
- Yuan, A., Yi, Z., Wang, Q., Sun, J., Li, Z., Du, Y., Zhang, C., Yu, T., Fan, J., Li, H., & Yu, S. (2012). ANK3 as a risk gene for schizophrenia: new data in Han Chinese and meta analysis. *American Journal of Medical Genetics. Part B, Neuropsychiatric Genetics*, 159B(8), 997-1005. <https://doi.org/10.1002/ajmg.b.32112>
- Zhang, P., Sun, Q., Zhao, C., Ling, S., Li, Q., Chang, Y. Z., & Li, Y. (2014). HDAC4 protects cells from ER stress induced apoptosis through interaction with ATF4. *Cellular Signalling*, 26(3), 556-563. <https://doi.org/10.1016/j.cellsig.2013.11.026>
- Zhang, Y., & Reinberg, D. (2001). Transcription regulation by histone methylation: interplay between different covalent modifications of the core histone tails. *Genes & Development*, 15(18), 2343-2360. <https://doi.org/10.1101/gad.927301>
- Zhao, X., Lenek, D., Dag, U., Dickson, B. J., & Keleman, K. (2018). Persistent activity in a recurrent circuit underlies courtship memory in *Drosophila*. *Elife*, 7. <https://doi.org/10.7554/eLife.31425>
- Zhao, X., Sternsdorf, T., Bolger, T. A., Evans, R. M., & Yao, T. P. (2005). Regulation of MEF2 by histone deacetylase 4- and SIRT1 deacetylase-mediated lysine modifications. *Molecular and Cellular Biology*, 25(19), 8456-8464. <https://doi.org/10.1128/MCB.25.19.8456-8464.2005>
- Zhou, D., Lambert, S., Malen, P. L., Carpenter, S., Boland, L. M., & Bennett, V. (1998). AnkyrinG is required for clustering of voltage-gated Na channels at axon initial segments and for normal action potential firing. *The Journal of Cell Biology*, 143(5), 1295-1304. <https://doi.org/10.1083/jcb.143.5.1295>

- Zhu, C. C., Bornemann, D. J., Zhitomirsky, D., Miller, E. L., O'Connor, M. B., & Simon, J. A. (2008). *Drosophila* histone deacetylase-3 controls imaginal disc size through suppression of apoptosis. *PLoS Genetics*, 4(2), e1000009. <https://doi.org/10.1371/journal.pgen.1000009>
- Zhu, S., Chiang, A. S., & Lee, T. (2003). Development of the *Drosophila* mushroom bodies: elaboration, remodeling and spatial organization of dendrites in the calyx. *Development*, 130(12), 2603-2610. <https://doi.org/10.1242/dev.00466>
- Zhu, Y., Huang, M., Bushong, E., Phan, S., Uytiepo, M., Beutter, E., Boemer, D., Tsui, K., Ellisman, M., & Maximov, A. (2019). Class IIa HDACs regulate learning and memory through dynamic experience-dependent repression of transcription. *Nature Communications*, 10(1), 3469. <https://doi.org/10.1038/s41467-019-11409-0>
- Zweifel, M. E., Leahy, D. J., Hughson, F. M., & Barrick, D. (2003). Structure and stability of the ankyrin domain of the *Drosophila* notch receptor. *Protein Science*, 12(11), 2622-2632. <https://doi.org/10.1110/ps.03279003>

6 Appendix

6.1 Fly strains

Fly strains (Shorthand names)	Genotype	Source
<i>w(cs10)</i>	<i>w[CS10]</i>	R.Davis
<i>elav-GAL4</i>	<i>w[CS10], P{w[+mW.hs]=GawB}elav[C155]</i>	BDSC 458
<i>Ank2₁₉₀₋₉₄₆-HA;</i> <i>DmHDAC4-Myc</i>	<i>w[CS10]; PBac{y+-attP-3B}VK22, UAS-Ank2-repeat-HA; UAS-DmHDAC4(WT)-Myc. Inserts into VK22(2R) 57F5 and P2:(3L) 68A4</i>	H.Fitzsimons
<i>DmHDAC4-Myc</i> <i>(DmHDAC4)</i>	<i>w[CS10]; P{y[+t7.7]=CaryP}attP2, UAS-DmHDAC4(WT)-Myc. Insert into P2:(3L) 68A4</i>	Genetivision, USA
<i>Ank2₁₉₀₋₉₄₆-HA</i> <i>(Ank2₁₉₀₋₉₄₆)</i>	<i>w[CS10]; PBac{y+-attP-3B}VK22, UAS-Ank-repeat-HA. Insert into VK22(2R) 57F5</i>	Genetivision, USA
<i>HDAC4::YFP</i>	<i>w[CS10]; P{w[+mW.hs]=GawB}elav[C155], CPTI-000077</i>	H.Fitzsimons
<i>Ank2 RNAi</i>	<i>[wCS10]; P{attP,y[+],w[3`] CG42734</i>	VDRC 107369
<i>HDAC4</i>	<i>w[CS10]; P{3xP3-RFP=attP-86F}, UAS-DmHDAC4</i>	Helen Fitzsimons
<i>HDAC4; Ank2 RNAi</i>	<i>w[CS10]; CG42734 RNAi (VDRC 107369); P{3xP3-RFP=attP-86F}, UAS-DmHDAC4</i>	Helen Fitzsimons
<i>HDAC4 RNAi</i>	<i>w[CS10]; P{GD9446}v20522</i>	VDRC #20522
<i>Ank2::EGFP</i>	<i>w[CS10]; PBac{EGFP-IV}ank2[KM0104]</i>	Kyoto Stock Centre #109758
<i>3A GAL4; UAS LifeAct</i>	<i>w[CS10]; P{w[+mW.hs]=GawB}3A, pUAS[Lifeact-GFP/CyO]</i>	Helen Fitzsimons
<i>GMR-GAL4</i>	<i>w[CS10]; P{w[+mC]=GAL4-ninaE.GMR}12</i>	Bloomington Stock Center 1104

<i>DmHDAC4 3A</i>	<i>w[CS10]; P{y[+t7.7]=CaryP}attP2, UAS-DmHDAC4-3A-Myc. Insert into P2:(3L) 68A4</i>	Genetivision, USA
<i>DmHDAC4Δ NLS</i>	<i>w[CS10]; P{y[+t7.7]=CaryP}attP2, UAS-DmHDAC4-ΔNLS-Myc. Insert into P2:(3L) 68A4</i>	Genetivision, USA
<i>DmHDAC4 ΔMEF</i>	<i>w[CS10]; P{y[+t7.7]=CaryP}attP2, UAS-DmHDAC4-ΔMEF2-Myc. Insert into P2:(3L) 68A4</i>	Genetivision, USA
<i>DmHDAC4 ΔAnk</i>	<i>w[CS10]; P{y[+t7.7]=CaryP}attP2, UAS-DmHDAC4-ΔAnk-Myc. Insert into P2:(3L) 68A4</i>	Genetivision, USA
<i>DmHDAC4 Y1142H</i>	<i>w[CS10]; P{y[+t7.7]=CaryP}attP2, UAS-DmHDAC4-Y1142H-Myc. Insert into P2:(3L) 68A4</i>	Genetivision, USA

Table 6.1. Genotypes and sources of *Drosophila melanogaster* strains used in this study. Abbreviations: R. Davis: Professor Ron Davis, The Scripps Institute, Florida. BDSC = Bloomington *Drosophila* Stock Centre. Genetivision, USA. VDRC = Vienna *Drosophila* Resource Centre, Kyoto Stock Centre, Japan.

6.2 Ank2₁₉₀₋₉₄₆-HA sequence

The 23 ANK repeats of Ankyrin2 are highlighted in red. The C-terminal 3x-HA tag is in bold.

```

1 MSNANGLNAL HLASKDGHFH VVSELLRRGA IVDSATKKGN TALHIASLAG QEEVVKLLLE
61 HNASVNVQSQ NGFTPLYMAA QENHDAVVRL LLSNGANQSL ATEDGFTPLA VAMQQGHDKV
121 VAVLLES DTR GKVRLPALHI AAKKDDVCAA TLLLDNDHNP DVTSKSGFTP LHIASHYGNQ
181 NIANLLIQKG ADVNYSAKHN ISPLHVAAKW GKTNMVSLLL EKGGNIEAKT RDGLTPLHCA
241 ARSGHEQVVD MLLERGAPIS AKTKNGLAPL HMAAQGEHVD AARILLYHRA PVDEVTVDYL
301 TALHVAACHG HVRVAKLLLD RNADANARAL NGFTPLHIAC KKNRLKVVEL LLRHGASISA
361 TTESGLTPLH VAAFMGCMNI VIYLLQHDAS PDVPTVRGET PLHLAARANQ TDIIRILLRN
421 GAQVDARARE QQTPLHIASR LGNVDIVMLL LQHGAQVDAT TKDMYTALHI AAKEGQDEVA
481 AVLIENGAAL DAATKKGFTP LHLTAKYGHI KVAQLLLQKE ADVDAQGKNG VTPHLVACHY
541 NNQQVALLLL EKGASPHATA KNGHTPLHIA ARKNQMDIAT TLLEYGALAN AESKAGFTPL
601 HLSSQEGHAE ISNLLIEHKA AVNHPAKNGL TPMHLCAQED NVNVAEILEK NGANIDMATK
661 AGYTPLHVAS HFGQANMVRV LLQNGANVDA ATSIGYTPLH QTAQQGHCHI VNLLLEHKAN
721 ANAQTVNGQT PLHIARKLGY ISVLDLSLTI TKEDETAAGG GYPYDVPDYA GYPYDVPDYA
781 GSYPYDVPDY A

```


6.3 HDAC4 variant sequences

DmHDAC4-Myc

Wild-type DmHDAC4 isoform D, aa 1 to 1252 with a C-terminal 6x-Myc tag sequence (bold).

```
1  MSSPDDRIP  HDLPSEAGSD  ERL LHITPAT  LTLDFKPHPA  VDIDQQIMEL  KKSQELQKQR
61  LINSFQEQSK  QMELEHKLQL  EHKYQFAVNS  HGAFQELRNE  SMVTAAAAAV  AQEQHRQQLH
121  QQQQQHQQQQ  QQQQHQQQQQ  QQQARGRDGM  KLKQNCSSANA  SPEVKQILNC  FILSRKSQAA
181  ASNGTTTTSP  YRNRGVVKSS  SGESLPAGTV  TSAHPYKIPQ  PPPSLLKYES  DFPLRKTAEE
241  PNLLKIRLKQ  SVIERKARIG  GPAGARRHER  LLQAAQRRQQ  KNSVLTCNS  TPDSGPNPSP
301  SAAALAVGVV  GSRGSPSAP  IQEENEESQ  YQPGQRSSIN  DLPLFSSPSL  PNISLGRPHL
361  PNSAQAAHQV  NAQVAAQAQA  QAQAQAQAA  MFAALAAAQG  GCGQPGYYP  LGMAFVGRQP
421  APLAMIPATG  IAPQQPSPV  RSASATSTSS  SQASLVGDVA  PPQAAHAATI  LPSSSSYMQQ
481  LGSVAGSGVN  LHAAAVAAAA  AAAAAAGSLP  PTNSHGHGHI  SHAHPHHAH  GHGHGHGHI
541  YAGHQHNVPI  TDAQVAQVHL  HKQGRPLGR  TQAAPLPLGH  PMLTGAVQLN  VVQTHYENSE
601  AERQAYEHQV  VNQKVRQTVL  TRSGAAAAAA  AAAGVSVVRE  AQLKEEDDD  AAEVMDLTDK
661  KKPPKTVLTS  TIATSTSQL  PEALAAAAAA  AAYRAPHNAS  SNSASATKSG  IKLRDQEYLO
721  QREQQLLLLQ  QEEELAKSLM  RPLSRTLASP  LVPLGPHGLS  QIPDTGQOPA  PIATSSSADH
781  IPPVNLSLPH  RQHRQLMSTL  YASQLRNHP  SASGSPPHKV  TTGLAYDPLM  LKHSCICGDN
841  AQHPEHSGRL  QSVWARLNET  DLVKRCRDLR  ARKATQEELQ  TVHTEAHAML  FGSNQCQLSR
901  PKLENTLSAS  FVRLSCGGLG  VDLDTWNEH  HTATAARMAA  GCVIDLALKT  AKGDLRNGFA
961  VVRPPGHAE  ANLAMGFCFF  NSIAIAAKLL  RQRMPEVRI  LIVDWDVHHG  NGTQQAFYQS
1021  PDILYLSIHR  HDDGNFFPGT  GGPTECGSGA  GLGFNVNLSW  SGALNPPLGD  AEYIAAFRTV
1081  VMPIARFNP  DIVLVSSGFD  AATGHPAPLG  GYHVSPACFG  FMTRELLQLA  NGKVVLALEG
1142  GYDLAAICDS  AQECVRALLG  DPAAPIAKAE  LERPPCQNAI  NTLQKTIAIQ  QTHWPCVRML
1201  EHTVGLSALE  TLKVEHDESE  TINAMAGLSM  QSMHRTLSRD  DSEEPMDQDE  TKGGGEQKLI
1261  SEEDLNEMEQ  KLISEEDLNE  MEQKLISEED  LNEMEQKLIS  EEDLNEMEQK  LISEEDLNEM
1321  ESLGDLTMEQ  KLISEEDL
```

DmHDAC4 3A

Mutations of three conserved serine residues in human HDAC4 prevent 14-3-3 binding, which is required for nuclear export, therefore accumulating HDAC4 in the nucleus. The corresponding *Drosophila* amino acids S239, S573 and S748 that have been mutated to alanine are shown in red bold. The C-terminal 6x-Myc tag sequence is in bold.

```
1  MSSPDDRIP I HDLPSEAGSD ERL LHITPAT LTLDFKPHPA V D I D Q Q I M E L K K S Q E L Q K Q R
61  L I N S F Q E Q S K Q M E L E H K L Q L E H K Y Q F A V N S H G A F Q E L R N E S M V T A A A A A V A Q E Q H R Q Q L H
121 Q Q Q Q H Q Q Q Q Q Q Q Q Q Q H Q Q Q Q Q Q Q Q Q A R G R D G M K L K Q N C S A N A S P E V K Q I L N C F I L S R K S Q A A
181 A S N G T T T T T S P Y R N R G V V K S S S G E S L P A G T V T S A H P Y K I P Q P P P S L L K Y E S D F P L R K T A A E
241 P N L L K I R L K Q S V I E R K A R I G G P A G A R R H E R L L Q A A Q R R Q Q K N S V L T N C N S T P D S G P N S P P
301 S A A A L A V G V V G S R G S P T S A P I Q E E N E E G S Q Y Q P G Q R S S I N D L P L F S S P S L P N I S L G R P H L
361 P N S A Q A H A Q V N A Q V A A Q A Q A Q A Q A Q A H A M F A A L A A A A Q G C G C Q P G Y Y N P L G M A F V G R Q P
421 A P L A M I P A T G I A P Q Q P S P V V R S A S A T S T S S S Q A S L V G D V A P P Q A H A A S T I L P S S S S Y M Q Q
481 L G S V A G S G V N L H A A A V A A A A A A A A A A A G S L P P T N S H G H G H G S H A H P H P H A H G H G H G H G H G I
541 Y A G H Q H N V P I T D A Q V A Q V H L H K Q G H R P L G R T Q A A P L P L G H P M L T G A V Q L N V V Q T H Y E N S E
601 A E R Q A Y E H Q V V N Q K V R Q T V L T R S G A A A A A A A A A A G V S V V R E A Q L K E E D D D S A A E V M D L T D K
661 K K P P K T V L T S T I A T S T S Q N L P E A L A A A A A A A A A Y R A P H N A S S N S A S A T K S G I K L R D Q E Y L Q
721 Q Q R E Q L L L L Q Q E E E L A K S L M R P L S R T L A S P L V P L G P H G L S Q I P D T G Q Q P A P I A T S S S A D H
781 I P P V N L S L P H R Q H R Q L M S T L Y A S Q L R N H Q P S A S G S P P H K V T T G L A Y D P L M L K H S C I C G D N
841 A Q H P E H S G R L Q S V W A R L N E T D L V K R C D R L R A R K A T Q E E L Q T V H T E A H A M L F G S N Q C Q L S R
901 P K L E N T L S A S F V R L S C G G L G V D L D T T W N E H H T A T A A R M A A G C V I D L A L K T A K G D L R N G F A
961 V V R P P G H H A E A N L A M G F C F F N S I A I A A K L L R Q R M P E V R R I L I V D W D V H H G N G T Q Q A F Y Q S
1021 P D I L Y L S I H R H D D G N F F P G T G G P T E C G S G A G L G F N V N I S W S G A L N P P L G D A E Y I A A F R T V
1081 V M P I A R S F N P D I V L V S S G F D A A T G H P A P L G G Y H V S P A C F G F M T R E L L Q L A N G K V V L A L E G
1142 G Y D L A A I C D S A Q E C V R A L L G D P A A P I A K A E L E R P P C Q N A I N T L Q K T I A I Q Q T H W P C V R M L
1201 E H T V G L S A L E T L K V E H D E S E T I N A M A G L S M Q S M H R T L S R D D S E E P M D Q D E T K G G G E Q K L I
1261 S E E D L N E M E Q K L I S E E D L N E M E Q K L I S E E D L N E M E Q K L I S E E D L N E M E Q K L I S E E D L N E M
1321 E S L G D L T M E Q K L I S E E D L
```

DmHDAC4 ΔAnk

Mutations of L351 and L354 of human HDAC4 abolishes binding of ANKRA2 (Xu et al., 2012). The consensus sequence for human ANKRA2 binding is the PxLPxI/L motif which is also present in *Drosophila* HDAC4. If either P349, L352, P352 or I354 of human HDAC4 are mutated to alanine, binding of HDAC4 to ANKRA2 is abolished. These amino acids are highlighted in bold red.

342 LPLYTS**PSLPNI**TLGLP Hs HDAC4

342 LPLFSSPSLPNISLGRP Dm HDAC4

In *Drosophila* HDAC4 these amino acids were mutated to alanine, as shown in bold blue, with a C-terminal 6x-Myc tag sequence (bold).

342 LPLFSSPSLPNISLGRP Dm HDAC4

342 LPLFSS**ASAANA**SLGRP Dm HDAC4 ΔAnk

```
1  MSSPDDRIP I HDLPSEAGSD ERL LHITPAT LTLDFKPHPA VDIDQQIMEL KKSQELQKQR
61  LINSFQE QSK QMELEHKLQL EHKYQFAVNS HGAFQELRNE SMVTAAAAAV AQEQHRQQLH
121 QQQQQHQQQQ QQQQQHQQQQ QQQARGRDGM KLKQNC SANA SPEVKQILNC FILSRKSQAA
181 ASNGTTTTSP YRNRGVVKSS SGESLPAGTV TSAHPYKIPQ PPPSLLKYES DFPLRKTAAE
241 PNLKIRLQ SVIERKARIG GPAGARRHER LLQAAQRRQ KNSVLTNCNS TPDSGPN SPP
301 SAAALAVGVV GSRGSP TSAP IQEENE EGSQ YQPGQRSSIN DLPLFSSASA ANASLGRPHL
361 PNSAQAHQV NAQVAAQAQA QAQAQAQAH A MFAALAAAQG GCGQPGYYP LGMAFVGRQP
421 APLAMIPATG IAPQQPSPV RSASATSTSS SQASLVGDVA PPQAHAASTI LPSSSSYMQQ
481 LGSVAGSGVN LHAAAVAAAA AAAAAAGSLP PTNSHGHGHG SHAHPH PHAH GHGHGHGHGI
541 YAGHQHN VPI TDAQVAQVHL HKQGHRPLGR TQAAPLPLGH PMLTGAVQLN VVQTHYENSE
601 AERQAYEHQV VNQKVRQTVL TRSGAAAAAA AAAGVSVVRE AQLKEEDDDS AAEVMDLTDK
661 KKPPKTVLTS TIATSTSQNL PEALAAAAAA AAYRAPHNAS SNSASATKSG IKLRDQEY LQ
721 QQREQLLLLQ QEEELAKSLM RPLSRTLASP LVPLGPHGLS QIPDTGQQPA PIATSSSADH
781 IPPVNLSLPH RQHRQLMSTL YASQLRNHQP SASGSPPHKV TTGLAYDPLM LKHSCICGDN
841 AQHPEHSGRL QSVWARLNET DLVKRC DRLR ARKATQEELQ TVHTEAHAML FGSNQCQLSR
901 PKLENTLSAS FVRLSCGGLG VDLDTTWNEH HTATAARMAA GCVIDLALKT AKGDLRNGFA
961 VVRPPGHAE ANLAMGFCFF NSIAIAAKLL RQRMPEV RRI LIVDWDVHHG NGTQQAFYQS
1021 PDILYLSIHR HDDGNFFPGT GGPTTECGSGA GLGFNVN ISW SGALNPPLGD AEYIAAFRTV
1081 VMPIARSFNP DIVLVSSGFD AATGHPAPLG GYHVSPACFG FMTRELLQLA NGKVVLALEG
1142 GYDLAAICDS AQECVRALLG DPAAPIAKAE LERPPCQNAI NTLQKTIAIQ QTHWPCVRML
1201 EHTVGLSALE TLKVEHDESE TINAMAGLSM QSMHRTL SRD DSEEPMDQDE TKGGGEQKLI
1261 SEEDLNEMEQ KLISEEDLNE MEQKLISEED LNEMEQKLIS EEDLNEMEQK LISEEDLNEM
1321 ESLGDLTMEQ KLISEEDL
```

DmHDAC4 ΔMEF2

Amino acids shown to be important for MEF2 binding to human HDAC4 (Jayathilaka et al., 2012; Wang & Yang, 2001) and are highlighted in bold red. The alignment between human and *Drosophila* HDAC4 identified the MEF2 binding domain at amino acids 162-175 in *Drosophila* HDAC4.

162 TEV**KMKLQEFV**LNK Hs HDAC4

162 PEV**KQILNCFILSR** Dm HDAC4

Conserved residues in *Drosophila* shown in bold blue were mutated to alanine, with a C-terminal 6x-Myc sequence (bold).

162 PEV**KQILNCFILSR** Dm HDAC4

162 PEV**AQIANCFALSR** Dm HDAC4 ΔMEF2

```
1  MSSPDDRIPI  HDLPSEAGSD  ERL LHITPAT  LTLDFKPHPA  VDI DQIMEL  KKSQELQKQR
61  LINSFQEQSK  QMELEHKLQL  EHKYQFAVNS  HGAFQELRNE  SMVTAAAAAV  AQEQHRQQLH
121 QQQQQHQQQQ  QQQQHQQQQQ  QQQARGRDGM  KLKQNC SANA  SPEVAQIANC  FALSRKSQAA
181 ASNGTTTTSP  YRNRGVVKSS  SGESLPAGTV  TSAHPYKIPQ  PPPSLLKYES  DFPLRKTA AE
241 PNLKIRLQK  SVIERKARIG  GPAGARRHER  LLQAAQRRQQ  KNSVLTNCNS  TPD SGPN SPP
301 SAAALAVGVV  GSRGSPTSAP  IQEENEESQ  YQPGQRSSIN  DLPLFSSPSL  PNISLGRPHL
361 PNSAQAHQV  NAQVAAQAQA  QAQAQAQAH  MFAALAAAQ  GCGQPGYYNP  LGMAFVGRQP
421 APLAMIPATG  IAPQQPSPVV  RSASATSTSS  SQASLVGDVA  PPQAHAASTI  LPSSSSYMQQ
481 LGSVAGSGVN  LHAAAVAAAA  AAAAAAGSLP  PTNSHGHHG  SHAHPHHAH  GHGHHGHHGI
541 YAGHQHNVPI  TDAQVAQVHL  HKQGHRPLGR  TQAAPLPLGH  PMLTGAVQLN  VVQTHYENSE
601 AERQAYEHQV  VNQKVRQTVL  TRSGAAAAAA  AAAGVSVVRE  AQLKEEDDDS  AAEVMDLTDK
661 KKPKKTVLTS  TIATSTSQNL  PEALAAAAAA  AAYRAPHNAS  SNSASATKSG  IKLRDQEYLQ
721 QQREQLLLLQ  QEEELAKSLM  RPLSRTLASP  LVPLGPHGLS  QIPDTGQQPA  PIATSSSADH
781 IPPVNLSLPH  RQHRQLMSTL  YASQLRNHQP  SASGSPPHKV  TTGLAYDPLM  LKHSCICGDN
841 AQHPEHSGRL  QSVWARLNET  DLVKRCDRLR  ARKATQEELQ  TVHTEAHAML  FGSNQCQLSR
901 PKLENTLSAS  FVRLSCGGLG  VDLDTTWNEH  HTATAARMAA  GCVIDLALKT  AKGDLRNGFA
961 VVRPPGHAE  ANLAMGFCFF  NSIAIAAKLL  RQRMPEVRR  LIVDWDVHHG  NGTQQAFYQS
1021 PDILYLSIHR  HDDGNFFPGT  GGPTECGSGA  GLGFNVNISW  SGALNPPLGD  AEYIAAFRTV
1081 VMPIARSFNP  DIVLVSSGFD  AATGHPAPLG  GYHVSPACFG  FMTRELLQLA  NGKVVLALEG
1142 GYDLAAICDS  AQECVRALLG  DPAAPIAKAE  LERPPCQNAI  NTLQKTIAIQ  QTHWPCVRML
1201 EHTVGLSALE  TLKVEHDESE  TINAMAGLSM  QSMHRTLSRD  DSEEPMDQDE  TKGGEQKLI
1261 SEEDLNEMEQ KLISEEDLNE MEQKLISEED LNEMEQKLIS EEDLNEMEQ LISEEDLNEM
1321 ESLGDLTMEQ KLISEEDL
```

DmHDAC4 ΔNLS

The NLS in human HDAC4 consists of three arginine-lysine rich clusters (Wang & Yang, 2001), which are highlighted in bold red.

242 NL**KLRSRLKQKVAERRS**---SPLL**RRK**DGPVVVTALKKRP Hs HDAC4

242 NL-L**KIRL**KQSVIE**RK**ARIGGPAGAR**RR**HERLLQAAQRRQ Dm HDAC4

Conserved residues in *Drosophila* are shown in bold blue, these were mutated to alanine residues with a C-terminal 6x-Myc tag sequence (bold).

242 NLL**KIRL**KQSVIE**RK**ARIGGPAGAR**RR**HERLLQAAQRRQ Dm HDAC4

242 NLL**AIALA**QSVIE**AA**ARIGGPAGA**AA**HERLLQAAQRRQ Dm HDAC4 ΔNLS

1 MSSPDDRIPI HDLPSEAGSD ERL LHITPAT LTLDFKPHPA VDIVDQIMEL KKSQELQKQR
61 LINSFQEQSK QMELEHKLQL EHKYQFAVNS HGAFQELRNE SMVTAAAAAV AQEQHRQQLH
121 QQQQHQQQQ QQQQHQQQQ QQQARGRDM KLKQNC SANA SPEVKQILNC FILSRKSQAA
181 ASNGTTTTSP YRNRGVV KSS SGE SLPAGTV TSAHPYKIPQ PPPSLLKYES DFPLRKTAEE
241 PNLL**AIALA**QSVIE**AA**ARIG GPAGAA**AA**HER LLQAAQRRQ KNSVLTNCNS TPDSGPN SPP
301 SAAALAVGVV GSRGSP TSAP IQEENE EGSQ YQPGQRSSIN DLPLFSSPSL PNISLGRPHL
361 PNSAQAHQV NAQVAAQAQA QAQAQAQAH MFAALAAAQ GCGQPGYYP LGMAFVGRQP
421 APLAMIPATG IAPQQP SPV RSASATSTSS SQASLVGDVA PPQAHAASTI LPSSSSYMQQ
481 LGSVAGSGVN LHAAAVAAAA AAAAAAGSLP PTNSHGHGHG SHAHPHFAH GHGHGHGHGI
541 YAGHQHNVPI TDAQVAQVHL HKQGHRPLGR TQAAPLPLGH PMLTGAVQLN VVQTHYENSE
601 AERQAYEHQV VNQKVRQTVL TRSGAAAAAA AAAGVSVVRE AQLKEEDDD SAAEVMDLTDK
661 KKPPKTVLTS TIATSTSQNL PEALAAAAAA AAYRAPHNAS SNSASATKSG IKLRDQEYLO
721 QQREQLLLLQ QEEELAKSLM RPLSRTLAS LVPLGPHGLS QIPDTGQQA PIATSSSADH
781 IPPVNLSLPH RQHRQLMSTL YASQLRNHP SASGSPPHKV TTGLAYDPLM LKHSCICGDN
841 AQHPEHSGRL QSVWARLNET DLVKRC DRLR ARKATQEELQ TVHTEAHAML FGSNQCQLSR
901 PKLENTLSAS FVRLSCGGLG VDLDTWNEH HTATAARMAA GCVIDLALKT AKGDLRNGFA
961 VVRPPGHAE ANLAMGFCFF NSIAIAAKLL RQRMPEVRI LIVDWDVHHG NGTQQAFYQS
1021 PDILYLSIHR HDDGNFFPGT GGPTTECGSGA GLGFNVN ISW SGALNPPLGD AEYIAAFRTV
1081 VMPIARSNP DIVLVSSGFD AATGHPAPLG GYHVSPACFG FMTRELLQLA NGKVVLALLEG
1142 GYDLAAICDS AQECVRALLG DPAAPIAKAE LERPPCQNAI NTLQKTIAIQ QTHWPCVRML
1201 EHTVGLSALE TLKVEHDESE TINAMAGLSM QSMHRTLSRD DSEEPMDQDE TKGGGE**QKLI**
1261 **SEEDLNEME Q KLISEEDLNE MEQKLISEED LNEME QKLIS EEDLNEME QK LISEEDLNEM**
1321 ESLGDLTME**Q KLISEEDL**

DmHDAC4 Y1142H

In human HDAC4, the H976Y mutation restores catalytic activity that is present in other HDACs including *Drosophila* HDAC4, this however, is lost in human HDAC4 (Lahm et al., 2007). In *Drosophila* the corresponding amino acid is Y1142 which is mutated to H in order to catalytically inactivate *Drosophila* HDAC4.

1137 LEGGHD Hs HDAC4

1137 LEGGYD Dm HDAC4

1137 LEGGHD Dm HDAC4 Y1142H

```

  1  MSSPDDRIP I HDLPSEAGSD ERL LHITPAT  LTLDFKPHPA  V D I D Q Q I M E L  K K S Q E L Q K Q R
 61  L I N S F Q E Q S K  Q M E L E H K L Q L  E H K Y Q F A V N S  H G A F Q E L R N E  S M V T A A A A A V  A Q E Q H R Q Q L H
121  Q Q Q Q H Q Q Q Q Q  Q Q Q Q H Q Q Q Q Q  Q Q Q A R G R D G M  K L K Q N C S A N A  S P E V K Q I L N C  F I L S R K S Q A A
181  A S N G T T T T S P  Y R N R G V V K S S  S G E S L P A G T V  T S A H P Y K I P Q  P P P S L L K Y E S  D F P L R K T A A E
241  P N L L K I R L K Q  S V I E R K A R I G  G P A G A R R H E R  L L Q A A Q R R Q Q  K N S V L T N C N S  T P D S G P N S P P
301  S A A A L A V G V V  G S R G S P T S A P  I Q E E N E E G S Q  Y Q P G Q R S S I N  D L P L F S S P S L  P N I S L G R P H L
361  P N S A Q A H A Q V  N A Q V A A Q A Q A  Q A Q A Q A Q A H A  M F A A L A A A Q G  G C G Q P G Y Y N P  L G M A F V G R Q P
421  A P L A M I P A T G  I A P Q Q P S P V V  R S A S A T S T S S  S Q A S L V G D V A  P P Q A H A A S T I  L P S S S S Y M Q Q
481  L G S V A G S G V N  L H A A A V A A A A  A A A A A A G S L P  P T N S H G H G H G  S H A H P H P H A H  G H G H G H G H G I
541  Y A G H Q H N V P I  T D A Q V A Q V H L  H K Q G H R P L G R  T Q A A P L P L G H  P M L T G A V Q L N  V V Q T H Y E N S E
601  A E R Q A Y E H Q V  V N Q K V R Q T V L  T R S G A A A A A A  A A A G V S V V R E  A Q L K E E D D D S  A A E V M D L T D K
661  K K P P K T V L T S  T I A T S T S Q N L  P E A L A A A A A A  A A Y R A P H N A S  S N S A S A T K S G  I K L R D Q E Y L Q
721  Q Q R E Q L L L L Q  Q E E E L A K S L M  R P L S R T L A S P  L V P L G P H G L S  Q I P D T G Q Q P A  P I A T S S S A D H
781  I P P V N L S L P H  R Q H R Q L M S T L  Y A S Q L R N H Q P  S A S G S P P H K V  T T G L A Y D P L M  L K H S C I C G D N
841  A Q H P E H S G R L  Q S V W A R L N E T  D L V K R C D R L R  A R K A T Q E E L Q  T V H T E A H A M L  F G S N Q C Q L S R
901  P K L E N T L S A S  F V R L S C G G L G  V D L D T T W N E H  H T A T A A R M A A  G C V I D L A L K T  A K G D L R N G F A
961  V V R P P G H H A E  A N L A M G F C F F  N S I A I A A K L L  R Q R M P E V R R I  L I V D W D V H H G  N G T Q Q A F Y Q S
1021  P D I L Y L S I H R  H D D G N F F P G T  G G P T E C G S G A  G L G F N V N I S W  S G A L N P P L G D  A E Y I A A F R T V
1081  V M P I A R S F N P  D I V L V S S G F D  A A T G H P A P L G  G Y H V S P A C F G  F M T R E L L Q L A  N G K V V L A L E G
1142  G H D L A A I C D S  A Q E C V R A L L G  D P A A P I A K A E  L E R P P C Q N A I  N T L Q K T I A I Q  Q T H W P C V R M L
1201  E H T V G L S A L E  T L K V E H D E S E  T I N A M A G L S M  Q S M H R T L S R D  D S E E P M D Q D E  T K G G G E Q K L I
1261  S E E D L N E M E Q  K L I S E E D L N E  M E Q K L I S E E D  L N E M E Q K L I S  E E D L N E M E Q K  L I S E E D L N E M
1321  E S L G D L T M E Q  K L I S E E D L
```

6.4 *Ank2* RNAi transcript targets

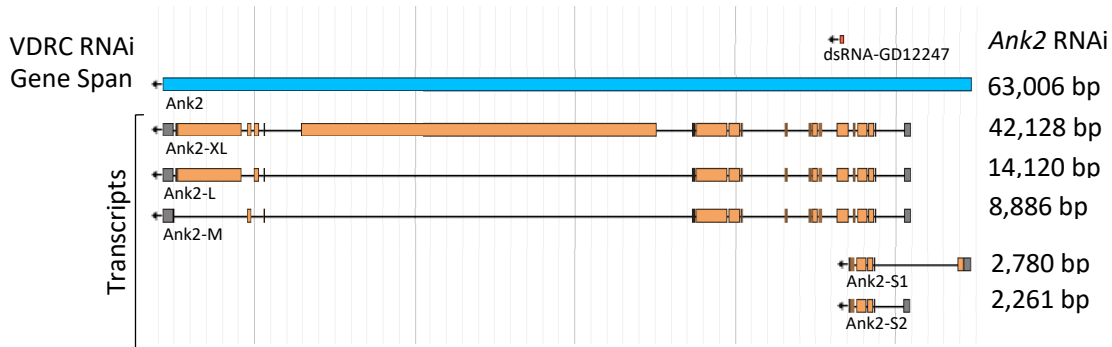


Figure 6.1. *Ank2* gene and transcript targets by the *Ank2* RNAi construct. The *Ank2* gene (Flybase ID: FBgn0261788) is shown in blue with the main transcripts; Ank2-XL, Ank2-L, Ank2-M, Ank2-S1, and Ank2-S2. dsRNA-GD12247 was the *Ank2* RNAi that was used throughout this study which targets the Ank2-XL, Ank2-L and Ank2-M isoforms and does not target the two short isoforms depicted here. Modified figure from (https://flybase.org/jbrowse/?data=data%2Fjson%2Fdmel&loc=3L%3A7645525..7732948&tracks=Gene_span%2CRNA%2Cper_product_5&highlight=). Abbreviations: VDRC = Vienna *Drosophila* Resource Centre, dsRNA = double stranded RNA.